

論文 / 著書情報
Article / Book Information

題目(和文)	
Title(English)	Fabrication and Heat Treatment of Spark Plasma Sintered Porous Ti-6Al-4V using Space Holder Method
著者(和文)	LANTANG YORINA S F
Author(English)	Yorina S F Lantang
出典(和文)	学位:博士(工学), 学位授与機関:東京工業大学, 報告番号:甲第9967号, 授与年月日:2015年9月25日, 学位の種別:課程博士, 審査員:小林 郁夫,熊井 真次,竹山 雅夫,木村 好里,生駒 俊之
Citation(English)	Degree:., Conferring organization: Tokyo Institute of Technology, Report number:甲第9967号, Conferred date:2015/9/25, Degree Type:Course doctor, Examiner:,,,,,
学位種別(和文)	博士論文
Type(English)	Doctoral Thesis

**Fabrication and Heat Treatment of
Spark Plasma Sintered
Porous Ti-6Al-4V using
Space Holder Method**

by

Yorina Sarah Franscoise Lantang

Doctoral Thesis

**Department of Metallurgy and Ceramics Science
Tokyo Institute of Technology**

2015

Abstract

Titanium and its alloy, especially Ti-6Al-4V have been widely used for biomaterial, especially bone implant, because of its high specific strength and excellent corrosion resistance. Big difference of Young's modulus or Modulus of elasticity between bone and this alloy has been a great concern for bone implants. This big difference of Young's modulus can cause the absent or less stress at the bone as the consequences of stress concentration on the metal implant as the stronger part of the structure, namely stress shielding. This present thesis mainly discussed the fabrication of porous Ti-6Al-4V through space holder method and the influence of heat treatment to porous Ti-6Al-4V in order to produce low Young's modulus of metal implant with compatible strength value to cortical bone properties which are around 10 – 30 GPa of Young's modulus and 70 – 280 MPa of compressive strength.

In order to obtain the effective condition of fabrication of porous Ti-6Al-4V, the influence of sintering parameters, space holder size and its distribution to the formation of macro- and micro-porosity were investigated. It was found that space holder distribution plays an important role to increase open porosity value of porous products. Open porosity of sample increase as the more homogenous space holder distribution produced suggests distribution of space holder is main aspect that control the macro-pore interconnectivity. There is no significant increase of open porosity number by varying the space holder size and shape implying the interconnectivity between macro-pore is independent on space holder size and shape. Additionally, sintering temperature and pressure are the main parameter to control micro-porosity. Increasing sintering pressure is more effective to reduce micro-porosity in the samples. Relative density produced is independent on heating rate. The most effective condition to produce less micro-porosity and more interconnected macro-porosity is utilization of any kind of space holder size with the addition of 10 wt. % ethanol as PCA and sintering at 700 °C, 60 MPa.

In the relation of porous products' mechanical properties, macro-porosity in the range of 50 – 800 μm plays more significant role to control mechanical properties of porous product. Irregular shape of macro-pore result about two times lower mechanical properties than cuboidal shape macro-pore while porous mechanical properties is insensitive to macro-porosity size. Homogenous macro-porosity will result more pore connectivity which result to higher number of open porosity and lower Young's modulus. Porous product strength is more dependent to pore wall thickness than its open porosity number. Micro-porosity in the size a few till a few

ten micrometer has no significant effect to both Young's modulus and mechanical properties of porous product.

Before doing heat treatment to porous products, solution treatment and aging were performed to spark plasma sintered Ti-6Al-4V. It was found that upon quenching, martensite phase only formed by sample solution treatment above 980 °C. Due to quite high vanadium content which stabilized the BCC structure, quenching below such temperature produced metastable β phase. Aging treatment enhances formation of β phase precipitate. Thus, after aging martensite decomposes to rich vanadium β phase, which form along the grain boundary of martensite and aligned along interface of martensite plate, and lean vanadium α -phase. The decomposition then decrease the hardness of the sample. The results of solution treatment also imply that the β transus temperature of spark plasma sintered Ti-6Al-4V is higher than 1050 °C.

Finally, the influence of solution treatment and oxygen to microstructure and mechanical properties of Porous Ti-6Al-4V are investigated. Oxygen content affects the phase's constituent of porous sample at elevated temperature. Due to relatively high oxygen content the β transus temperature of the sample increase till between 1200 and 1300 °C. Even though oxygen increase the β transus temperature, it also increase the compressive strength of porous sample. Solution treatment at temperature 850 – 1000 °C followed by ice water quenched produces microstructure which is similar to spark plasma sintered Ti-6Al-4V and increases the mechanical properties of porous Ti-6Al-4V. Solution treatment at single β phase area at 1300 – 1400 °C produce a very fine Widmanstätten α and β phase which successfully results to the increase of mechanical properties of porous Ti-6Al-4V, compatible with cortical bone properties.

“Have I not commanded you? Be strong and courageous. Do not be frightened, and do not be dismayed, for the LORD your God is with you wherever you go.”

Joshua 1:9

Table of Contents

Chapter 1 General Introduction	1
1.1 Background.....	1
1.2 Porous metal for bone replacement	1
1.3 Solid-state state space holder method.....	3
1.4 Heat treatment of Ti-6Al-4V alloy	4
1.5 Objective of the present thesis	5
1.6 Outline of the present thesis.....	6
1.7 References.....	9
Chapter 2 Fabrication of Porous Ti-6Al-4V through Space Holder Method	12
2.1 Introduction.....	12
2.2 Experimental Procedures	13
2.2.1 Materials.....	13
2.2.2 Mixing condition.....	14
2.2.3 Spark Plasma Sintering	15
2.2.4 Characterization	15
2.2.4.1 Density and Open Porosity.....	15
2.2.4.2 Relative Density	16
2.2.4.3 Image analysis	16
2.3 Results.....	17
2.3.1 Microstructure and densification of porous Ti-6Al-4V	17
2.3.2 Space holder size and distribution in relation with porous product porosity and sinter-ability	24
2.4 Discussion.....	32
2.4.1 Influence of sintering parameter to the formation of macro- and micro-porosity ...	32
2.4.2 Influence of space holder distribution to the formation of macro-porosity	35

2.5 Conclusions.....	36
2.6 References.....	37
Chapter 3 Effect of Macro- and Micro-porosity on Mechanical Properties of a Porous Ti-6Al-4V	40
3.1 Introduction.....	40
3.2 Experimental Procedures	40
3.3 Results.....	43
3.3.1 Influence of sintering parameter to mechanical properties	43
3.3.2 Influence of space holder size and distribution to mechanical properties.....	44
3.4 Discussion.....	53
3.4.1 Effect of micro-porous to mechanical properties	53
3.4.2 Effect of macro-porous to mechanical properties	54
3.5 Conclusions.....	56
3.6 References.....	57
Chapter 4 Influence of Solution Treatment and Aging to Microstructure and Hardness of Bulk Spark Plasma Sintered Ti-6Al-4V	58
4.1 Introduction.....	58
4.2 Experimental Procedures	59
4.3 Results.....	60
4.3.1 Microstructural change after heat treatment.....	60
4.3.2 Hardness after heat treatment.....	73
4.4 Discussion.....	75
4.4.1 Influence of solution treatment to microstructure and hardness	75
4.4.2 Influence of aging to microstructure and hardness	80
4.5 Conclusions.....	80
4.6 References.....	81
Chapter 5 Influence of Solution Treatment and Oxygen Content to Microstructure and Mechanical Properties of Porous Ti-6Al-4V.....	82

5.1 Introduction.....	82
5.2 Experimental Procedures	82
5.2.1 Fabrication of porous sample	82
5.2.2 Heat treatment	83
5.3 Results.....	84
5.3.1 Oxygen concentration change	84
5.3.2 High-temperature XRD	85
5.3.3 Microstructural change after solution treatment	86
5.3.4 Mechanical properties after solution treatment.....	86
5.4 Discussion.....	100
5.4.1 Influence of oxygen.....	100
5.4.2 Influence of solution treatment to micro-structure and mechanical properties of porous Ti-6Al-4V	102
5.5 Conclusions.....	104
5.6 References.....	105
Chapter 6 General Conclusions	107

Chapter 1 General Introduction

1.1 Background

Titanium and its alloy, especially Ti-6Al-4V have been widely used for biomaterial, especially bone implant, because of its high specific strength and excellent corrosion resistance. Moreover, it is widely known that titanium provides bone osteoinduction which is defined as “the induction of undifferentiated inducible osteoprogenitor cells that are not yet committed to the osteogenic lineage to form osteoprogenitor cells” (Friedenstein, 1968) [1]. To be simple, osteoinduction means that primitive, undifferentiated and pluripotent cells are somehow stimulated to develop into the bone-forming cell lineage [2] or the process when osteogenesis/bone growing process is induced [3].

Big difference of Young’s modulus or Modulus of elasticity between bone and this alloy has been a great concern for the application for bone implants material. Several researches reported the difference of Young’s modulus between bone and metal implant can lead to the implantation failure. This big difference of Young’s modulus can cause less stress at the bone as the consequences of stress concentration on the metal implant as the stronger part of the structure, namely stress shielding. Thus, metal implant have to have not only high strength, good corrosion resistant and good biocompatibility, but also low Young’s modulus, comparable to Young’s modulus of bone. Porous product could be one of the best alternatives to produce low Young’s modulus of the metal implant. Consequently, the reduction of Young’s modulus is followed by the decrease of its strength. Thus, a porous implant has to have comparable proper strength to bear the body physical stress.

1.2 Porous metal for bone replacement

The application of porous metal for implant fixation started in the late 1970s after numerical basic studies from laboratory and animal trial program [4]. Porous metal alloys have become alternate implant substance, include total hip joint and tooth root replacements, bone lesion site fillers and segmental replacement. Ever since several research have been performed

in several topics, e.g. mechanical properties and stability, tissue remodeling, biomechanical function, chemical characteristics, etc.

Lewangrowshi *et al.* reported for polyethylene – calcium salt composite samples implanted into mouse's tibia more bone ingrowth was observed in more calcium content sample in which more porosity produced [5]. Bone growth in the implant relate to aggregation and infiltration of bone cell, osteocyte, to the implant. Higher porosity also generated more bone ingrowth for porous polyethylene, containing 20 wt. % of hydroxyapatite, rat's apex implant fabricated by free solid forming [6].

Meanwhile, mechanical properties of porous structure will also strongly affect by porosity. Gibson-Ashby model [7] below show us the relation between mechanical properties of open porous foam and porosity volume fraction.

$$\frac{E}{E_s} = C \left(\frac{\rho}{\rho_s} \right)^n = Cp^n \quad 1.1$$

$$\frac{\sigma}{\sigma_s} \approx 0.3 \left(\frac{\rho}{\rho_s} \right)^{3/2} \quad 1.2$$

Where C and n is constant, E, σ and ρ is Young modulus, strength and density of metal foam and E_s , σ_s while ρ_s is properties of solid metal and p is porosity.

1.3 Solid-state state space holder method

Several methods have been performed to produce porous metal either by liquid state or solid state. Titanium and titanium alloys are known to have high melting point and high reactivity especially to form oxide and carbide. Hence, unlike forming porous metal or metal foam through liquid state fabrication process, solid state process is still preferable, especially in the high melting point of view. In this study, space holder method was selected due to its simplicity and its ability to produce greater porosity and shape control porosity.

The process begins by mixing the metal powders with an appropriate space holder and is followed by the mixture to form a green body. Space holder size should be higher than the average powder size of metal powder. The green body is then subjected to heat treatment process that is sintering process, leads to growth of sinter neck and densification of green products which associated with the improvement of structural integrity [8]. The schematic of the process is shown in figure 1.1. Due to its non-toxic characteristic, its high melting temperature, its chemical stability and its ease to remove sodium chloride is chosen to be space holder in this research.

Many researches have been publish about the morphology of space holder and its effect to the mechanical properties and biocompatibility of porous metal product. Bekoz *et al.* [9] compare the mechanical properties of irregular and spherical shape carbamide to the mechanical properties of stainless steel foam while Zhang *et al.* [10] confirmed the increase of compressive strength polymeric porous product which is produced by spherical shape space holder rather than the one produced by cuboidal shape space holder. Although its significance to the total porosity produced and its influence to the mechanical properties, only limited reports about space holder distribution are found. Li *et al.* [11] reported sieved space holder increase the compression strength of porous NiTi, implies the importance of space holder size distribution. Niu *et al.* [12] used finite element method (FEM) to relate the relation between random pore distributions to elastic modulus of titanium scaffolds. In this thesis, the influence of space holder distribution to the properties of porous products, such as porosity, density, Young's modulus and compressive strength will be explored.

In order to avoid inhomogeneity distribution of macro-pores, as well as space holder distribution inhomogeneity, several researchers have been trying to add binder or process

control agent (PCA) during mixing process. Several kinds of binder have been used such as water [13], polyvinyl-alcohol (PVA) [14], polyethylene-glycol (PEG) [15], ethanol [16] and stearic acid (SA) [17]. Despite the importance, its role, its effectivity and its influence of PCA addition to distribution of space holder as well as macro-pores distribution is rarely discussed. In this research the quantitative analysis is performed to show the influence of PCA to pore distribution and its effect to the open porosity and mechanical properties of porous Ti-6Al-4V. In addition, the influence of macro-porosity produced by space holder and micro-porosity produced during sintering is also investigated.

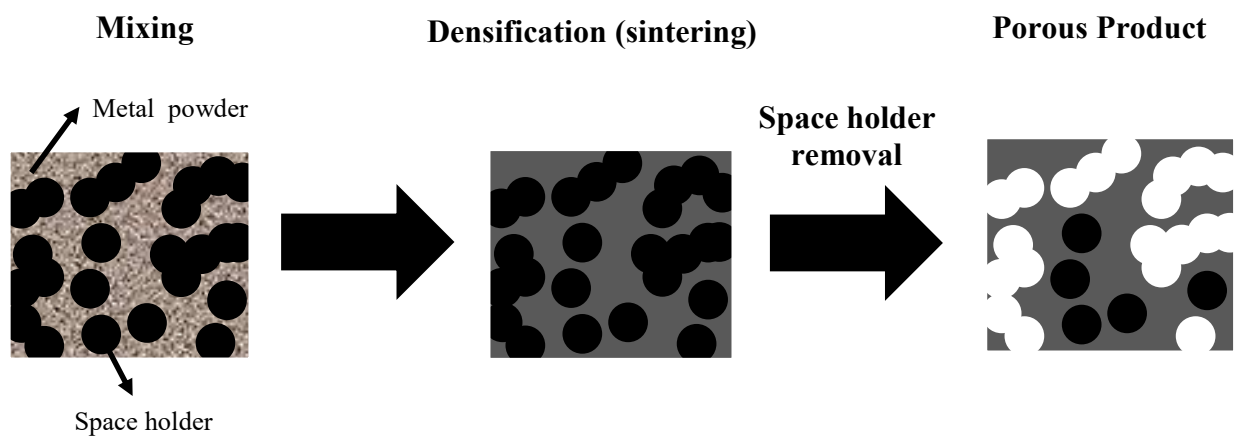


Figure 1. 1 Schematic of solid-state space holder method

1.4 Heat treatment of Ti-6Al-4V alloy

From the equations 1.1 and 1.2, it is obvious that as the consequences of the reduction of the apparent Young's modulus of porous metal, its strength will also decrease. Thus, a compromising reduction of apparent Young's modulus should be attained in order to maintain the strength of porous metal. Another pursuit is to increase the porous product without changing so much its Young's modulus. Such pursuit can be obtained by performing heat treatment to porous metal.

Depending on cooling rate and prior heat treatment, e.g. annealing, thermo-mechanical process, solution treatment and aging, Ti-6Al-4V alloy microstructure can be modified into several types microstructure, such as α allotriomorph, globular α or primary α , Widmanstätten, basket-weave, and martensitic phase [18]. However, Titanium and titanium alloys produced

through powder metallurgy route, which usually have Widmanstätten structure, not always effectively strengthened by the combination of solution treatment and aging [19]. In this thesis the effectivity of combination of solution treatment and aging to porous product that is produced by solid-state method or powder metallurgy route and sintered by spark plasma sintering is discussed.

1.5 Objective of the present thesis

This present thesis mainly discussed the fabrication of porous Ti-6Al-4V through space holder method and the influence of heat treatment to porous Ti-6Al-4V in order to produce low Young's modulus of metal implant with compatible strength value to cortical bone properties which are around 10 – 30 GPa of Young's modulus and 70 – 280 MPa of compressive strength. Thus the main objectives of this thesis are describe as follow

- (1) To investigate the influence of sintering parameters, space holder size and its distribution to the formation of macro- and micro-porosity in order to obtain the effective condition of fabrication of porous Ti-6Al-4V
- (2) To investigate the influence of macro- and micro-porosity to the mechanical properties of porous Ti-6Al-4V. Thus, the optimum fabrication condition and mechanical properties can be achieved.
- (3) To confirm the effect of solution treatment and aging to the mechanical properties of spark plasma sintered Ti-6Al-4V in order to implement them to the porous product
- (4) To investigate the influence of oxygen content and solution treatment to the microstructure and mechanical properties of porous Ti-6Al-4V

1.6 Outline of the present thesis

In the present thesis, the fabrication of porous Ti-6Al-4V through space holder method and the influence of heat treatment to porous Ti-6Al-4V in order to produce low Young's modulus value of metal implant with compatible strength value to cortical bone properties i.e. around 10 – 30 GPa of Young's modulus and 70 – 280 MPa of compressive strength are discussed. The flow chart of the thesis is given in figure 1.2.

The back ground of this research is explained in *Chapter 1 General Introduction*. This chapter also describe the development of space holder technique to produce porous metal. In addition the introduction of heat treatment process of Ti-6Al-4V and porous metal characteristic are also explained.

Chapter 2 Fabrication of porous Ti-6Al-4V through space holder method

The influence of sintering parameters (heating rate, sintering temperature and sintering pressure), space holder size and its distribution to the formation of both micro- and macro-porosity is investigated in order to achieve the effective condition of fabrication of porous Ti-6Al-4V using sodium chloride as the space holder. The original developed image analysis of samples' macro-image was used in order to quantitatively analyze the space holder distribution as well as the pore distribution of the samples. The main parameters to control in this process are space holder distribution, sintering pressure and sintering temperature.

Chapter 3 Effect of macro- and micro-porosity on mechanical properties of a porous Ti-6Al-4V

In this chapter, the influence of macro-porosity and micro-porosity to the mechanical properties of porous Ti-6Al-4V fabricated by solid-state space holder method is discussed. Macro-porosity in the range of 50 – 800 μm plays more significant role to control mechanical properties of porous product while micro-porosity in the size a few till a few ten micrometer has no significant effect to both Young's modulus and compressive strength of porous product.

Chapter 4 Influence of solution treatment and aging to microstructure and hardness of bulk spark plasma sintered Ti-6Al-4V

In order to confirm the effect of solution treatment and aging to the mechanical properties of spark plasma sintered Ti-6Al-4V, solution treatment and aging was performed. Solution treatment above 980 °C introduces martensite phase which strengthened the samples upon quenching. Solution treatment increase the hardness of spark plasma sintered Ti-6Al-4V whereas aging treatment decrease the hardness of solution treated samples. The results of solution treatment also imply that the β transus temperature of spark plasma sintered Ti-6Al-4V is higher than 1050 °C.

Chapter 5 Influence of solution treatment and oxygen content to microstructure and mechanical properties of Porous Ti-6Al-4V

In this chapter, the influence of solution treatment and oxygen to microstructure and mechanical properties of Porous Ti-6Al-4V are discussed. Solution treatment increase oxygen content in porous samples. Oxygen influences the phase constituent of sample at elevated temperature. Even though oxygen increase the β transus temperature, it also increase the compressive strength of porous sample. Solution treatment at single β phase area at 1300 – 1400 °C produces a very fine Widmanstätten α and β phase which later results to more increase of mechanical properties of porous Ti-6Al-4V comparable with cortical bone properties.

The general conclusions of this thesis is summarized in ***Chapter 6 General conclusions.***

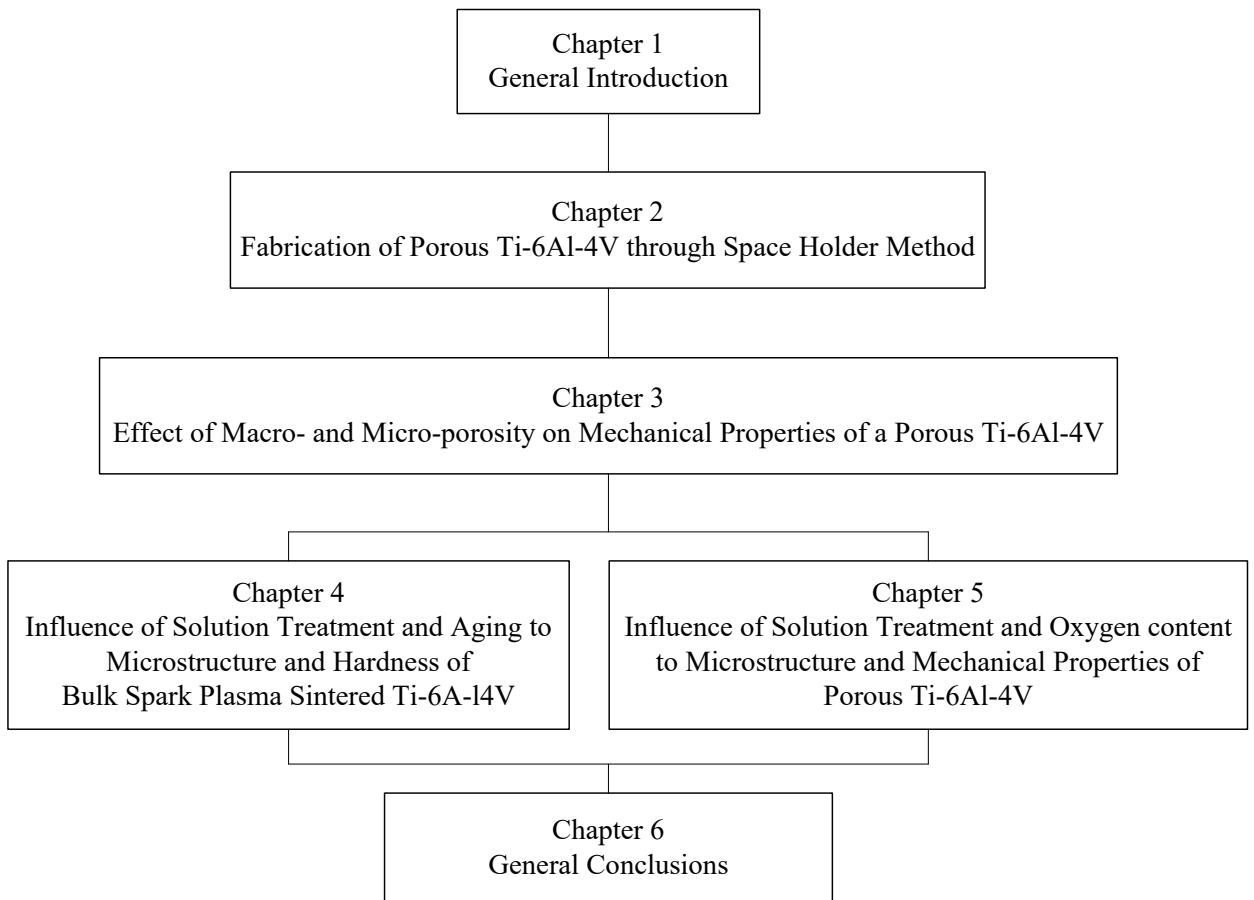


Figure 1. 2 Outline of the present thesis

1.7 References

- [1] A. Friedenstein, "Induction of bone tissue by transitional epithelium," *Clinical Orthopaedics and Related Research*, vol. 59, pp. 21-37, 1968.
- [2] T. Albrektsson and C. Johansson, "Osteoinduction, osteoconduction and osseointegration," *European Spine Journal*, vol. 10, no. 2 Supplement, pp. S96-S1011, 2001.
- [3] J. Wilson-Hench, "Osseointegration," in *Progress in Biomedical Engineering: Definition in Biomaterials*, D. F. Williams, Ed., Chester, Elsevier, 1987, p. 29.
- [4] J. Lemons and L. Lucas, "Properties of Biomaterials," *The Journal of Arthroplasty*, vol. 1, no. 2, pp. 143-147, 1986.
- [5] K.-U. Lewandrowski, J. D. Gresser, S. P. Bondre, A. E. Silva, D. L. Wise and D. J. Trantolo, "Developing porosity of poly(propylene glycol-co-fumaric acid) bone graft substitutes and the effect on osteointegration: A preliminary histology study in rats," *Journal of Biomaterials Science, Polymer Edition*, vol. 11, no. 8, pp. 879-889, 2000.
- [6] T. D. Roy, J. L. Simon, J. L. Ricci, E. D. Rekow, V. P. Thompson and J. R. Parsons, "Performance of degradable composite bone repair products made via three-dimensional fabrication techniques," *Journal of Biomedical Materials Research A*, vol. 66A, no. 2, pp. 283-291, 2003.
- [7] L. Gibson and M. F. Ashby, "Cellular Solids: Structure and Properties," Cambridge, Cambridge University Press, 1997, p. 189 and 206.
- [8] G. Ryan, A. Pandit and D. P. Apatsidis, "Fabrication methods of porous metals for use in orthopaedic applications," *Biomaterials*, vol. 27, pp. 2651-2670, 2006.

- [9] N. Bekoz and E. Oktay, "Effects of carbamide shape and content of processing and properties of steel foam," *Journal of Materials Processing Technology*, vol. 212, pp. 2109-2116, 2012.
- [10] J. Zhang, L. Wu, D. Jing and J. Ding, "A comparative study of porous scaffolds with cubic and spherical macropores," *Polymer*, vol. 46, no. 13, pp. 4979-4985, 2005.
- [11] D. S. Li, Y. Zhang, X. Ma and X. P. Zhang, "Space-holder engineered porous NiTi shape memory alloys with improved pore characteristics and mechanical properties," *Journal of Alloys and Compounds*, vol. 474, no. 1-2, pp. L1-L5, 2009.
- [12] W. Niu, S. Gill, H. Dong and C. Bai, "A two-scale model for predicting elastic properties of porous titanium formed with space-holders," *Computational Materials Science*, vol. 50, pp. 172-178, 2010.
- [13] O. Smorygoa, A. Marukovicha, V. Mikutskia, A. A. Gokhaleb, G. J. Reddyb and J. V. Kumarb, "High-porosity titanium foams by powder coated space holder compaction method," *Materials Letters*, vol. 83, pp. 17-19, 2012.
- [14] Z. Esen and S. Bor, "Characterization of Ti-6Al-4V alloy foams synthesized by space holder technique," *Materials Science Engineering A*, vol. 528, pp. 3200-3209, 2011.
- [15] W. Niu, C. Bai, G. Qiu and Q. Wang, "Processing and properties of porous titanium using space holder technique," *Materials Science and Engineering: A*, vol. 506, no. 1-2, pp. 148-151, 2009.
- [16] M. Dewidar, H. F. Mohamed and J.-K. Lim, "A New Approach for Manufacturing a High Porosity Ti-6Al-4V," *Journal of Materials Science and Technology*, vol. 24, pp. 931-935, 2008.
- [17] C. E. Wen, Y. Yamada and P. D. Hodgson, "Fabrication of novel TiZr alloy foams for biomedical applications," *Materials Science and Engineering C*, vol. 26, pp. 1439-14444, 2006.
- [18] G. Lütjering, "Influence of processing on microstructure and mechanical properties of (α + β) titanium alloys," *Materials Science and Engineering: A*, vol. 243, no. 1-2, pp. 32-45, 1998.

- [19] F. Hideki, "Strengthening of $\alpha+\beta$ titanium alloys by thermomechanical processing," *Materials Science and Engineering: A*, vol. 243, p. 103–108, 1998.

Chapter 2 Fabrication of Porous Ti-6Al-4V through Space Holder Method

2.1 Introduction

In order to produce porous metals or metal foams, several methods have been developed recently. In general, all the available methods can be categorized into big two categories, i.e. solid-state method or liquid-state method [1]. Titanium and its alloys, including Ti-6Al-4V, generally have high melting point that is not preferable to produce porous metals through liquid-state method [2], such as gas injection molding [1], vapor deposition, and foaming agent in molten metal [3] [4]. The solid-state method through powder metallurgy route using space holder as pore maker, such as polymethylmethacrylate (PMMA) polymer [5], magnesium [6], sodium chloride [7], and ammonium hydro carbonate [8], has been known to exhibit some advantages to permit simple and accurate control of pore fraction, shape and connectivity [7].

The production of porous metals through the powder metallurgy route will produce two kinds of porosity, namely micro-porosity – produced due to unfinished neck growth – and macro-porosity – produced by the space holder. These two porosities will influence the mechanical properties of porous product. Micro-porosity production is strongly related with the densification process during sintering, while macro-porosity is usually mimic characteristic of the space holder. Thus, sintering parameters are crucial in this process as well as choice of space holder and mixing process. In this chapter the influence of sintering parameters (heating rate, sintering temperature and sintering pressure), space holder size and its distribution to the formation of both micro- and macro- porosity is discussed in order to achieve the effective condition of fabrication of porous Ti-6Al-4V using sodium chloride as the space holder.

2.2 Experimental Procedures

2.2.1 Materials

In this study, spherical gas atomization Ti-6Al-4V powder (Osaka Titanium technologies Co., Ltd) was used as the metal powder and sodium chloride (Nascalai Tesque, Inc.) was used as the space holder. Sodium chloride is used because of its non-toxic characteristic and high dissolubility in water. The metal powder size is less than 45 μm , while the space holder powder is varied from 600 μm to 106 μm . The chemical composition and morphology of metal powder are shown in table 2.1 and figure 2.1.

Table 2.1 Chemical composition of as received Ti-6Al-4V powder

	Ti	Fe	Al	H	N	C	O	V
%	Bal.	0.070	5.91	0.009	0.008	0.015	0.190	3.94

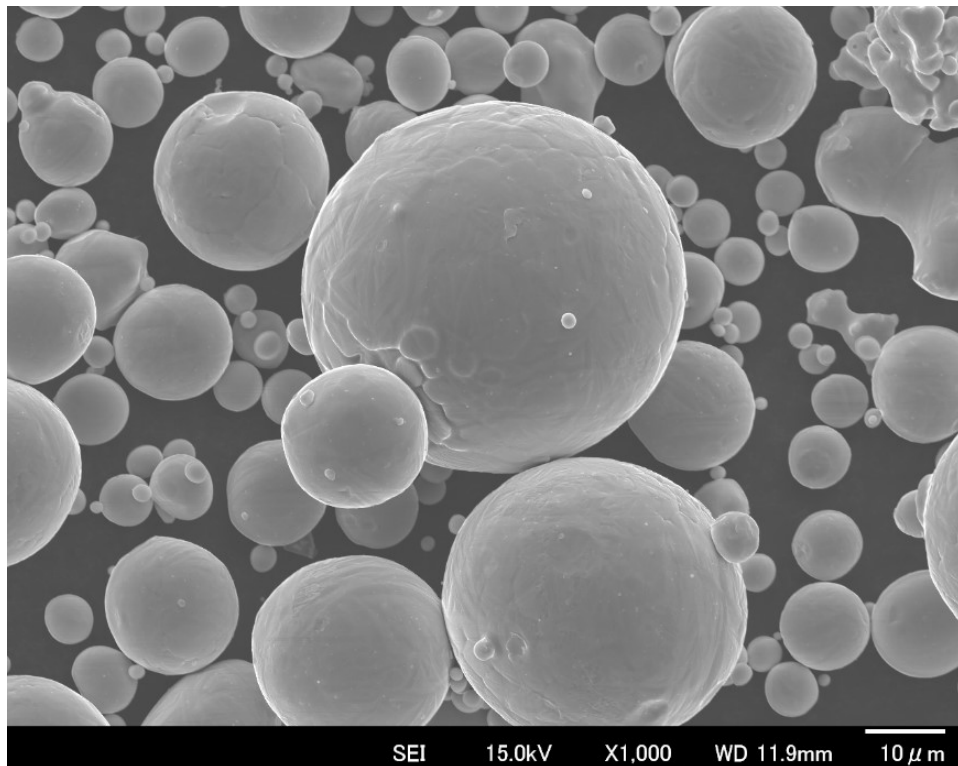


Figure 2.1 SEM image of Ti-6Al-4V powder

2.2.2 Mixing condition

The volume fraction of the metal powder and the space holder was decided to be 50: 50 vol. % and 40: 60 vol. %. A little amount of process control agent (PCA), i.e. stearic acid (SA) and ethanol are added in order to improve the distribution of space holder powder. Both of the process control agent are considered as less-toxic chemical. Powder mixing was performed by several mixing parameter and condition as shown in table 2.2 using a planetary micro mill machine (Pulverisette 7, Fritsch). Mixed powder then compacted in a 20 mm inner diameter graphite die.

Table 2.2 Mixing condition of powder

Ti-6Al-4V : NaCl (vol. %)	NaCl Size (μm)	Process Control Agent (PCA)	Balls for mixing	Mixing Parameter
50 : 50	600 – 425	No	No	100 rpm, 1h
		1 wt. % SA	1:1 1-mm-ZrO ₂ -ball	100 rpm, 1h
		5 wt. % SA	1:1 1-mm-ZrO ₂ -ball	100 rpm, 1h
		10 wt. % molten SA	No	Hand mixing
	10 wt. % ethanol	No	100 rpm, 1h	
	600 – 425 and 212 – 106 (with weight ratio 1:1)	10 wt. % ethanol	No	100 rpm, 1h
40 : 60	600 – 425	10 wt. % ethanol	No	100 rpm, 1h
	600 – 425 and 212 – 106 (with weight ratio 1:1)			
	425 – 212			
	425 – 212 and 106 - (with weight ratio 1:1)			
	212 – 106			
	Less than 106			

2.2.3 Spark Plasma Sintering

Spark plasma sintering process (SPS) is known as a process that is effective to sinter high melting temperature metal. It allows densification in much lower sintering temperature and shorter sintering time. In the case of sintering of titanium and its alloy, sintering temperature and time can be reduced to 700 – 900 °C for several minutes, compare to conventional sintering process and hot isostatic pressing, i.e. 900 – 1200 °C for 8 – 12 hours and 700 – 900 °C for 1 – 8 hours.

Sintering process was performed using a spark plasma sintering machine (SPS 511S, SPS Syntex) under a vacuum condition less than 13 Pa with different sintering program (figure 2.2) and sintering parameters by varying heating rate, sintering temperature (700 – 725 °C) and sintering pressure (30 – 60 MPa).

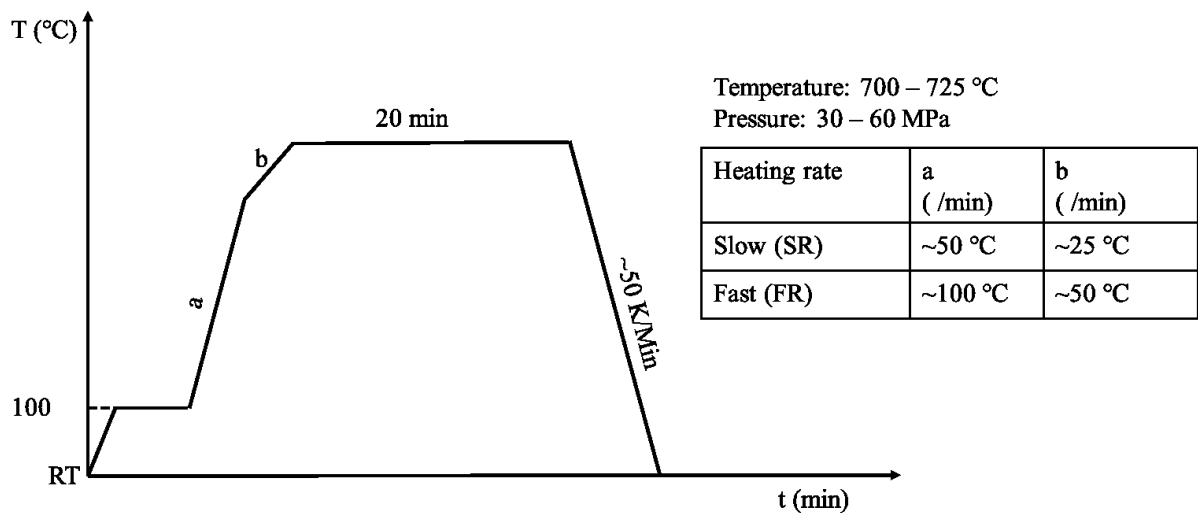


Figure 2.2 Sintering temperature profile program

2.2.4 Characterization

Cylindrical sintered samples were cut and then subjected to characterization including density and open porosity calculation, macro image and its image analysis, and SEM.

2.2.4.1 Density and Open Porosity

In order to calculate density and open porosity of porous samples, the dried mass difference before and after of a columnar shape samples immersed in an ultrasonic cleanser

machine filled by warm distilled water for 30 minutes was measured. Equation (2.1) and (2.2) were used to calculate samples density and open porosity. Samples' density was simply defined as the ratio between porous sample weight and its volume while porosity was calculated by dividing the volume of dissolved sodium chloride over sample's volume.

$$\text{Density } (\rho) = \frac{w_{\text{after dissolution}}}{v_{\text{sample}}} \quad 2.1$$

$$\text{Open Porosity } (OP) = \frac{\Delta w}{v_{\text{sample}} \times \rho_{\text{NaCl}}} \times 100\% \quad 2.2$$

2.2.4.2 Relative Density

The relative density of the samples is calculated by comparing the sintered product density at certain time of sintering time and theoretical density of Ti-6Al-4V/sodium chloride composite calculated by the rule of mixture (3.3 g/cm³ for composite containing 50 vol. % sodium chloride and 3.074 g/cm³ for composite containing 60 vol. % sodium chloride), as describe in equations below.

$$\text{Relative Density} = \frac{\rho_{\text{actual}}^{\text{Ti-6Al-4V/NaCl}}}{\rho_{\text{theoretical}}^{\text{Ti-6Al-4V/NaCl}}} \quad 2.3$$

$$\rho_{\text{theoretical}} = \% \text{ vol. Ti-6Al-4V} \times \rho_{\text{Ti-6Al-4V}} + \% \text{ vol. NaCl} \times \rho_{\text{NaCl}} \quad 2.4$$

$$\rho_{\text{actual}} = \frac{w}{v_t} \quad 2.5$$

$$v_t = \text{volume at } t \text{ sintering time} \quad 2.6$$

2.2.4.3 Image analysis

An original developed image analysis was performed by calculating each square pore area and pore wall thickness – the distance between pore - of samples' cross sectional macro image which is divided into several number of 2 mm x 2 mm squares as shown in figure 2.3.

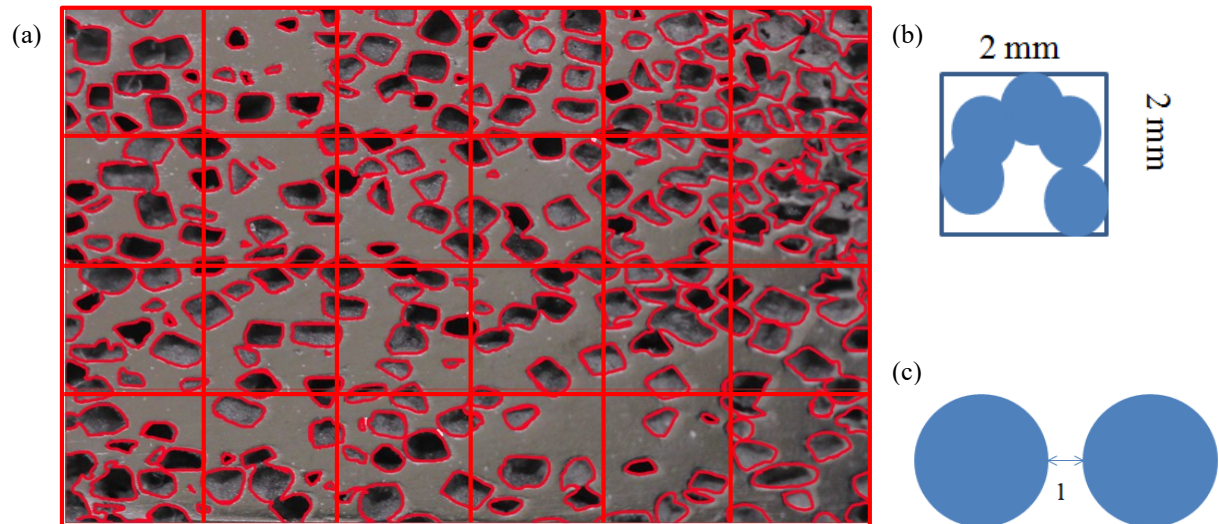


Figure 2.3 Schematic of image analysis include sliced macro image (a), pore area for each square (b), and pore wall thickness (c)

2.3 Results

2.3.1 Microstructure and densification of porous Ti-6Al-4V

The microstructure of sintered powder mixture of 50 vol. % Ti-6Al-4V: 50 vol. % sodium chloride size 600 – 425 μm after sodium chloride dissolution shown in figure 2.4. At low magnification, it is seen that the morphology of macro-pores mimics the cuboidal shape of sodium chloride as space holder. Rough surface of pore surface was built from the spherical shape of metal powder, pointed by white arrow. At high magnification, micro-porosity and necks between powders are clearly observed. Figure 2.5 shows the SEM images of 50 vol. % Ti-6Al-4V: 50 vol. % sodium chloride size 600 – 425 μm sintered with slow heating rate sintering program and varied sintering condition. It is clearly shown that micro-porosity is reduced as the sintering temperature and pressure increase. Sintering the powder mixture at 700 $^{\circ}\text{C}$, 30 MPa gives more micro-porosity compare to the other sintering conditions. This results on the micro-pore fraction consistent with the densification curves in figure 2.6 and 2.7 that increasing temperature and pressure increase the relative density of powder mixture which related with the reduction of micro-porosity.

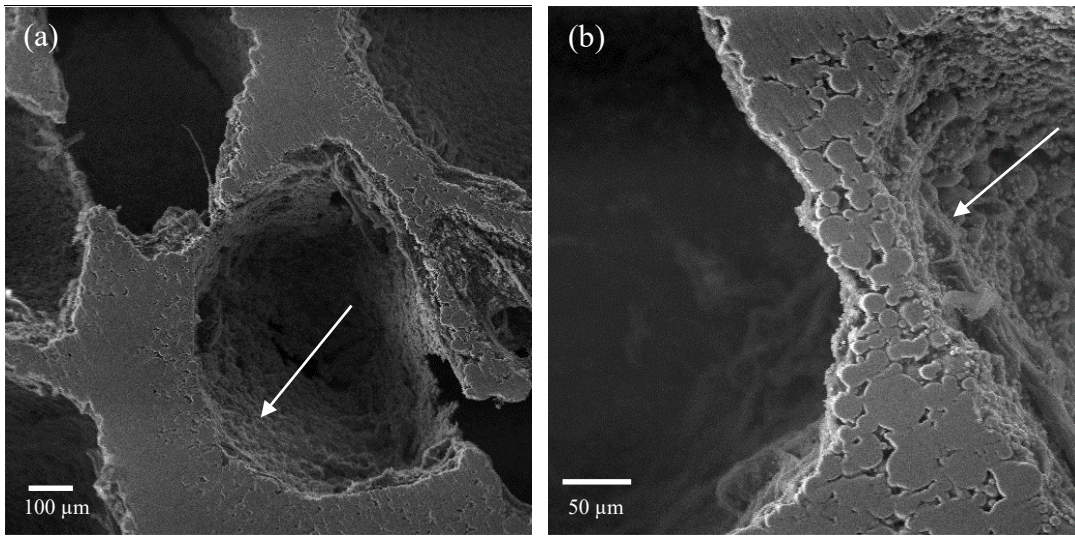


Figure 2.4 SEM image of 50 vol. % Ti-6Al-4V: 50 vol. % sodium chloride size 600 – 425 μm sintered at 700 $^{\circ}\text{C}$, 30 MPa for low magnification (a) and high low magnification (b)

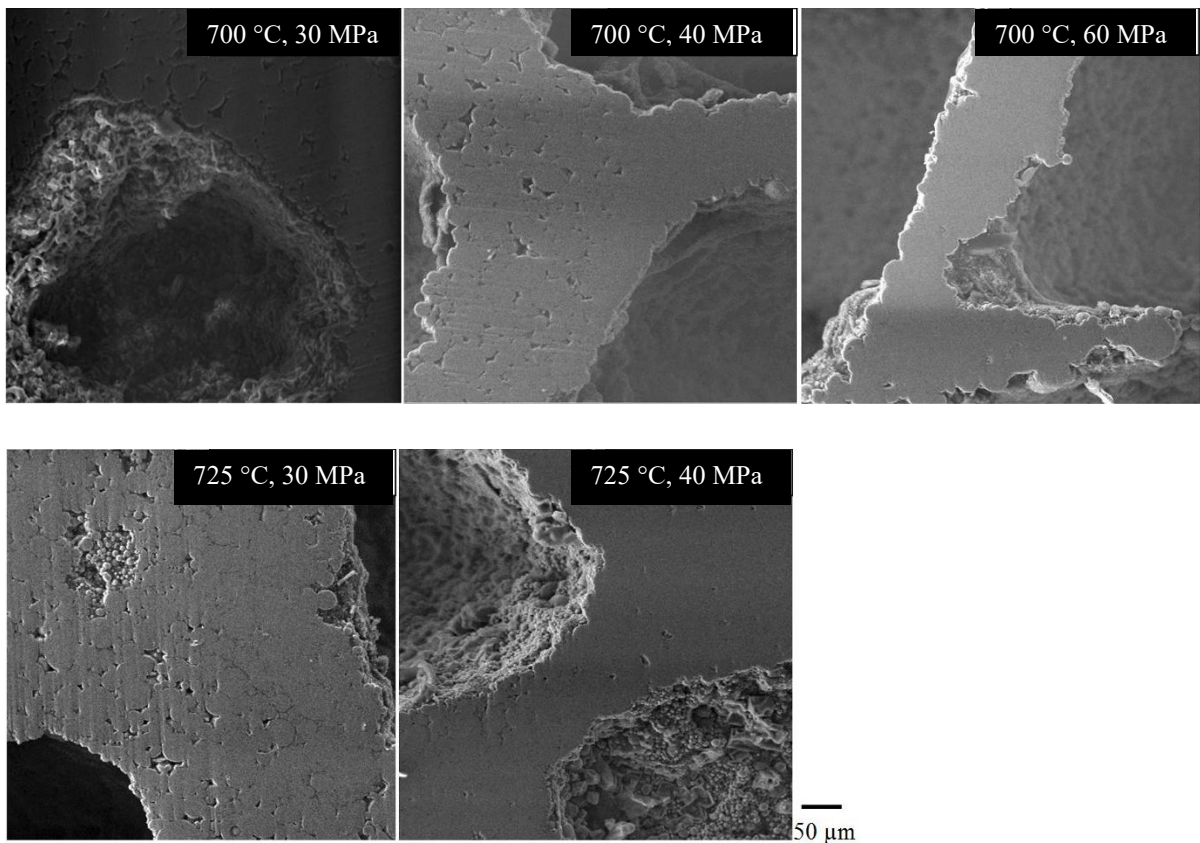


Figure 2.5 SEM image of 50 vol. % Ti-6Al-4V: 50 vol. % sodium chloride size 600 – 425 μm sintered at different sintering condition

At the initial process of the sintering, the powder mixture was expanded in the response of increasing of sintering temperature during constant pressure of 10 MPa. This was observed as the small decrease of relative density at the first four minutes of densification curves in figure 2.6 (black line). This process was not observed when sintering pressure was increased till 60 MPa while sintering at 30 MPa longer the process till the first nine and a half minutes of sintering process (fig. 2.6). This imply that the densification process was delayed as the decrease of sintering pressure. This result is in agreement with Ye *et al.* that relative density increase as sintering pressure increase [7].

Relative density then increase as the sintering time, temperature and pressure increase, reaching its sintering temperature of 700 °C and each designated pressure of 30, 40, and 60 MPa at the 17th minutes (fig. 2.6). Powder mixture then was sintered at designated temperature and time for 20 minutes. As shown in figure 2.6 increasing sintering pressure results higher relative density of powder mixture.

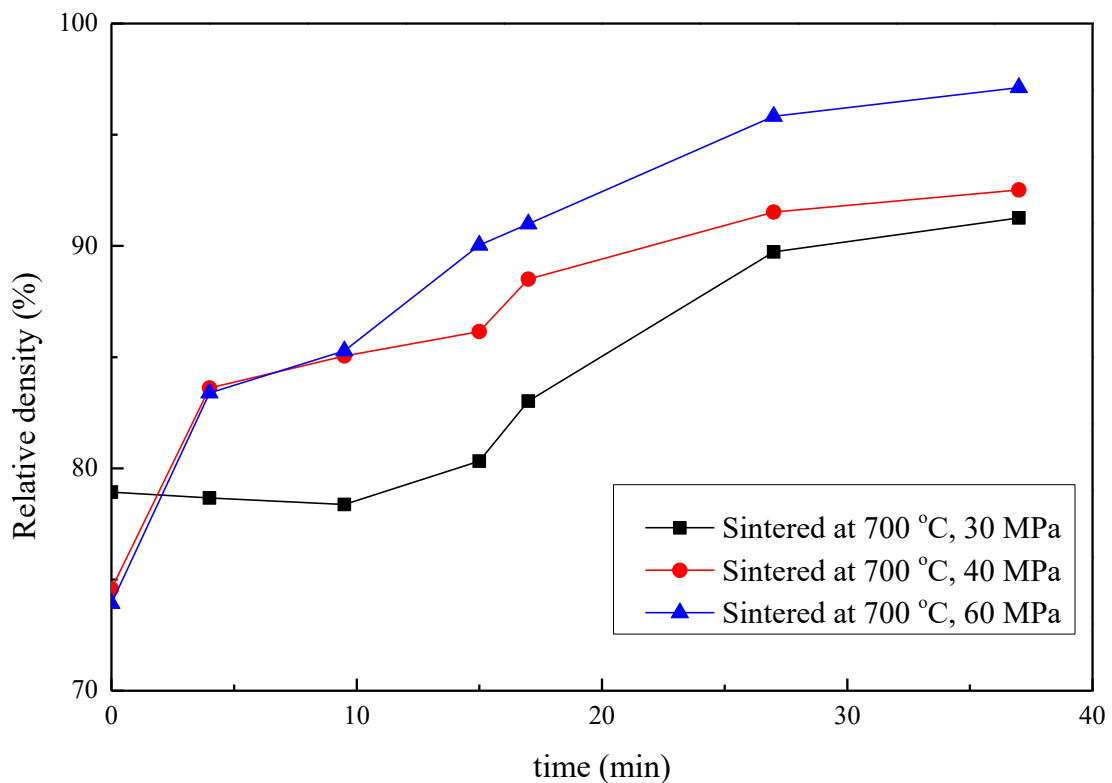


Figure 2.6 Densification curves of powder mixed contain 50 vol. % Ti-6Al-4V: 50 vol. % sodium chloride size 600 – 425 μm during sintering process at 700 °C temperature at different pressure

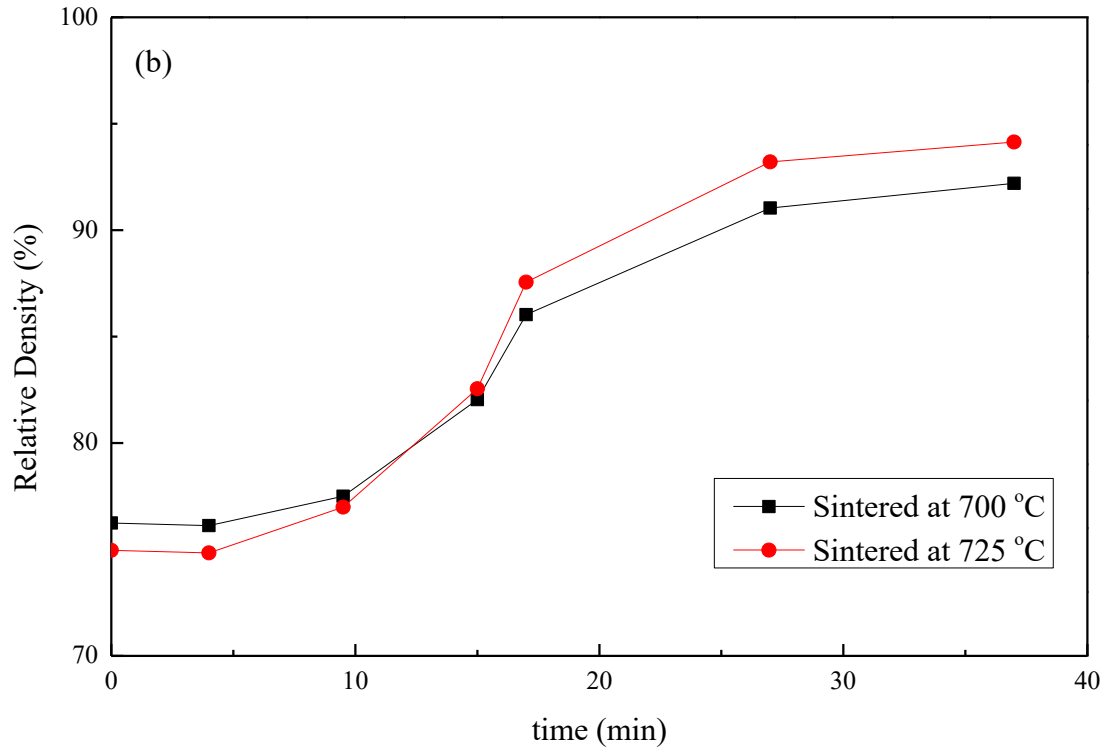
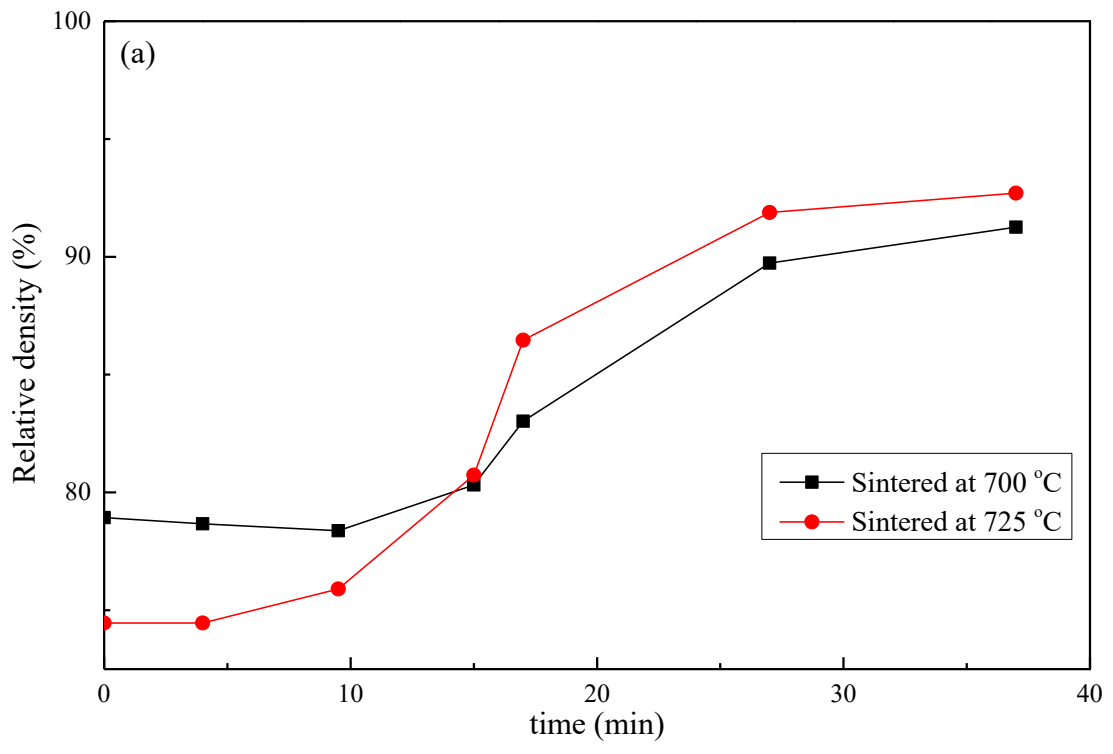


Figure 2.7 Densification curves of powder mixed contain 50 vol. % Ti-6Al-4V: 50 vol. % sodium chloride size 600 – 425 μm during sintering process at 30 MPa pressure (a), 40 MPa (b), and different temperature

The effect of sintering temperature to the increase of relative density during sintering process is shown in figure 2.7. The results is consistent with the samples microstructure in figure 2.5 in both applied pressure of 30 and 40 MPa, increasing sintering temperature will increase the relative density.

The microstructural change of samples sintered with different heating program of slow and high heating rate is shown in figure 2.8. There is no microstructural change both in low magnification and high magnification of samples sintered using slow and high heating rate especially in term of micro-porosity reduction. The effect of heating rate during SPS process is clearer observed in figure 2.9. Increasing the heating rate appears to change a little of relative density during sintering process. At the same sintering time, it is observed that at same sintering temperature and pressure, higher heating rate produces a little higher relative density. Comparing each composite relative density at the final sintering process, higher heating rate results a little lower relative density than samples sintered using slower heating rate. Munir *et al.* describe arguable effect of sintering rate during spark plasma sintering method [9]. Higher heating rate generates densification process, but several results from Shen *et al.*, Zhou *et al.* , and Chen *et al.* show independency of final relative density to heating rate [10] [11] [12]. In this case, since only small change of final relative density were observed, heating rate is considered to have no significant effect to micro-porosity reduction of the samples.

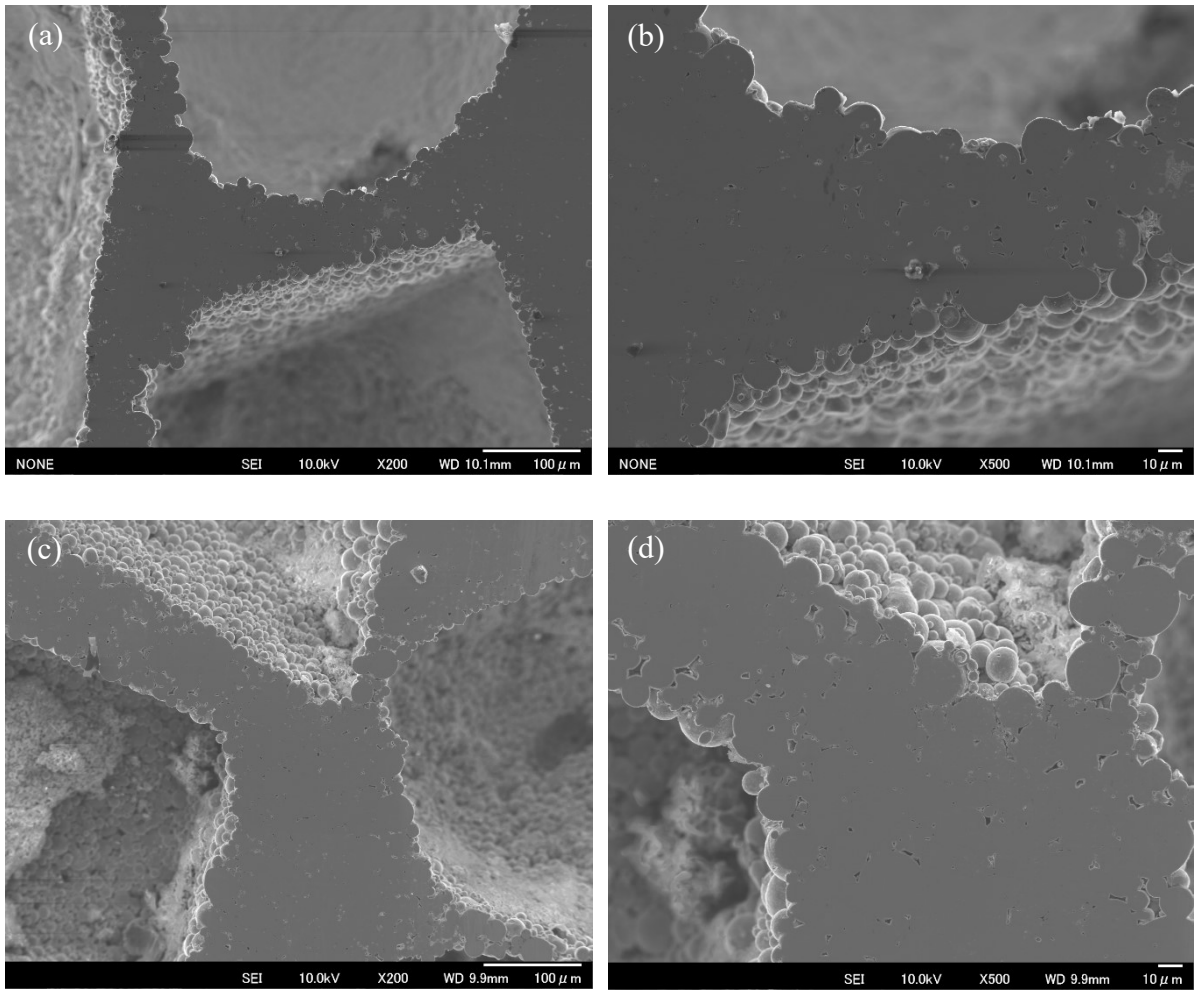


Figure 2.8 SEM image of 50 vol. % Ti-6Al-4V: 50 vol. % sodium chloride size 600 – 425 μm sintered at 700 °C, 40 MPa by high heating rate program at low magnification (a) and high magnification (b); slow heating rate program at low magnification (c) and high magnification (d)

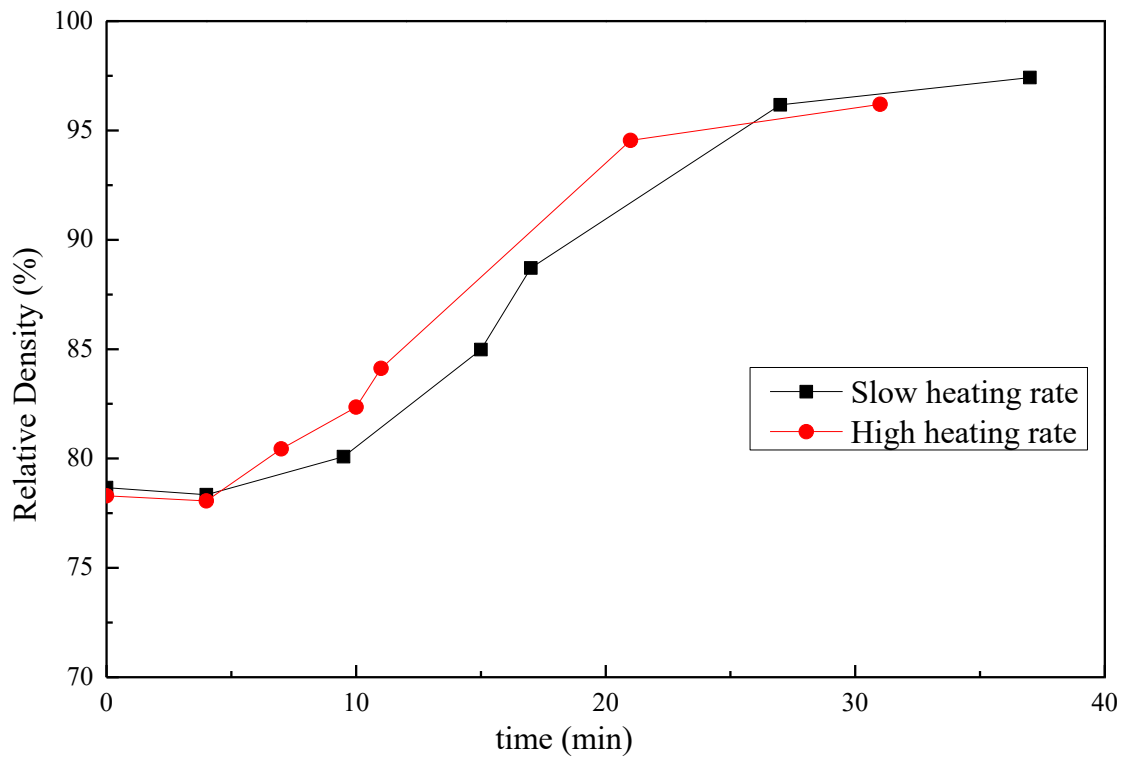


Figure 2.9 Densification curves of powder mixed contain 50 vol. % Ti-6Al-4V: 50 vol. % sodium chloride size 600 – 425 μm during sintering process at 700 $^{\circ}\text{C}$, 60 MPa with different sintering program

2.3.2 Space holder size and distribution in relation with porous product porosity and sinter-ability

The space holder distribution was investigated by the macro image of sintered product after sodium chloride removal in warm water. Figure 2.10 shows the macro image of each sintered powder mixtures with and without the addition of PCA. It is observed that the morphology of the pore mimics the cuboidal shape of sodium chloride, in accordance with the SEM results in section 2.3.1. It is also shown that the pore shape was slightly deformed along the direction of sintering pressure due to sodium chloride's low strength. Qualitatively, the addition of PCA improve the distribution of sodium chloride as space holder. Addition of 5 wt. % of stearic acid, 10 wt. % molten stearic acid and 10 wt. % ethanol during mixing process improve the distribution of the macro-pore which strongly related with the distribution of space holder. Porous sample structural segregation was observed in figure 2.10 (a) i.e. big dense area and isolated close pore.

Further analysis through quantitative analysis of each samples macro-image described in section 2.2 suggests the same results. Image analysis histogram of pore area in figure 2.11 shows the addition of process control agent results to narrower distribution of pore area which considered as homogeneous space holder distribution. The quantitative report of the image analysis in table 2.4 also implies the same results. Addition of process control agent decrease the difference between maximum value and minimum value of pore area – describe as $\Delta_{\max-\min}$ in table 2.4 – and standard deviation of pore area of each square, indicating the improvement of space holder distribution.

The relation between additions PCA to the open porosity produced after sodium chloride removal is describe in figure 2.12. Comparing the image analysis results and open porosity calculation results, it is known the improvement of space holder distribution results the increase of open porosity number suggest that homogenous pore structure will result more interconnectivity between pores. The significance of the increase is analyzed by one step ANOVA. The result shows that the probability of the null hypothesis of no significance of PCA to open porosity number is 0.0004, smaller than the decided significance criteria of null hypothesis of 0.05. The relation between density and pore distribution is not clearly described since the density is simply calculated by equation 2.1 which is include both macro-, micro-porosity and isolated pore filled by sodium chloride.

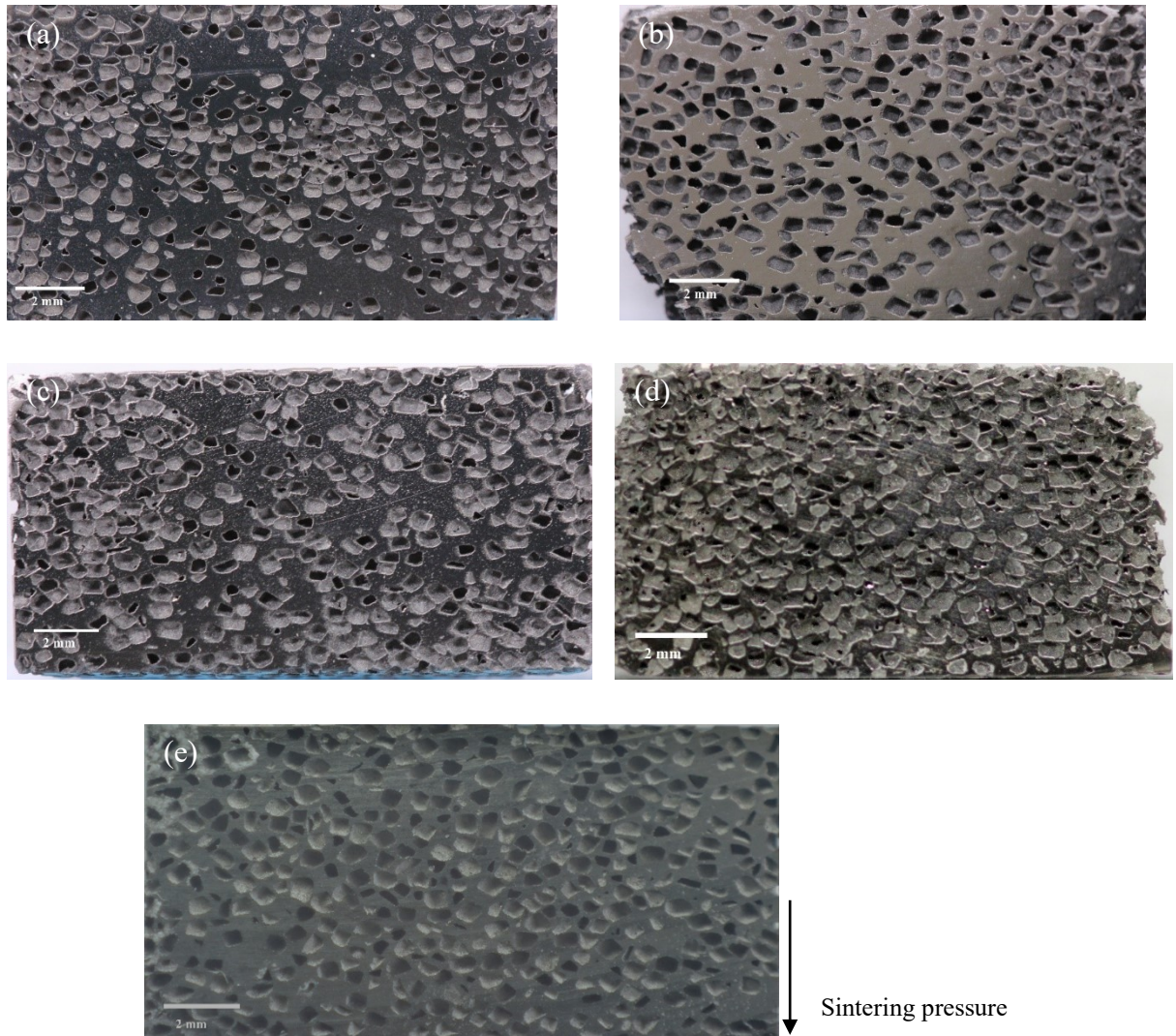


Figure 2.10 Macro image of porous samples mixed without addition of PCA (a), 1 wt. % (b), 5 wt. % (c), 10 wt. % melted stearic acid (SA) (d), and 10 wt. % ethanol as process control agent (PCA)

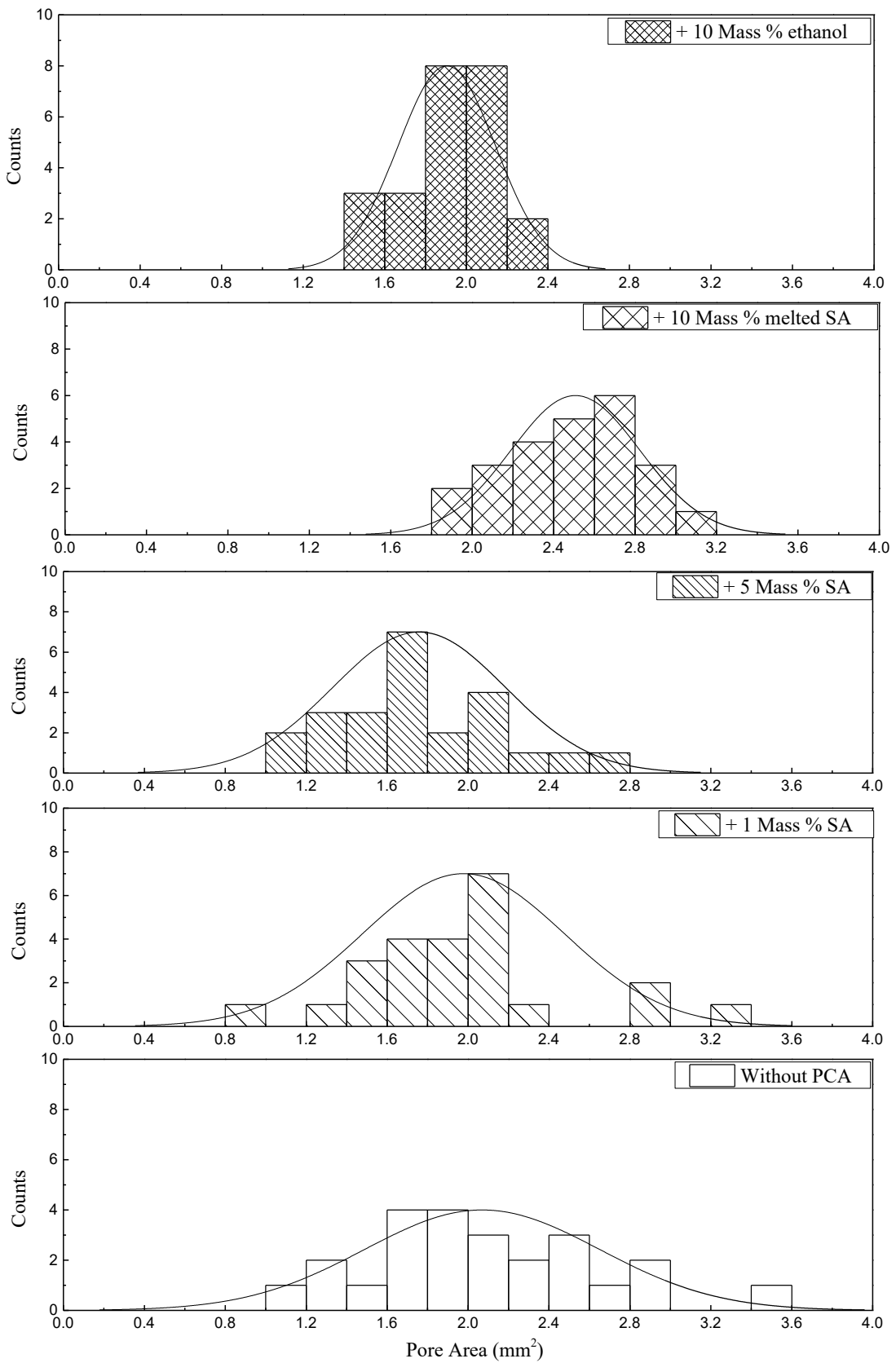


Figure 2.11 Histogram of image analysis results of sintered powder mixtures with the addition of different process control agent

Table 2.3 Results of quantitative image analysis of pore area for sintered powder mixtures with addition of different PCA

PCA	Mean (mm)	Std. deviation	Max. pore area (mm ²)	Min. pore area (mm ²)	Δ max – min (mm ²)	laverage (mm)
no	2.07	0.58	3.55	1.05	2.5	0.47±0.45
1 wt. % Stearic Acid	1.98	0.49	3.31	0.97	2.34	0.41±0.35
5 wt. % Stearic Acid	1.76	0.43	2.69	1.04	1.65	0.43±0.37
10 wt. % melted Stearic Acid	2.5	0.32	3.05	1.83	1.22	0.40±0.76
10 wt. % Ethanol	1.9	0.24	2.21	1.4	0.81	0.43±0.34

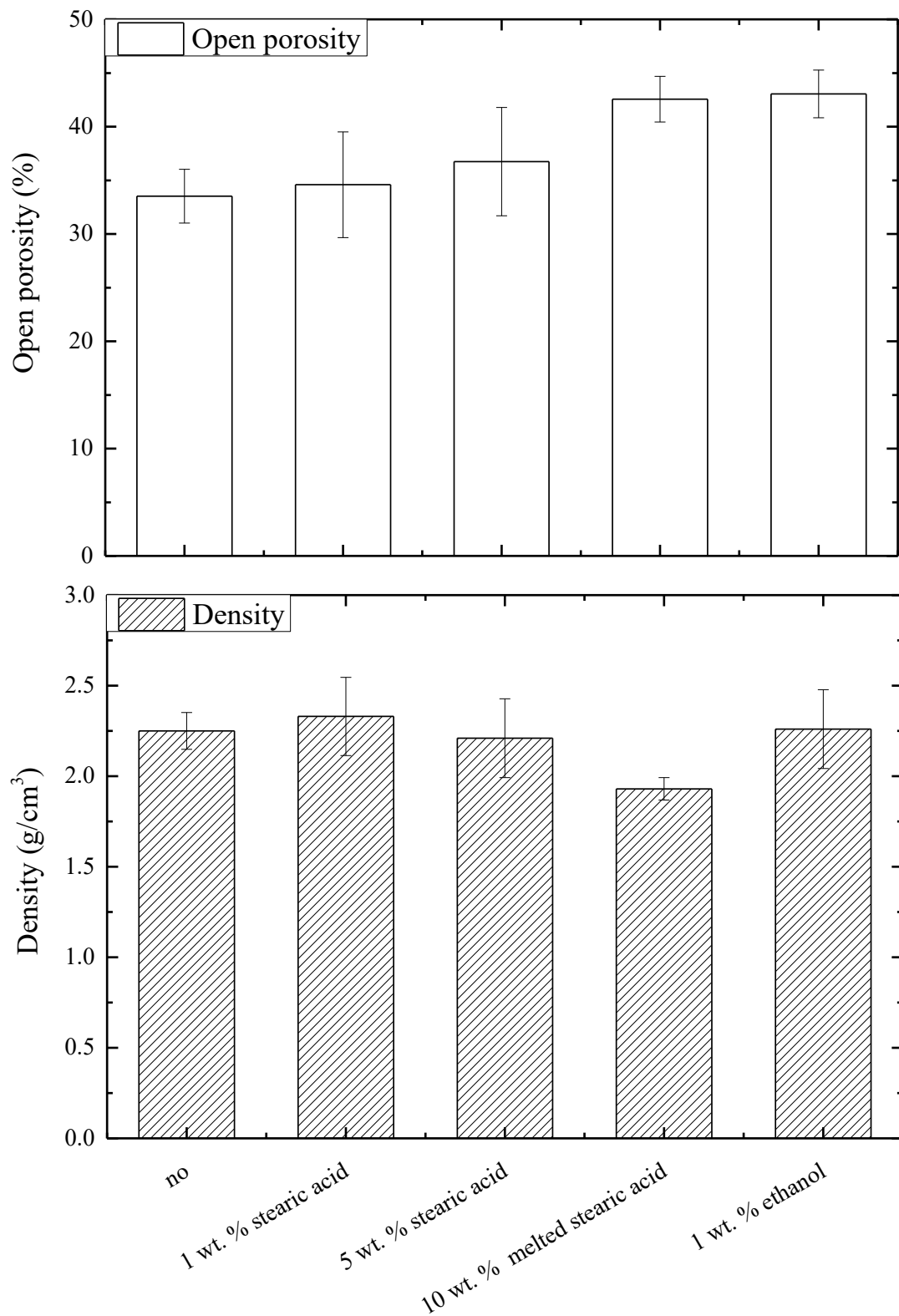


Figure 2.12 Density and open porosity change of sintered powder mixtures with addition of different PCA

Figure 2.13 shows the densification curves of powder mixture containing 40 vol. % Ti-6Al-4V: 60 vol. % with varied size of sodium chloride sintered at 700 °C, 60 MPa which mixed with addition of ethanol as PCA. At the early process of sintering, powder mixture containing smaller size sodium chloride gives a steep slope of relative density's increase compare to the other powder mixtures. This happen due to the compact-ability of powder is increase as the decrease of its size. Additionally, the shape of small size sodium chloride (less than 425 μm) used in this research is not cuboidal but irregular. The increase of densification rate at the early stage of sintering is in accordance with Bouvard *et al.* result that the densification rate increases with decreasing size ratio of the two powders pack together [13] [14]. Arzt et al. [15] is also modeled that at the initial stage of sintering the relative density is inversely proportional to powder size.

Although the result shows reduction of sodium chloride size generate the densification at the early process, the final relative density of sintered samples is not significantly changed. In the results of titanium foams produced by sodium chloride replication, Ye *et al.* shows there is no significant different on the final relative density of titanium and different size sodium chloride blend (between 50 – 500 μm) which is sintered at 780 °C using uniaxial hot press machine [7]. In the densification model built by Schuh et al. [16] and Arzt et al. [15] show that there is no relation between space holder size and final relative density.

The influence of space holder size to open porosity produced is also describe in figure 2.14. Varying sodium chloride powder gives no significant change to the open porosity produced, implying that open porosity produces is independent to space holder size. The ANOVA results also suggest the same relation of significance of null hypothesis. The probability of null hypothesis is 0.31, bigger than the decided significance criteria of null hypothesis of 0.05.

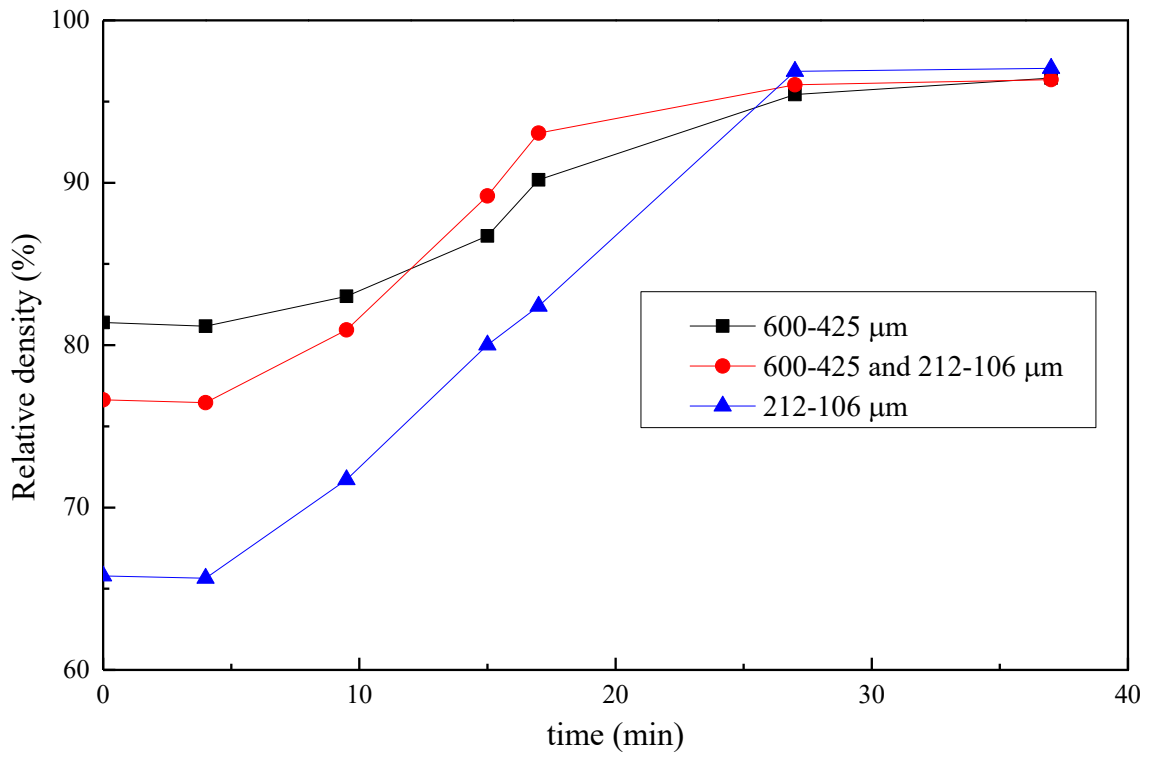


Figure 2.13 Densification curves of powder mixed contain 40 vol. % Ti-6Al-4V: 60 vol. % varied size of sodium chloride sintered at 700 °C, 60 MPa with addition of ethanol as PCA

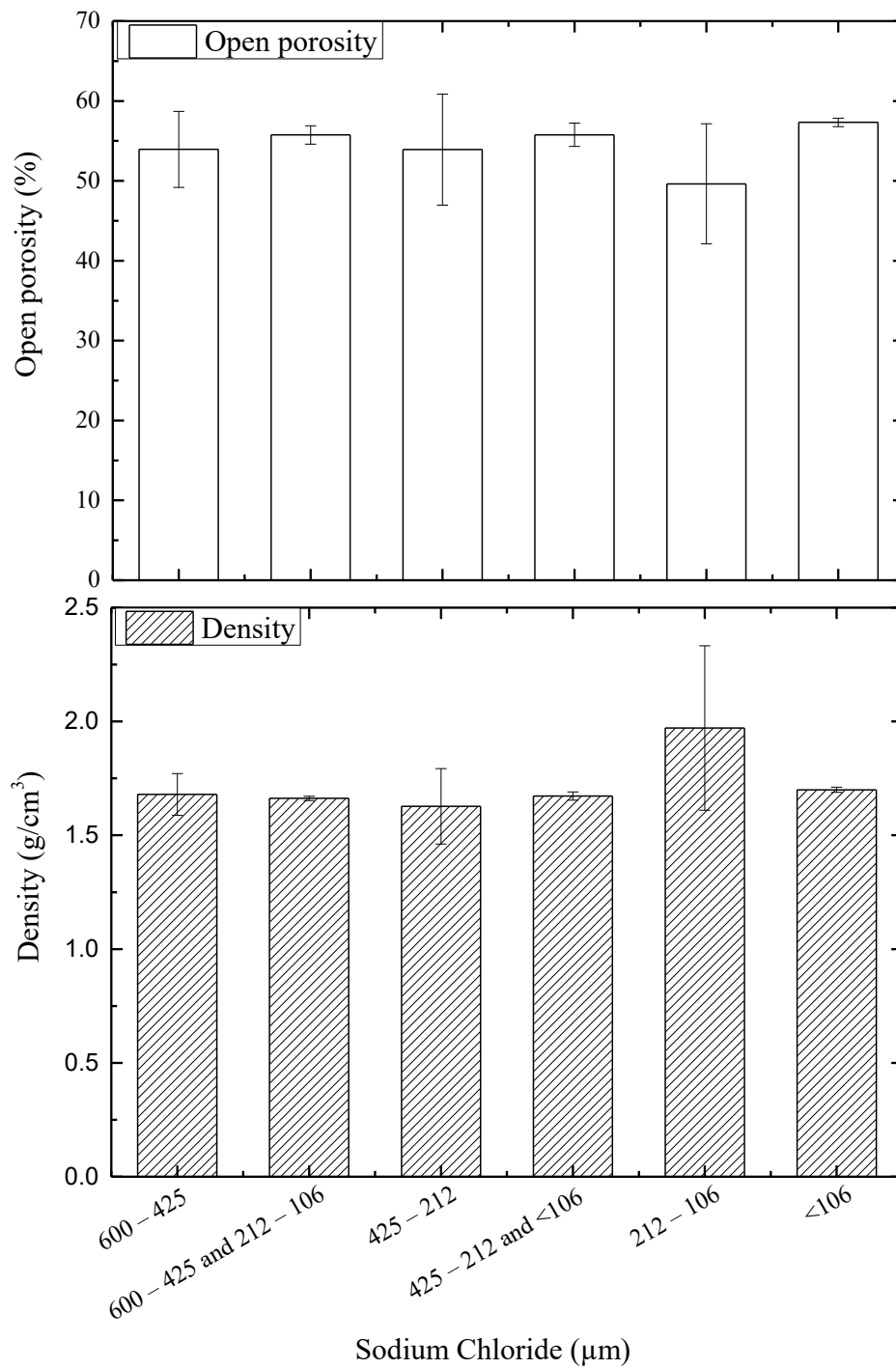


Figure 2.14 Open porosity change of sintered powder mixtures with different space holder size

2.4 Discussion

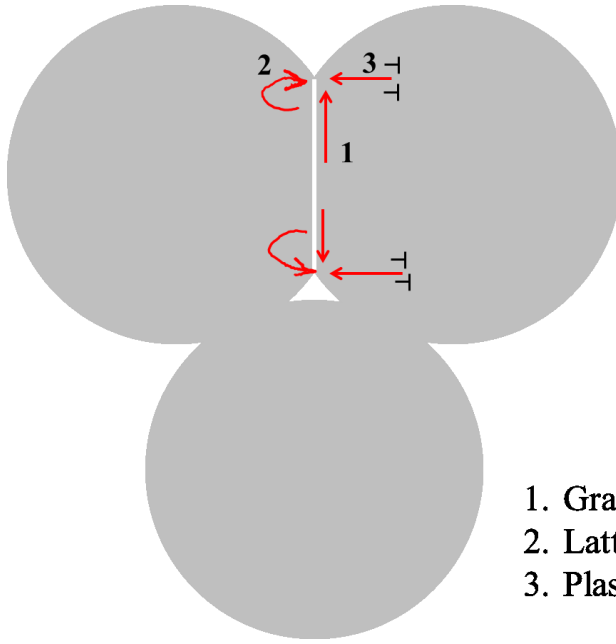
2.4.1 Influence of sintering parameter to the formation of macro- and micro-porosity

In this research, sodium chloride was used as the space holder. The melting point of space holder is around 803°C. Thus, this is the upper limit of sintering temperature. In this research work and also similarly with Quan *et al.* work [17], increasing sintering temperature to 750 °C will melt sodium chloride that it lost its function as space holder. Due to its soft characteristic (relatively low hardness) compare to the metal powder, macro-porosity produced is in the shape of slightly deformed sodium chloride. This kind of shape may affects the isotropy of porous properties especially its mechanical properties as reported by Tuncer *et al.* [18]. Since in this research there is no reaction between space holder and metal powder, it is rather difficult to relate the influence of heating rate to the formation of macro-porosity.

The formation of micro-porosity is strongly related with the densification process and densification rate. Increasing sintering temperature and pressure increase number of relative density of composite Ti-6Al-4V/NaCl. Densification process for sintering polycrystalline materials such as metal is usually occur through diffusion. The mechanism is usually classified through several mechanism as follow [19] [20] [21] :

- Surface diffusion
- Vapor Transport
- Surface lattice diffusion
- Grain boundary diffusion
- Grain boundary lattice diffusion
- Plastic deformation or dislocation lattice diffusion

From the mechanisms above, only grain boundary diffusion, grain boundary lattice diffusion, and dislocation lattice diffusion give the densifying effect. The mechanism micro-porosity reduction in relation with temperature is described in figure 2.15.



1. Grain Boundary diffusion
2. Lattice diffusion from the grain boundary
3. Plastic flow

Figure 2. 15 Schematic mechanism of densification process as well as micro-porosity reduction [22]

A model build by Coble [23] shows the relation between temperature and densification rate during sintering of polycrystalline materials as describe below [21]:

Lattice diffusion:
$$\frac{1}{\rho} \frac{d\rho}{dt} \approx \frac{AD_l \gamma_{sv} \Omega}{\rho G^3 kT} \quad 2.7$$

Grain boundary diffusion:
$$\frac{1}{\rho} \frac{d\rho}{dt} \approx \frac{4}{3} \left(\frac{D_{gb} \gamma_{sv} \Omega \delta_{gb}}{G^4 kT \rho (1-\rho)^{1/2}} \right) \quad 2.8$$

where ρ is the density, A is a constant, G is the grain size, D_l and D_{gb} is diffusion coefficients for lattice and grain boundary diffusion, δ_{gb} is thickness of grain boundary diffusion, γ_{sv} specific surface energy, Ω is atomic volume, k is Boltzmann constant, and T is temperature. As stated in his paper Ye *et al.* consider that the densification of Ti/NaCl composite is control mostly by the densification of Ti powders rather than sodium chloride powders [7].

In general the relation between temperature and densification rate is describe in equation below [9]:

$$\frac{d\rho}{(1-\rho)dt} = B \left(g \frac{\gamma}{x} + P \right) \quad 2.9$$

Where ρ is the density, B is a term that includes diffusion coefficient and temperature, g is a geometric constant, γ is the surface energy, x is the parameter that represent a size scale.

In addition, applying higher pressure not only will enhance plastic flow (fig. 2.15), it will also increase the number of inter-particles contact which generates densification process by increasing the driving force of sintering [24]. Furthermore, the influence of pressure to micro-porosity reduction is described in figure 2.16.

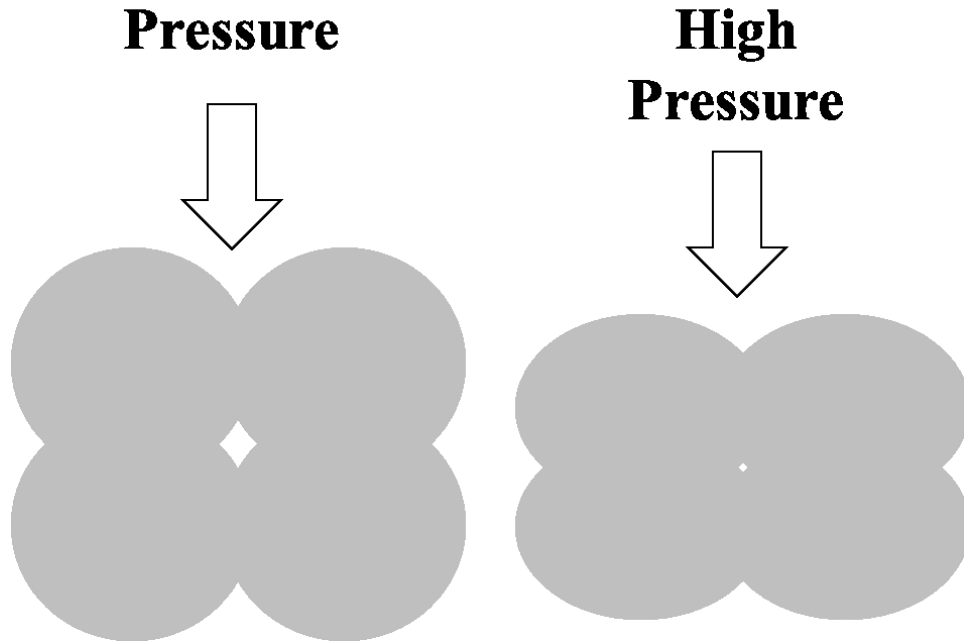


Figure 2. 16 Mechanism of reduction of micro-porosity at higher sintering pressure

Although there is no significant difference of final relative density produced by the varying space holder size. At the early stage of sintering process the densification rate of composite contained Ti-6Al-4V/NaCl increase as the decrease of space holder size. This is explained by Artz *et al.* that at the initial stage of sintering densification rate can be modelled as equation below [15]:

$$D = 3(D^2\dot{D}_0)^{1/3}\dot{\gamma}/R \quad 2.10$$

where \dot{D} is the densification rate, D is the relative density, D_0 is the initial relative density, $\dot{\gamma}$ is the initial particle radius. Decreasing space holder size is also generating sintering process by increasing the number of soft-hard contact particles [13] [14]. During pressure mode sintering process one of main densification mechanism is happened due to inter-particles plastic deformation [14]. Smaller size of space holder provides more soft-hard inter-particles contact that increase the compact ability of powder mixtures which generate the densification process [13].

2.4.2 Influence of space holder distribution to the formation of macro-porosity

Space holder distribution is connected to the macro-pore distribution. Without addition of process control agent, composite contained 50 vol. % of sodium chloride only produce around 30 % of open porosity. The space holder method is known to be a good alternative to produce porous metal for its simplicity and accuracy to control pore fraction, shape and connectivity [7], but in practical it only gives accurate control of pore shape. High weight ratio between metal powder and space holder that used in this research is the main reason of the ineffectiveness of sodium chloride utilization as space holder. Due to this high weight ratio, metal powder will bear bigger centrifugal force during mixing process. Thus, powder mixtures is not properly mixed. Addition of process control agent (PCA) improve the distribution of powder mixtures by providing a bond between powders during the mixing process, the schematic figure of powder mixing with and without PCA is shown in figure 2.17.

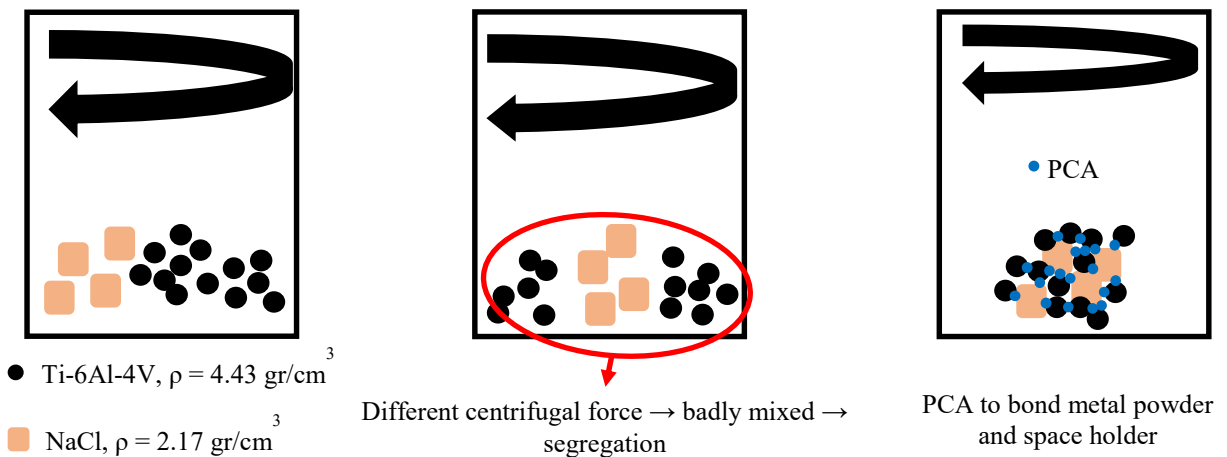


Figure 2. 17 Schematic of PCA role during mixing process

Addition of PCA results more interconnectivity of macro-pore that increase the open porosity number of samples. Addition of ethanol and melted stearic acid gives the highest number of open porosity, while the addition of 1 wt. % of stearic acid only give no significant increase of open porosity number. In such small amount of stearic acid – most likely exist in semi-solid condition during mixing due to its low melting temperature – is not having an ability to provide enough bond between the powders [25].

2.5 Conclusions

In this chapter the influence of sintering parameters (heating rate, temperature and pressure), space holder size and distribution to the formation of both micro- and macro-porosity is investigated. In summary the influence is define below:

- (1) Sintering temperature and pressure are the main parameter to control micro-porosity. Increasing sintering pressure is more effective to reduce micro-porosity in the samples. Relative density produced is independent on heating rate.
- (2) Although changing the densification rate during the initial process of sintering, varying space holder size has no significant change of final relative density.
- (3) Open porosity of sample increase as the more homogenous space holder distribution produced, suggests that distribution of space holder is main aspect which control the macro-pore interconnectivity.
- (4) There is no significant increase of open porosity number by varying the space holder size and shape, implies that the interconnectivity between macro-pore is independent on space holder size and shape.
- (5) The main parameter to control in this process is space holder distribution and sintering pressure and sintering temperature.
- (6) The most effective condition to produce less micro-porosity and more interconnected macro-porosity is the utilization of any kind of space holder size with the addition of 10 wt. % ethanol as PCA and sintering at 700 °C, 60 MPa.

2.6 References

- [1] C. Körner and R. F. Singer, "Processing of Metal Foams - Challenges and Opportunities," *Advanced Engineering Materials*, vol. 2, no. 4, pp. 159-165, 2000.
- [2] D. C. Dunand, "Processing of Titanium Foams," *Advanced Engineering Materials*, vol. 6, no. 6, pp. 369-376, 2004.
- [3] J. Banhart, "Manufacture, characterisation and application of cellular metals and metal foams," *Progress in Materials Science*, vol. 46, pp. 559-632, 2001.
- [4] V. Gergely, D. Curran and T. Clyne, "The FOAMCARP process: foaming of aluminium MMCs by the chalk-aluminium reaction in precursors," *Composites Science and Technology*, vol. 63, pp. 2301-2310, 2003.
- [5] G. Engin, B. Aydemir and H. Ö. Gülsoy, "Injection molding of micro-porous titanium alloy with space holder technique," *Rare Metals*, vol. 30, no. 6, pp. 565-571, 2011.
- [6] T. Aydoğmuş and Ş. Bor, "Processing of porous TiNi alloys using magnesium as space holder," *Journal of Alloys and Compounds*, Vols. 705-710, p. 478, 2009.
- [7] B. Ye and D. C. Dunand, "Titanium foams produced by solid-state replication of NaCl powders," *Materials Science and Engineering A*, vol. 528, pp. 691-697, 2010.
- [8] F. Zhang, E. Otterstein and E. Burkel, "Spark Plasma Sintering, Microstructures, and Mechanical," *Advanced Engineering Materials*, vol. 12, no. 9, pp. 863-872, 2010.
- [9] Z. Munir, U. Anselmi-Tiburini and M. Ohyanagi, "The effect of electrical field and pressure on the synthesis and consolidation of materials: A review of the spark plasma sintering method," *Journal of Materials Science*, vol. 41, pp. 763-777, 2006.
- [10] Z. Shen, M. Johnsson, Z. Zhao and M. Nygren, "Spark Plasma Sintering of Alumina," *Journal of the american ceramics society*, vol. 85, no. 8, pp. 1921-1927, 2002.
- [11] Y. Zhou, K. Hirao, Y. Yamauchi and S. Kanzaki, "Effects of heating rate and particle size on pulse electric current sintering of alumina," *Scripta Materialia*, vol. 48, no. 12, pp. 1631-1636, 2003.

- [12] D. J. Chen and M. J. Mayo, "Rapid Rate Sintering of Nanocrystalline ZrO₂-3 mol% Y₂O₃," *Journal of the American Ceramic Society*, vol. 79, no. 4, pp. 906-912, 2005.
- [13] N. Tuncer, G. Arslan, E. Maire and S. Luc, "Investigation of Spacer Size Effect on Architecture and Mechanical Properties of Porous Titanium," *Materials Science and Engineering A*, vol. 530, pp. 633-642, 2011.
- [14] D. Bouvard, "Densification behaviour of mixtures of hard and soft powders under pressure," *Powder Technology*, vol. 111, pp. 231-239, 2000.
- [15] E. Arzt, M. F. Ashby and K. E. Easterling, "Practical Application of Hot-Isostatic Pressing Diagrams : Four Case Studies," *Metallurgical Transaction A*, vol. 14, pp. 211-221, 1983.
- [16] C. Schuh, P. Noel and D. C. Dunand, "Enhanced Densification of Metal Powders by Transformation-Mismatch Plasticity," *Acta Materialia*, vol. 48, pp. 1639-1653, 2000.
- [17] Y. Quan, F. Zhang, H. Rebl, B. Nebe, O. Keßler and E. Burkel, "Ti6Al4V foams fabricated by spark plasma sintering with post-heat treatment," *Materials Science and Engineering A*, vol. 565, pp. 118-125, 2013.
- [18] N. Tuncer, G. Arslan, E. Maire and L. Salvo, "Influence of cell aspect ratio on architecture and compressive strength of titanium foams," *Materials Science and Engineering A*, vol. 528, pp. 7368-7374, 2011.
- [19] D. Richerson, *Modern Ceramic Engineering: Properties, Processing and Use in Design*, New York: Marcel Dekker, 1992.
- [20] M. Rahaman, *Ceramic Processing and Sintering*, New York: Marcel Dekker, 2003.
- [21] J. N. Calata, *Densification Behavior of Ceramic and Crystallizable Glass Materials Constrained on a Rigid Substrate*, Blackburg, Virginia: Virginia Polytechnic Institute and State University, 2005.
- [22] M. N. Rahaman, in *Ceramic Processing and Sintering*, New York, Marcel Dekker, Inc., 2003, p. 472.

- [23] R. Coble, "Sintering of crystalline solids I: Intermediate and final state diffusion models," *Journal of applied physics*, vol. 32, pp. 787-792, 1961.
- [24] S. B. Z. Esen, "Characterization of Ti-6Al-4V alloy foams synthesized by space holder technique," *Materials Science Engineering A*, vol. 528, pp. 3200-3209, 2011.
- [25] Y. S. F. Lantang, E. Kobayashi, H. Tezuka and T. Sato, "Effect of macro- and micro-porosity on mechanical properties of a Porous Ti-6Al-4V alloy fabricated using solid-state space-holder method," *Materials transaction*, vol. 55, pp. 1428-1433, 2014.

Chapter 3 Effect of Macro- and Micro-porosity on Mechanical Properties of a Porous Ti-6Al-4V

3.1 Introduction

The mechanical properties of porous materials is strongly affected by its porosity. Gibson-Ashby modeled [1] the relation between mechanical properties of porous materials, describe in chapter 1. As mentioned before, the production of porous metals through solid-state method or powder metallurgy route will produce two kinds of porosity namely macro-porosity and micro-porosity. In chapter 2, it was discussed that the production of micro-porosity is related with densification process during sintering which affected by sintering parameter – temperature, applied pressure, heating rate – while macro-porosity is obviously related with the space holder used. Thus, the mechanical properties of porous samples is also effected with the factors mentioned above.

Zeng *et al.* result shows the influence of pore shape to the mechanical properties of porous PZT 95/5 ceramics. The result shows that irregular pore shape lowered the mechanical properties of PZT 95/5 ceramics [2]. In addition, Bin *et al.* in their work of open cell aluminum shows the independence of compression strength to pore size [3]. In this chapter, the influence of macro-porosity and micro-porosity to the mechanical properties of porous Ti-6Al-4V fabricated by solid-state space holder method will be discussed.

3.2 Experimental Procedures

All porous samples obtained in chapter 2 shown in table 3.1 then mechanically tested by compression test. Compression test was performed in order to acquire the mechanical properties of columnar shape (fig. 3.1) porous samples using a universal testing machine, Autograph AG-IC, Shimadzu with 0.2 mm/min of cross head movement parallel to sintering pressure direction. Strain was measured by two strain gages mounted in parallel circuit system as shown in figure 3.2.

Table 3. 1 Summary of samples sintering condition and mixing process for compression test

Sintering Program	%vol. NaCl	Sintering parameter (T/°C, P/MPa)	NaCl Size (µm)	Process Control Agent (PCA)	Mixing parameter (ball mill, rotating speed, time)	
Slow heating rate (SR)	50	700, 30	600 – 425	No	No ball, 100 rpm, 1 h	
				1 % wt. SA	1:1 Zr-ball, 100 rpm, 1h	
				5 % wt. SA	1:1 Zr-ball, 100 rpm, 1h	
				10 % wt. ethanol	No ball, 100 rpm, 1h	
		700, 40	600 – 425	No	No ball, 100 rpm, 1 h	
				10 % wt. melted SA	hand mix	
		700, 60	600 – 425	5 % wt. SA	1:1 Zr-ball, 100 rpm, 1h	
				10 % wt. ethanol	No ball, 100 rpm, 1h	
		725, 30	600 – 425	No	No ball, 100 rpm, 1 h	
		725, 40	600 – 425	No	No ball, 100 rpm, 1 h	
		60	700, 60	600 – 425	10 % wt. ethanol	No ball, 100 rpm, 1h
				600 – 425 and 212 – 106 (with weight ratio 1:1)		
212 - 106						
Fast heating rate (FR)	50	700, 60	600 – 425	10 % wt. ethanol	No ball, 100 rpm, 1h	
			600 – 425 and 212 – 106 (with weight ratio 1:1)			
	60	700, 60	600 - 425	10 % wt. ethanol	No ball, 100 rpm, 1h	
			425 - 212			
			425 – 212 and less than 106 (with weight ratio 1:1)			
		Less than 106				

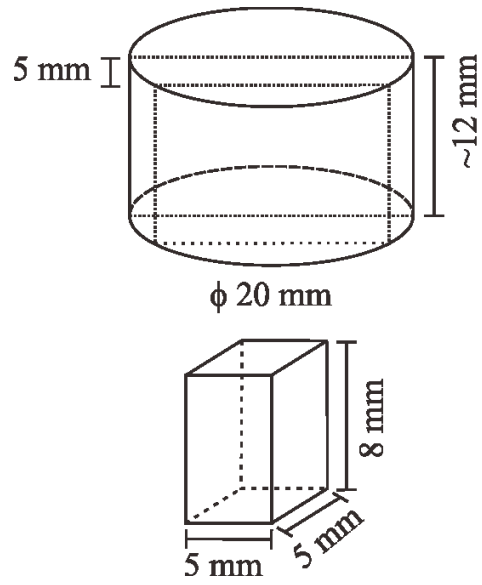


Figure 3. 1 Schematic of compression test sample dimension

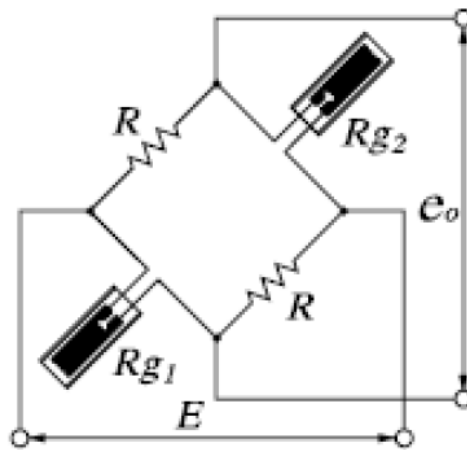


Figure 3. 2 Circuit diagram of two parallel strain gages method

3.3 Results

3.3.1 Influence of sintering parameter to mechanical properties

Table 3.2 shows the is the compression test results of powder mixture contained 50 vol. % 600 – 425 μm size sodium chloride sintered at different sintering temperature and pressure. From chapter 2, it is understood that relative density is strongly related with the micro-porosity existed in the sample. When samples sintered at different sintering pressure of 30 MPa (figure 3.3 (a)), the increase of sintering temperature results a little increase of sample's relative density and mechanical properties, i.e. compression strength and Young's modulus of the samples, but the same relation is not observed at higher sintering temperature of 40 MPa (figure 3.3 (b)). At such pressure increasing sintering temperature slightly decrease the Young's modulus of the samples. This happened due to the samples' open porosity sintered at 700 °C is slightly smaller than samples sintered at 725 °C (table 3.2). Figure 3.3 (b) also shows that at same sintering pressure and temperature of 700 °C, 40 MPa, both Young's modulus and compression strength of the samples decrease even though the relative density of samples increase. This result implies that both Young's modulus and compression strength of the samples are decided by samples' open porosity rather than relative density.

Figure 3.4 shows the influence of pressure to the mechanical properties of powder mixture contained 50 vol. % 600 – 425 size sodium chloride sintered at different sintering pressure and temperature. Additionally, the powder mixture mixed with 10 wt. % of molten stearic acid and 5 wt. % of stearic acid sintered respectively at 700 °C, 40 MPa and 700 °C, 60 MPa. The results also show that Young's modulus and compression strength of samples are varied independently on relative density. At same sintering temperature of 725 °C (fig. 3.4(b)), increasing sintering pressure, as well as increasing samples' relative density, slightly increase the strength of the samples but decrease its Young's modulus. At 700 °C, the increase of sintering pressure results to a slight increment of Young's modulus while at 725 °C the increase of sintering pressure decrease samples' Young's modulus. Comparing the open porosity number of the samples (table 3.2), it is shown that at sintering temperature 725 °C, samples sintered at 30 MPa have slightly higher open porosity number than samples sintered at 40 MPa. This tendency is also shown for samples sintered at the same sintering pressure and different sintering temperature (fig. 3.3 (b)). These results suggest that besides open porosity number, strength of the samples also depend on another factor will be discussed later.

Table 3.3 shows the compression test results of powder mixture contained 50 vol. % and 60 vol. % 600 – 425 μm size sodium chloride sintered at different sintering program. The influence of heating rate to the mechanical properties is shown in figure 3.5. Increasing the heating rate which decrease the samples' relative density also only gives small improvement of samples strength while the relation between samples' Young's modulus and heating rate is not clearly shown. The results change in the same manner in samples which sintered at different sintering pressure and temperature. Figure 3.5 (a) shows increasing heating rate result small increment of samples' Young's modulus while figure 3.5 (b) shows inversely influence. The results also suggests that the mechanical properties of the samples are decided by samples' open porosity rather than relative density.

3.3.2 Influence of space holder size and distribution to mechanical properties

Mechanical properties of powder mixture contained 60 vol. % of different size of sodium chloride mixed with the addition of 10 wt. % ethanol then sintered at same sintering temperature and pressure of 700 °C, 60 MPa but different heating rate, i.e. slow heating rate and high heating rate is summarized in figure 3.6. It is necessary to be noted as mentioned in chapter 2 that sodium chloride used for the size under 425 μm was irregular-shape crunched powder. The macro image of samples is shown in figure 3.7 and 3.8. The mechanical properties, both Young's modulus and strength of porous samples decrease as the decrease of spacer size due to the spacer shape change from cuboidal shape to irregular shape. Bekoz *et al.* showed the utilization of irregular carbamide as space holder result to lower value of both Young's modulus and strength compare to spherical shape of carbamide in their work of steel foams[4]. - Results of Zhen *et al.* on porous PZT ceramics had the same tendency of lower compressional strength of samples with irregular shape pore [2]. Irregular shape pore introduces stress concentration at sample that lowered its mechanical properties. The effect of irregular shape is then clearly shown by comparing the mechanical properties of sample with two kinds of pore shape and size of cuboidal 600 – 425 μm and mixture of cuboidal 600 – 425 μm and irregular 212 – 106 μm . Both Young's modulus and strength of sample with mixture of cuboidal and irregular shape pore have about a half Young's modulus and compressional strength.

In order to separate the influence of space holder size and shape to the mechanical properties of porous samples, figure 3.9 was presented. The figure shows only a little change of Young's modulus and strength by varying spacer size. This result is consistent with Bin *et al.* that no significant change of compressional strength by changing pore size of aluminum foam [3].

Table 3. 2 Compression test results of samples sintered at different sintering temperature and pressure

Sintering parameter	Composite's relative density (%)	Open porosity (%)	Mechanical Properties	
(T/°C, P/ MPa)			Young's Modulus (GPa)	Compressive strength (MPa)
700, 30	91.26	33.52	40 ± 3	121 ± 13.59
700, 40	92.20	31.33	50 ± 7	144 ± 22.85
	92.52	42.56	19.4 ± 0.53	78 ± 9.74
700, 60	97.12	39.50	36.5 ± 7.50	82 ± 14.81
	97.42	46.00	13.7 ± 2.41	139 ± 14.28
725, 30	92.70	31.33	49.7 ± 3.51	132 ± 17.91
725, 40	94.14	33.50	44.3 ± 5.03	155 ± 19.05

Table 3. 3 Compression test results of samples sintered at 700 °C, 60 MPa sintered at sintering heating rate

Sintering program	% vol. NaCl	Composite's relative density (%)	Open porosity (%)	Mechanical Properties	
				Young's Modulus (GPa)	Compressive strength (MPa)
Slow heating rate (SR)	50	97.42	46	13.7 ± 2.41	139 ± 14.28
	60	96.44	54	15.7 ± 6.17	59 ± 8.09
Fast Heating rate (FR)	50	96.19	46	17.3 ± 4.65	136 ± 5.16
	60	96.01	54	12.9 ± 1.59	112 ± 4.49

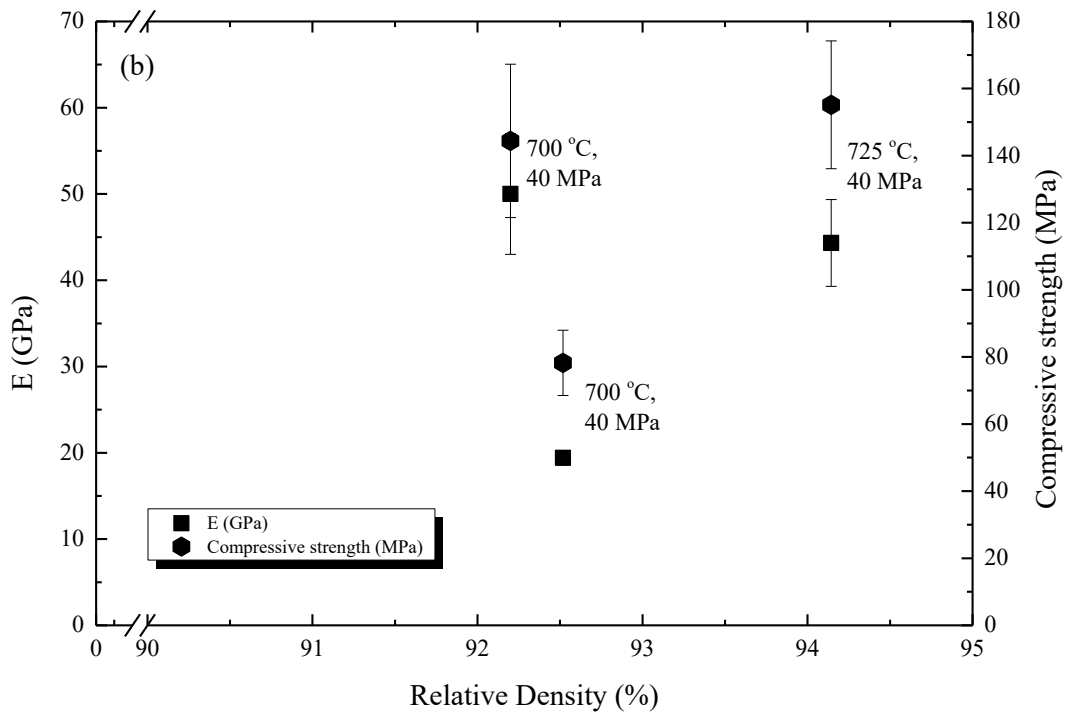
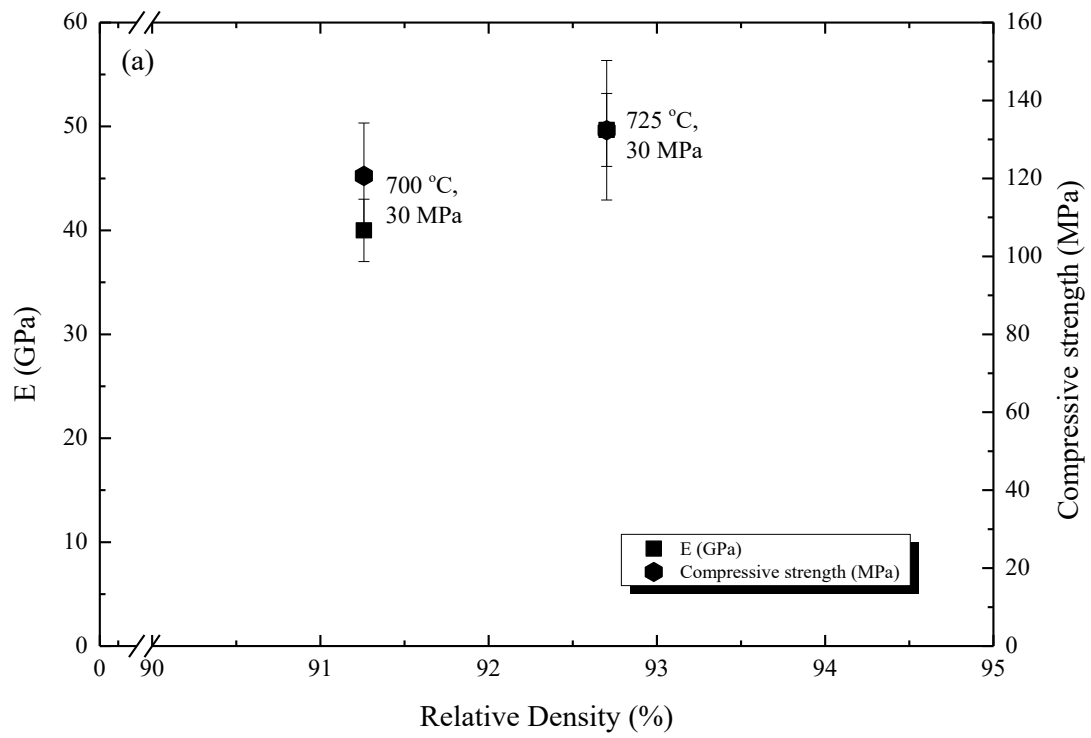


Figure 3. 3 Mechanical properties of samples sintered at different sintering temperature and different sintering pressure of 30 MPa (a) and 40 MPa (b)

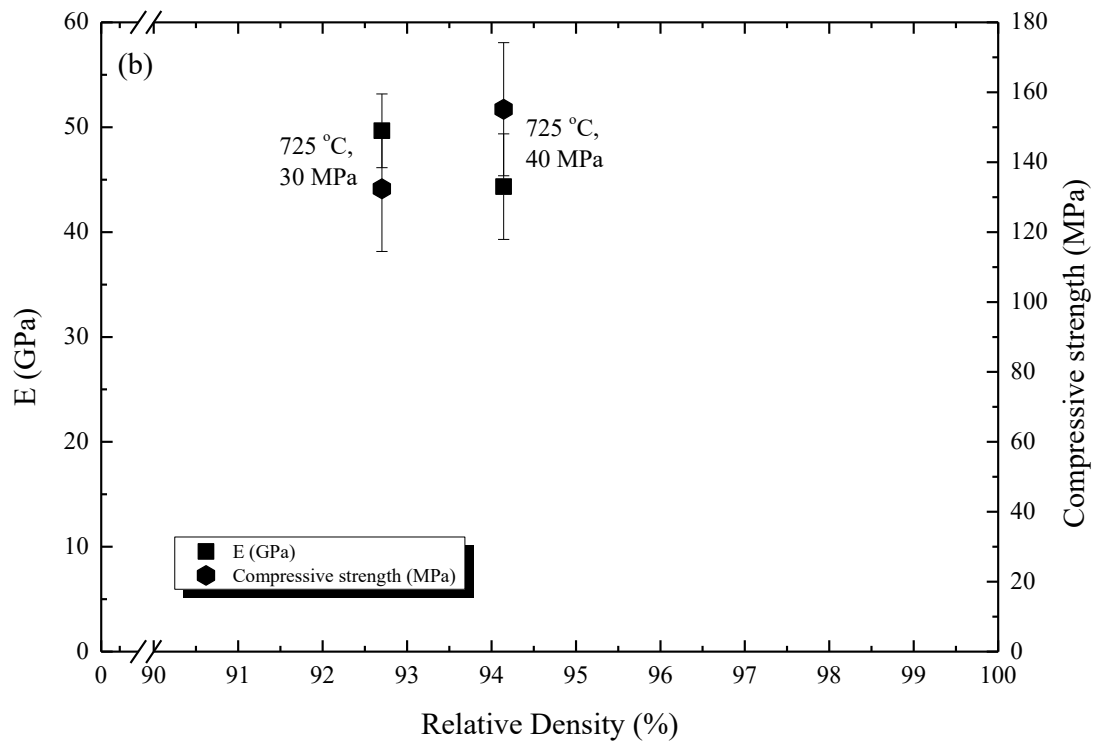
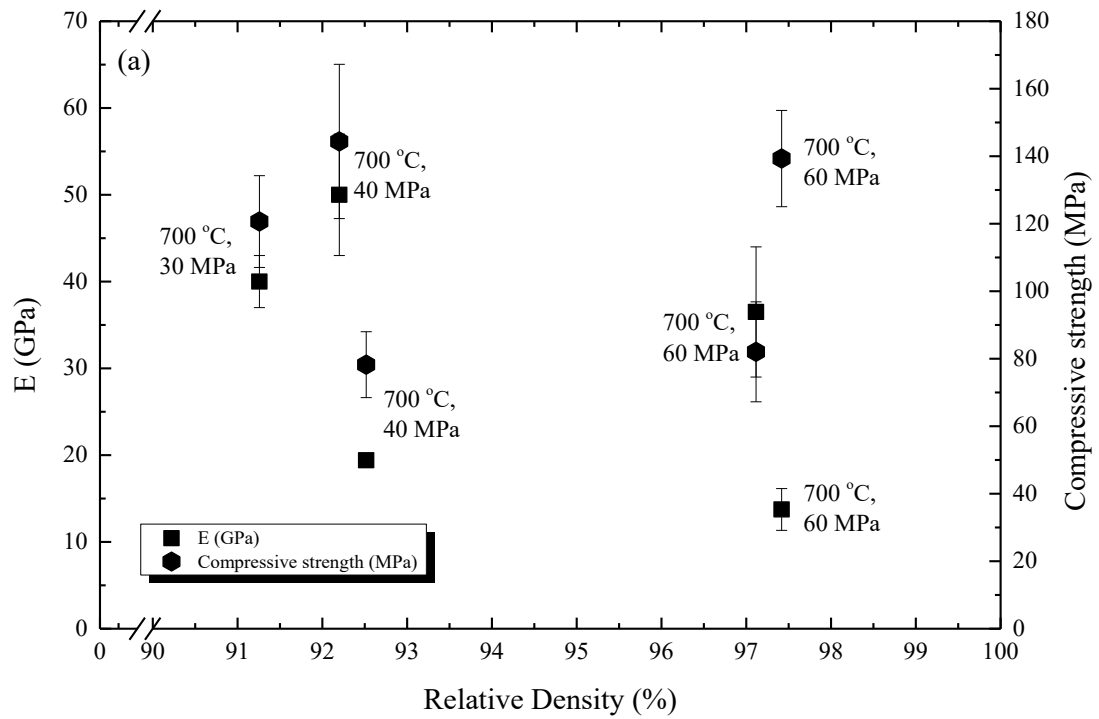


Figure 3. 4 Mechanical properties of samples sintered at different sintering pressure and different sintering temperature of 700 °C (a) and 725 °C (b)

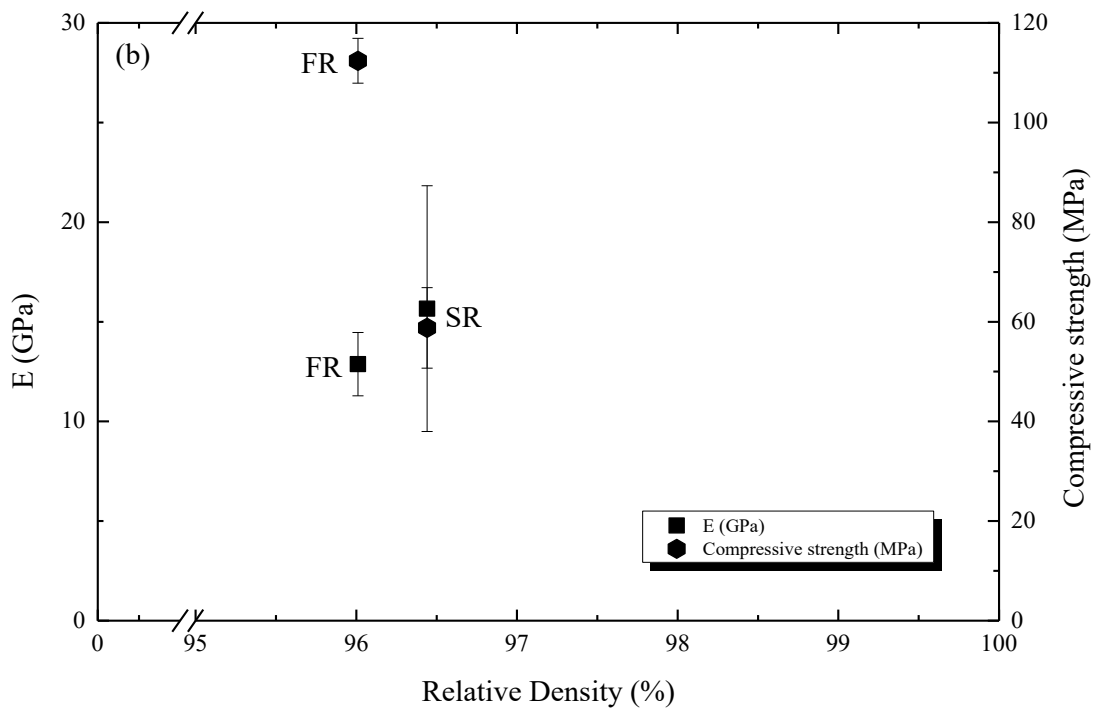
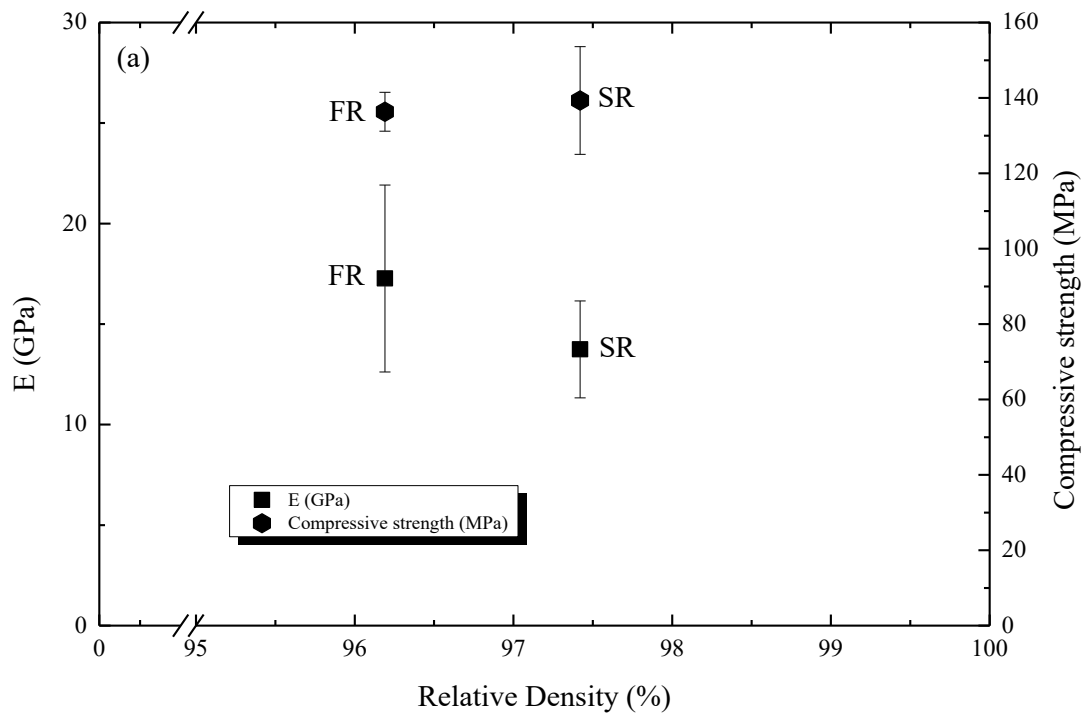


Figure 3. 5 Mechanical properties of samples sintered at 700 °C, 60 MPa with different heating rate and different sodium chloride contained 50 vol. % (a) and 60 vol. % (b). FR is fast heating rate and SR is slow heating rate.

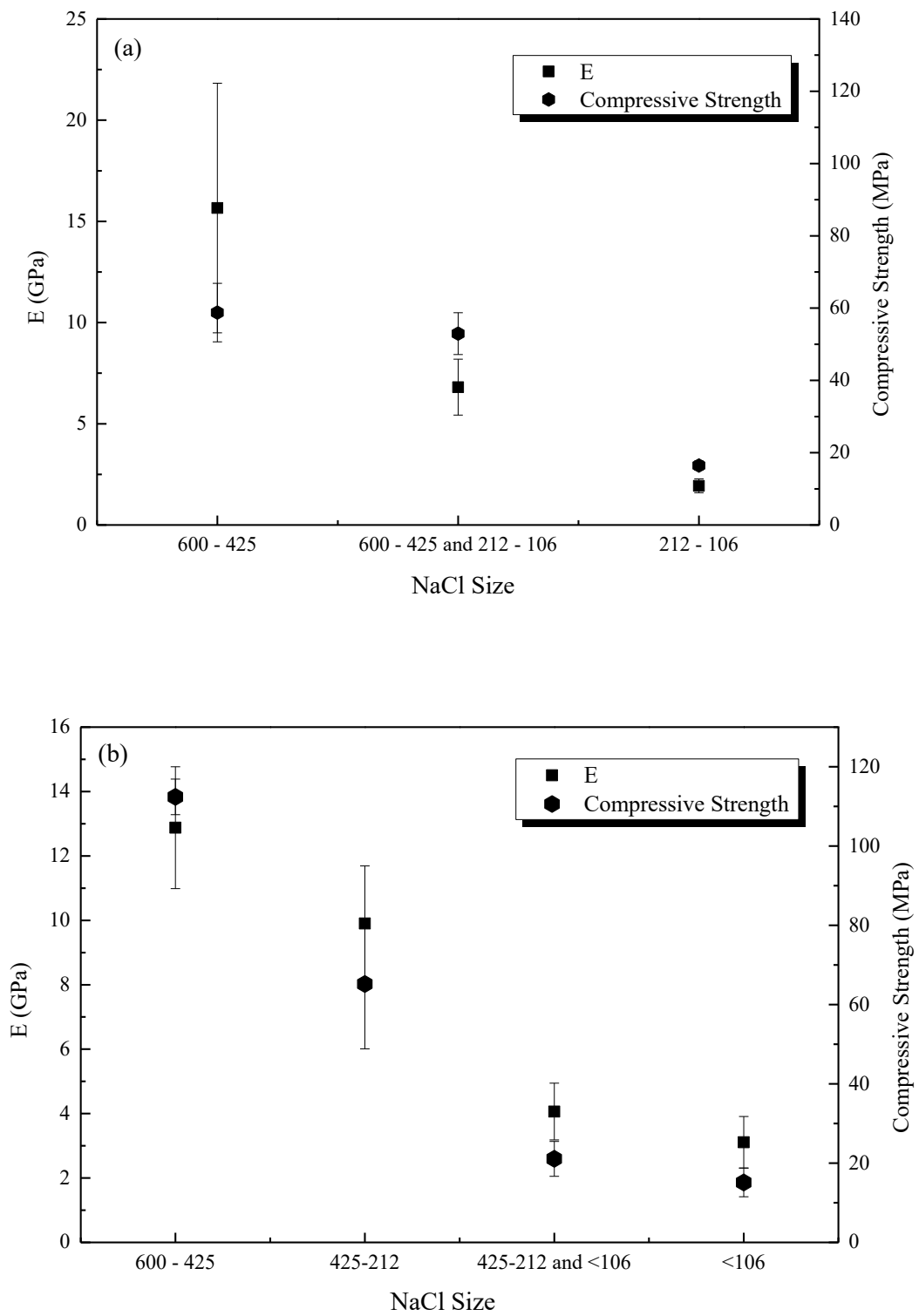


Figure 3. 6 Mechanical properties of powder mixture contained 60 vol. % varied size sodium chloride sintered at 700 °C, 60 MPa using slow heating rate (a) and high heating rate (b)

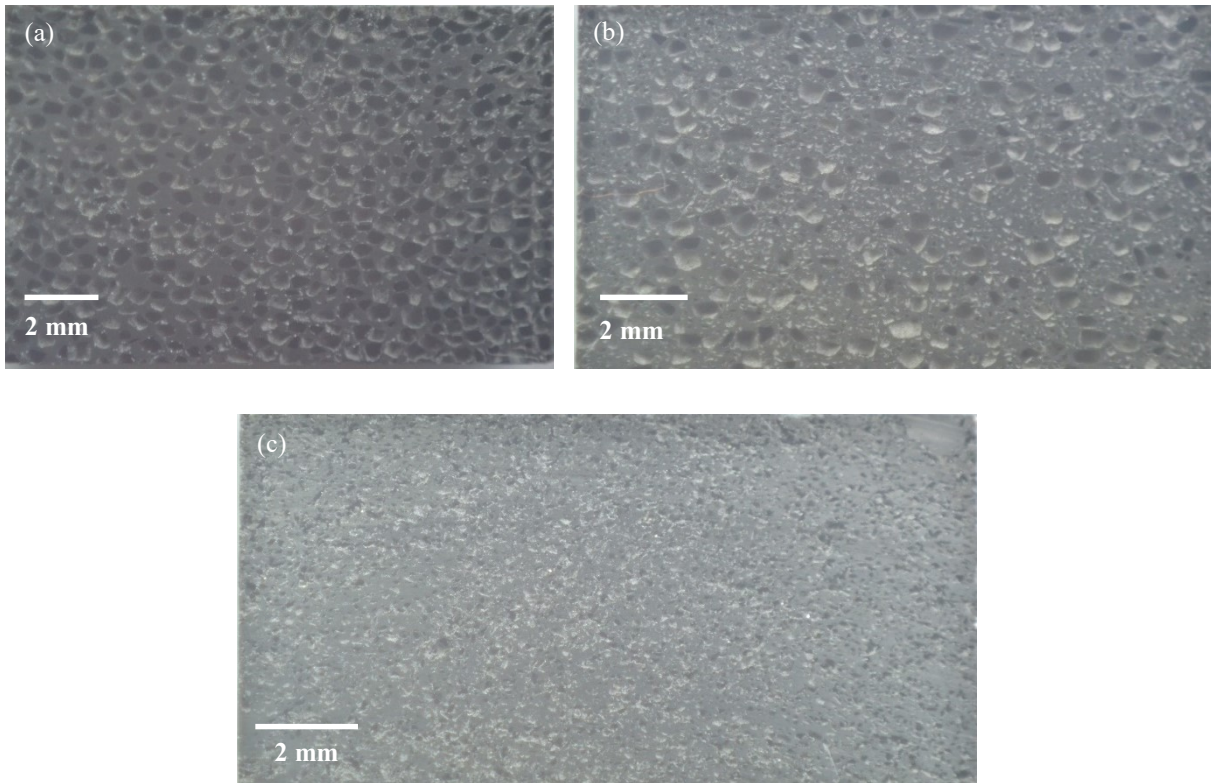


Figure 3. 7 Macro-image of powder mixture contained 60 vol. % sodium chloride size of 600 – 425 μm (a), 600 – 425 + 212 – 106 μm (b), and 212 – 106 μm (c) mixed with addition of 10 wt. % of ethanol sintered at 700 $^{\circ}\text{C}$, 60 MPa using slow heating rate program

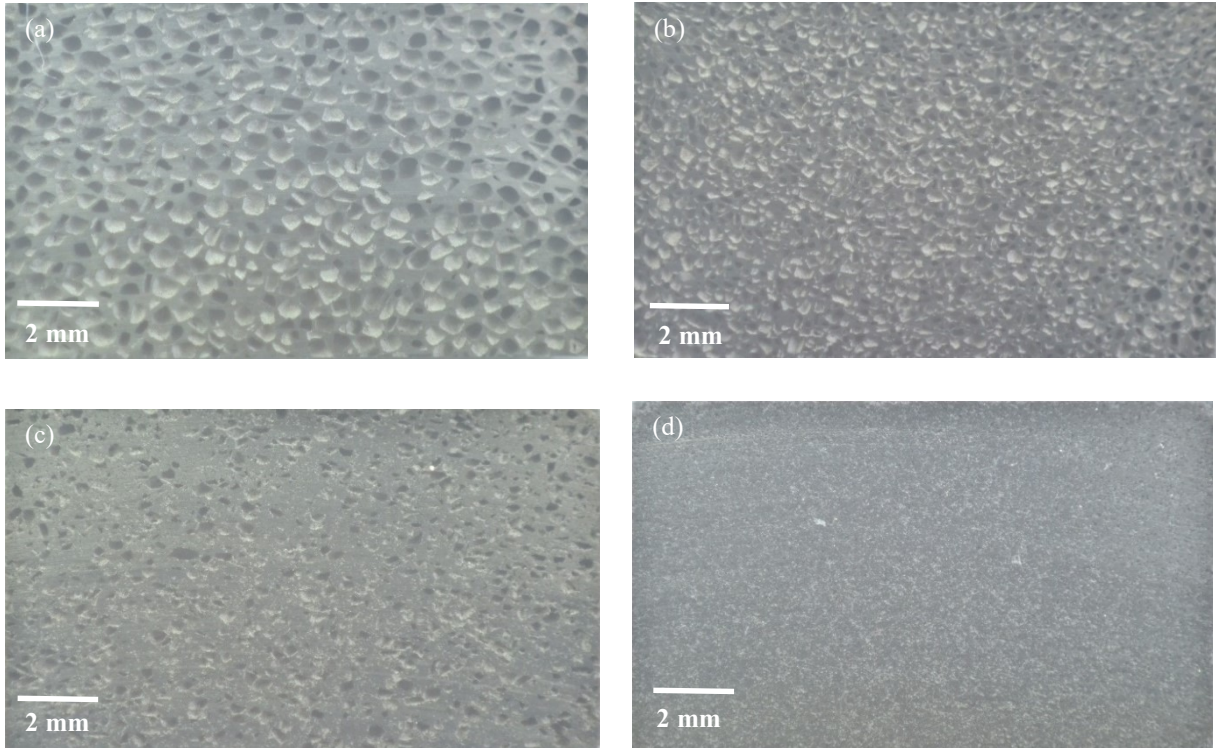


Figure 3. 8 Macro-image of powder mixture contained 60 vol. % sodium chloride size of 600 – 425 μm (a), 425 – 212 (b), 425 – 212 + <106 μm (c), and <106 μm (d) mixed with addition of 10 wt. % of ethanol sintered at 700 $^{\circ}\text{C}$, 60 MPa using slow heating rate program

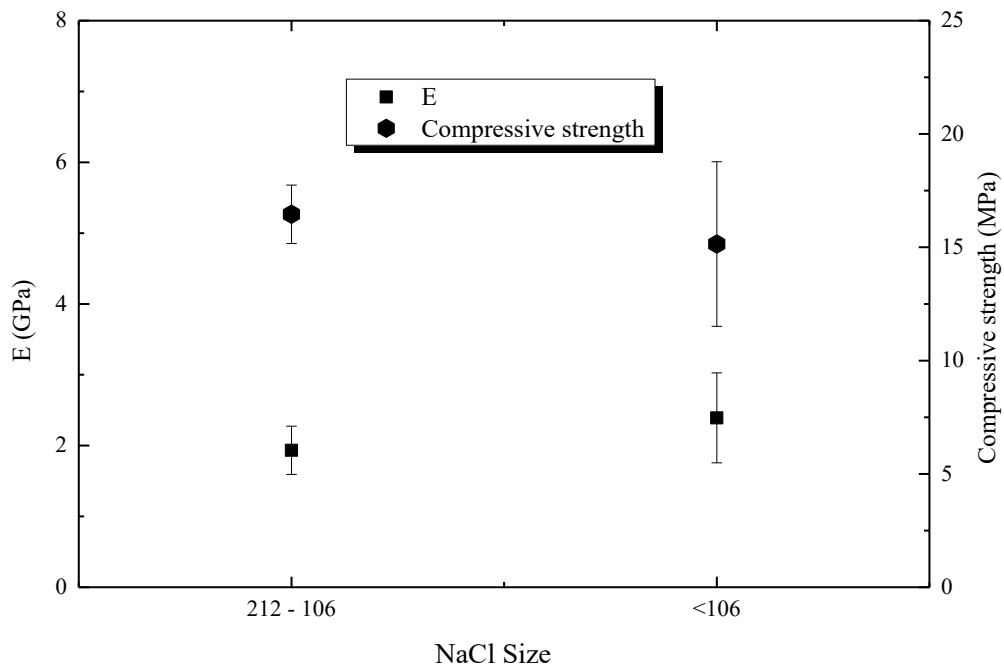


Figure 3. 9 Mechanical properties of powder mixture contained 60 vol. % varied size sodium chloride sintered at 700 °C, 60 MPa

From Chapter 2, it was understood that the addition of process control agent (PCA) resulted in the improvement of space holder distribution during mixing process. The addition of 5 wt. % stearic acid, 10 wt. % molten stearic acid and 10 wt. % ethanol during mixing process improve the distribution of the macro-pore as well as the distribution of space holder. Table 2.4 in Chapter 2 shows the results of quantitative analysis of pore are for sintered powder mixtures with addition of different PCA while table 3.4 shows the summary open porosity number and mechanical properties of the samples. Comparing table 2.4 and number of open porosity of the samples (table 3.4), the improvement of pore distribution results to the increment of open porosity number which decrease sample's Young's modulus.

Comparing the mechanical properties of samples which have about the same open porosity number, i.e. samples mixed without PCA and with 1 wt. % SA, the two samples have about the same Young's modulus but they have notable compression test. This tendency also happened for sample mixed with 10 wt. % melted SA and 10 wt. % ethanol. From the calculation of pore wall thickness of these two samples, sample which has higher mechanical properties has higher pore wall thickness.

Table 3. 4 Summary of open porosity and mechanical properties of sintered powder mixtures contained 50 vol. % 600 – 425 μm size sodium with addition of different PCA

Process control agent	Open porosity, OP (%)	Young's modulus, E (GPa)	Proof Strength, σ (MPa)
no	33.52 ± 2.51	40 ± 3	121 ± 13.59
1% mass Stearic Acid	34.59 ± 4.92	39 ± 4.17	92 ± 17.96
5% mass Stearic Acid	36.74 ± 5.04	45 ± 9.5	106 ± 14.58
10 mass% melted Stearic Acid	42.56 ± 2.12	19.41 ± 0.53	78 ± 9.74
10 wt. % ethanol	43.05 ± 2.22	16 ± 2.49	143 ± 17.18

3.4 Discussion

3.4.1 Effect of micro-porous to mechanical properties

From figure 3.3-5 even though reducing micro-porosity by adjusting sintering parameters, including sintering temperature, pressure and heating rate, results on a little increase of mechanical properties of porous product, there is no relation between relative density and mechanical properties. In addition, the t-test of the all the results of samples sintered at different sintering parameters give probability number bigger than 0.05 which lead to the conclusion that reducing micro-porosity has insignificant increase to the mechanical properties. The results are in accordance with the model build by Niu *et al.* in the relation of micro- and macro-porosity of porous titanium produced by space-holder [5]. The fitting function for the correlation between micro- and macro- density for the porous titanium is only give a weak interaction where micro-density only gives a little influence to the Young's modulus of porous product.

3.4.2 Effect of macro-porous to mechanical properties

In contrast to micro-porosity, remarkable change of both Young's modulus and compression strength of the samples are observed as the distribution and shape of macro-pore differs. Irregular shape of macro-pore will result to lower mechanical properties while changing the size of macro pore only results to insignificant change of mechanical properties. The results imply mechanical properties is only affected by macro-pore shape. Homogenous pore distribution as the results of PCA utilization produces more pore interconnectivity which decrease Young's modulus of samples. This finding opposes results of Cramer *et al.* on elastic properties of aluminum alloy 6061-T6 which show insensitive response of elastic properties to the actual pore distribution [6].

Figure 3.5 is the summary of mechanical properties of samples mixed with different PCA in table 3.4. It is clearly shown that both Young's modulus and compression strength of the samples decrease as the open porosity increase and comparing them with Gibson-Ashby model [1], the data are lower than the fitting line of Gibson-Ashby model.

More homogeneity yields to lower pore wall thickness (l_{average}) which results to the decrease of compressional strength of samples (table 2.4). From the compression test result in figure 3.5 (b), for nearly the same open porosity number, one sample is scattered far from the fitting line. It was already mentioned before that there is another factor affects more sample's compression strength. Comparing table 2.4 and table 3.4, for about the same open porosity number compressional strength may differ due to different pore wall thickness. It is clearly shown that high compression strength sample has thicker pore wall thickness. This implies that compare to Young's modulus, compressional strength is less dependent to the open porosity number. This relation is described by Gibson-Ashby that the increase of t_i/t lead to stronger porous materials as shown in figure 3.10 [7].

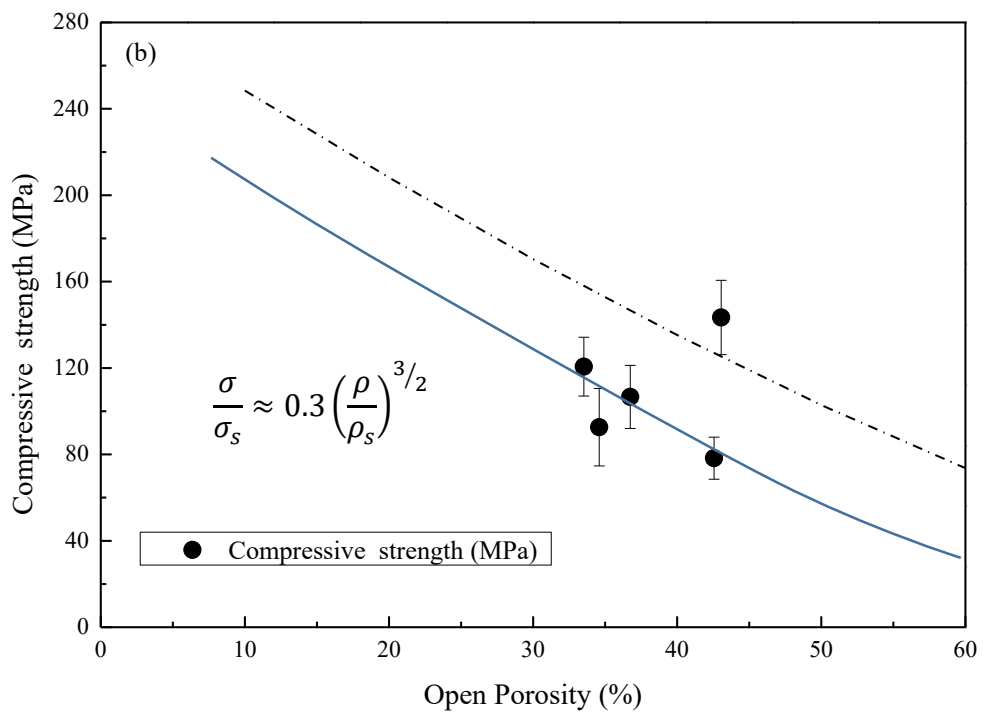
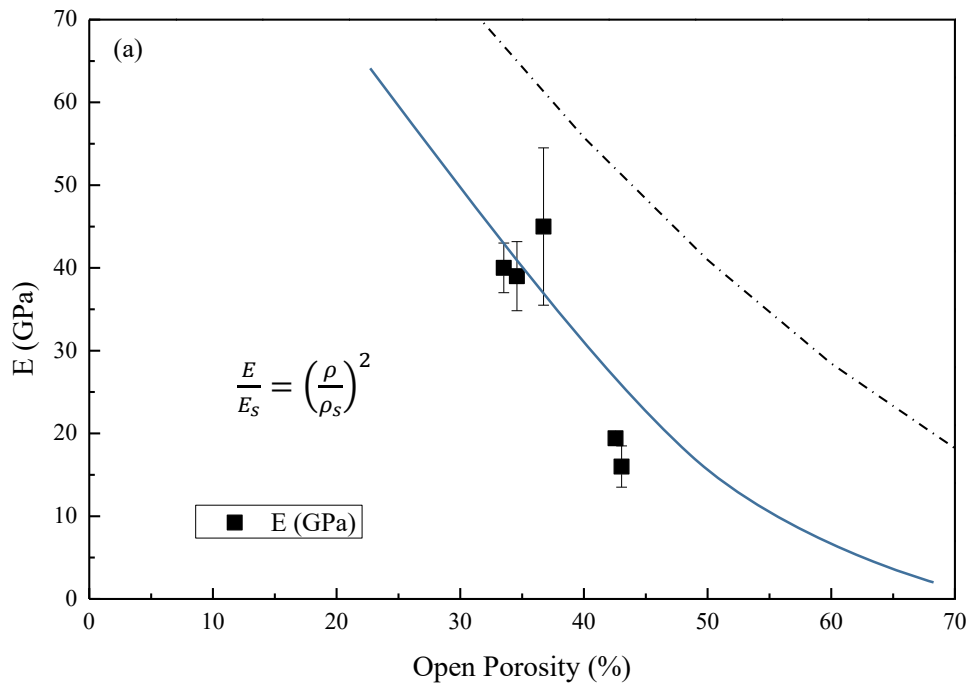


Table 3. 5 Comparison of Young's Modulus (a) and compressive strength (b) with Gibson-Ashby model of samples mixed with different PCA. The dash line is the fitting line of Gibson-Ashby model [1].

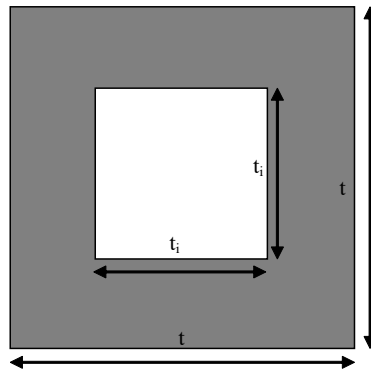


Figure 3. 10 Cross section of a strut with a box like central tubular void [7]

3.5 Conclusions

In this chapter, the influence of micro- and macro-porosity to the mechanical properties, including Young's modulus and compression strength, of porous Ti-6Al-4V produce by solid-state space holder method is discussed. In summary the influence is define below:

- (1) Micro-porosity in the size a few till a few ten micrometer has no significant effect to both Young's modulus and mechanical properties of porous product
- (2) Macro-porosity in the range of 50 – 800 μm plays more significant role to control mechanical properties of porous product
- (3) Irregular shape of macro-pore result about two times lower mechanical properties than cuboidal shape macro-pore while porous mechanical properties is insensitive to macro-porosity size
- (4) More homogenous macro-porosity will result more pore connectivity which result to higher number of open porosity and lower Young's modulus. Porous product strength is more dependent on pore wall thickness than its open porosity number

3.6 References

- [1] L. J. Gibson and M. F. Ashby, "Cellular Solids: Structure and Properties," Cambridge, Cambridge University Press, 1997, p. 186; 206.
- [2] T. Zeng, X. Dong, C. Mao, Z. Zhou and H. Yang, "Effect of pore shape and porosity on the properties of porous PZT 95/5 ceramics," *Journal of the European Ceramic Society*, vol. 27, pp. 2025-2029, 2007.
- [3] J. Bin and Z. N. Wang Zejun, "Effect of pore size and relative density on the mechanical properties of open cell aluminum foams," *Scripta Materialia*, vol. 56, pp. 169-172, 2007.
- [4] N. Bekoz and E. Oktay, "Effects of carbamide shape and content of processing and properties of steel foamc," *Journal of Materials Processing Technology*, vol. 212, pp. 2109-2116, 2012.
- [5] W. Niu, S. Gill, H. Dong and C. Bai, "A two-scale model for predicting elastic properties of porous titanium formed with space-holders," *Computational Materials Science*, vol. 50, pp. 172-178, 2010.
- [6] M. Cramer and I. Sevostianov, "Effect of pore distribution on elastic stiffness and fracture toughness of porous metal," *International Journal of Fracture*, vol. 160, pp. 189-196, 2009.
- [7] L. J. Gibson and M. F. Ashby, "Cellular Solids: Structure and Properties," Cambridge, Cambridge University Press, 1997, p. 211.

Chapter 4 Influence of Solution Treatment and Aging to Microstructure and Hardness of Bulk Spark Plasma Sintered Ti-6Al-4V

4.1 Introduction

Ti-6Al-4V alloy with the addition of aluminum as α phase stabilizer and vanadium as β phase stabilizer has performed high weight to strength ratio, high corrosion resistance and biocompatibility. Depending on cooling rate and prior heat treatment, e.g. annealing, thermo-mechanical process, solution treatment and aging, this alloy microstructure is divided into several types microstructure, such as α allotriomorph, globular α or primary α , Widmanstätten, basket-weave, and martensitic phase [1]. Martensite type of α' will be formed when β phase is quenched or cooled under high cooling rate. The martensite has two different structure, α' with hexagonal crystal structure and α'' with orthorhombic crystal structure [2] [3]. Solution treatment temperature and vanadium content in β phase strongly affect the formation of α' and/or α'' type martensite. More vanadium content in β phase will stabilize and retain its BCC crystal structure. Vanadium enrichment of the β phase occurs in proportion to the reduction of volume fraction of α phase. If β phase contains about 10 at% vanadium (approximately in temperature range 750 - 900 °C) is quenched, it partly transforms into soft orthorhombic α'' martensite. Higher solution treatment temperature (above 900 °C phase) will reduce vanadium enrichment in β , enhancing transformation of hard hexagonal α' [4] [5] [6] [7].

However, titanium and titanium alloys produced through powder metallurgy method, which usually have Widmanstätten structure, not always effectively strengthened by the combination of solution treatment and aging [8]. In this present study the effect of combination of solution treatment and aging to spark plasma sintered Ti-6Al-4V widely used for biomaterials especially bone implant is investigated.

4.2 Experimental Procedures

Same gas spherical gas atomization Ti-6Al-4V powder in Chapters 2 and 3 was used in this study. Bulk samples were sintered without space holder with different sintering condition between 700 – 725 °C and 30 – 40 MPa. Sintering was performed under a vacuum condition around 13 Pa using a spark plasma sintering machine (SPS 511S, SPS Syntex) with slow heating rate program as described in Chapter 2.

Solution treatment was performed at temperature between 850 – 1050 °C for 1 hour in argon flow furnace followed by ice water quenching. All solution treated (ST) samples then aged (STA) at 530 °C for 6 hours followed by air cooling. To understand the phases form during aging, ST 1000 sample also aged at 530 °C for 6 hours followed by ice water quenched. Table 4.1 shows the heat treatment condition for the samples. After the heat treatment, the samples then subjected to some characterization including XRD, SEM/EDS, and micro-Vickers test.

Table 4. 1 Availability of heat treated samples for several solution treatment and aging treatment

Sintering Condition	Solution treatment temperature (°C)	Aging Condition			
		No aging	530 °C, 3h	530 °C, 6h	700 °C, 6h
700 °C, 30 MPa	850	O	X	O	X
	900	O	X	O	X
	980	O	X	O	X
	1000	O	X	O	O
	1050	O	O	O	X
725 °C, 40 MPa	850	O	X	O	X
	900	O	X	O	X
	980	O	X	O	X
	1000	O	X	O	X

4.3 Results

4.3.1 Microstructural change after heat treatment

Microstructure of as sintered sample at 700 °C, 30 MPa and 725 °C, 40 MPa are shown in figure 4.1. At lower magnification, numbers of micro-pores are observed while at high magnification the microstructure inside the powder shows some small lighter particles in between α phase. The EDS results from figure 4.2 shows that this lighter particles have higher vanadium content, suggest that these lighter particles are β phase. In general, there is no much different of microstructure from varying sintering temperature and pressure.

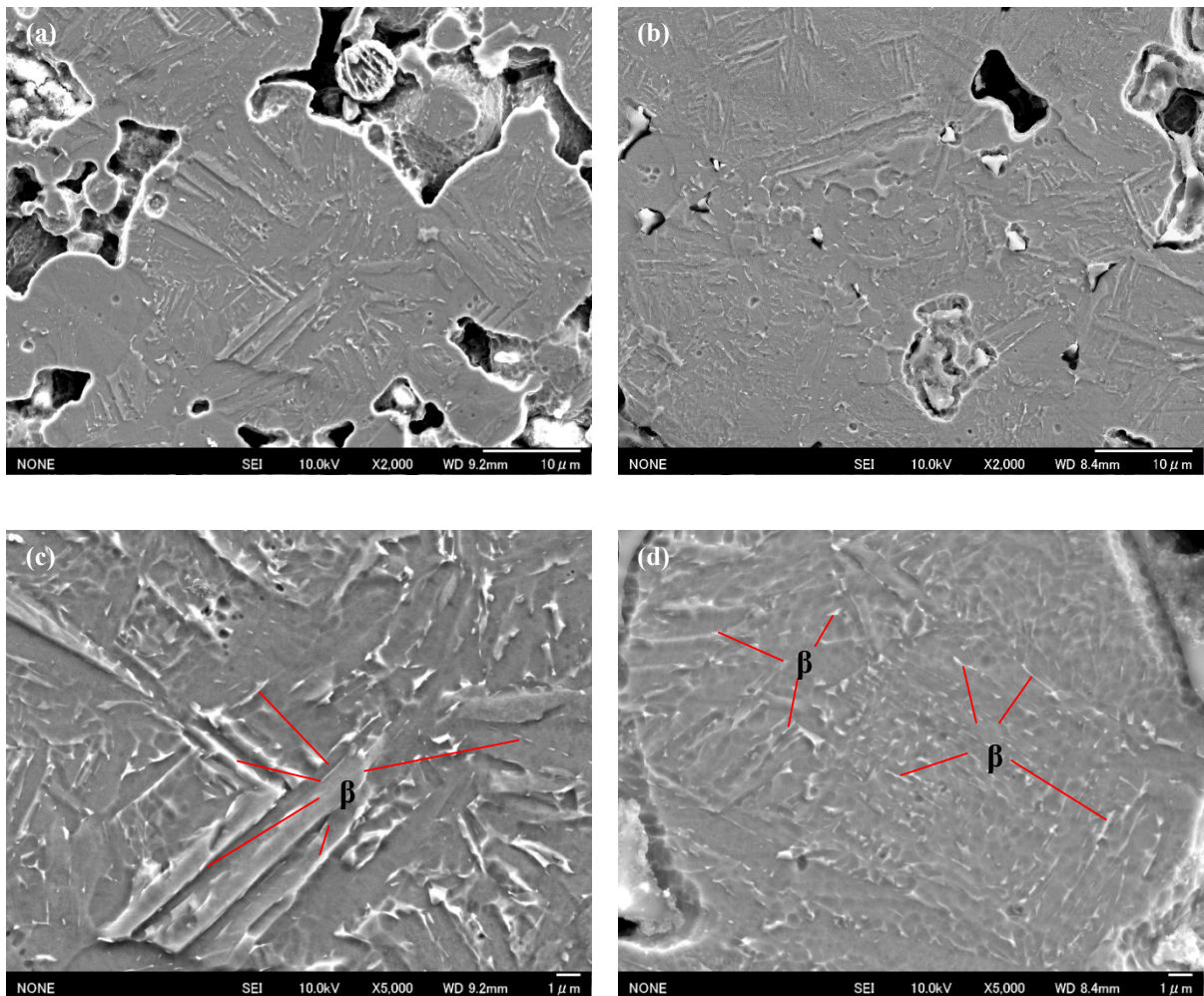


Figure 4. 1 SEM images of bulk Ti-6Al-4V sintered at respectively 700 °C, 30 MPa (a) and 725 °C, 40 MPa (b) at low magnification and high magnification (c-d)

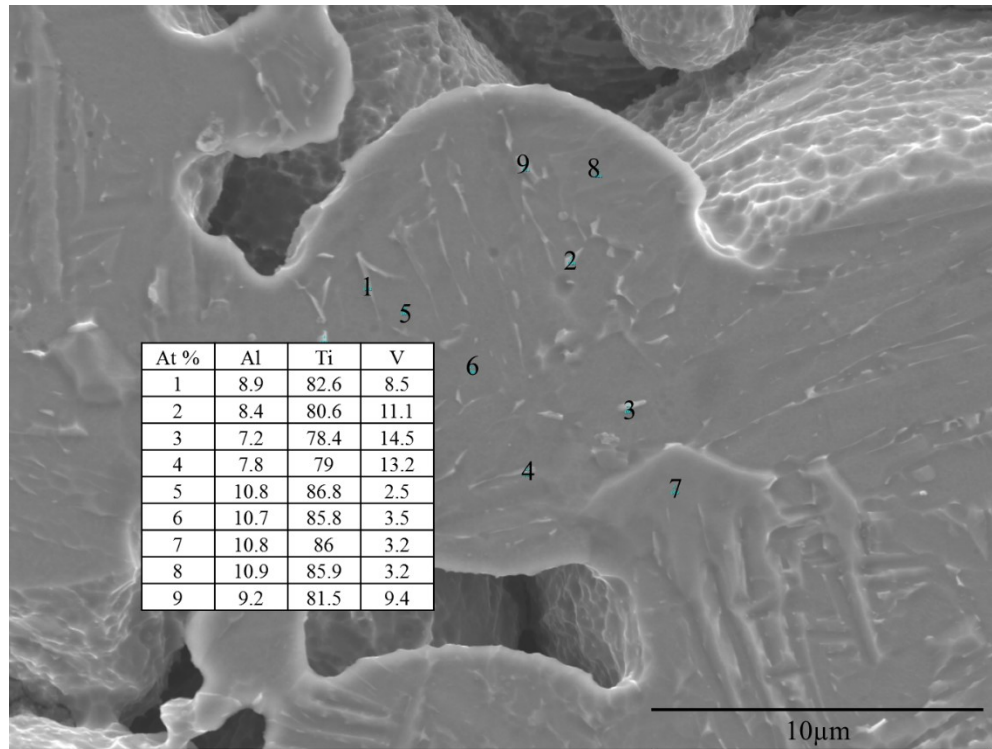


Figure 4. 2 EDS results of sample sintered at 700 °C, 30 MPa

The microstructures of samples sintered at different condition then solution treated at several temperatures are shown in figure 4.3 – 4.6. At low temperature, micro-porosities are observed in all samples. As the solution treatment temperature increase, the neck between powders also grow. This process is more obviously observed at samples sintered at 725 °C, 40 MPa. At high magnification, figure 4.4 and 4.6, upon quenching, solution treatment above 980 °C produces an acicular structure of hexagonal α' martensite while solution treatment at 850 and 900 °C only produce thin layer β meta stable phase in between α phase. The XRD result shown in figure 4.7 confirms that samples heat treated above 980 °C do not have β phase peak. Lee *et al.* result on heat treated and quenched powder metallurgy Ti-6Al-4V shows that vanadium content more than 15 wt.%, β phase tends to retain its BCC structure after quenching while at 10 wt.% α phase partly transform into soft orthorhombic α'' martensite [4]. Thus, upon quenching below 980 °C, β phase still presences.

Figure 4.8 and 4.9 are the SEM images of samples sintered at 700 °C, 30 MPa and 725 °C, 40 MPa after solution treatment at several temperature then aged at 530 °C for 6 hours. After aging at 530 °C, dispersed small lighter particles are observed along the grain boundary and interior of metastable β phase for ST 850 and ST 900 samples. For ST 980 and ST 1000 samples, these small particles are also observed along α' grain boundary and interior of α' martensite.

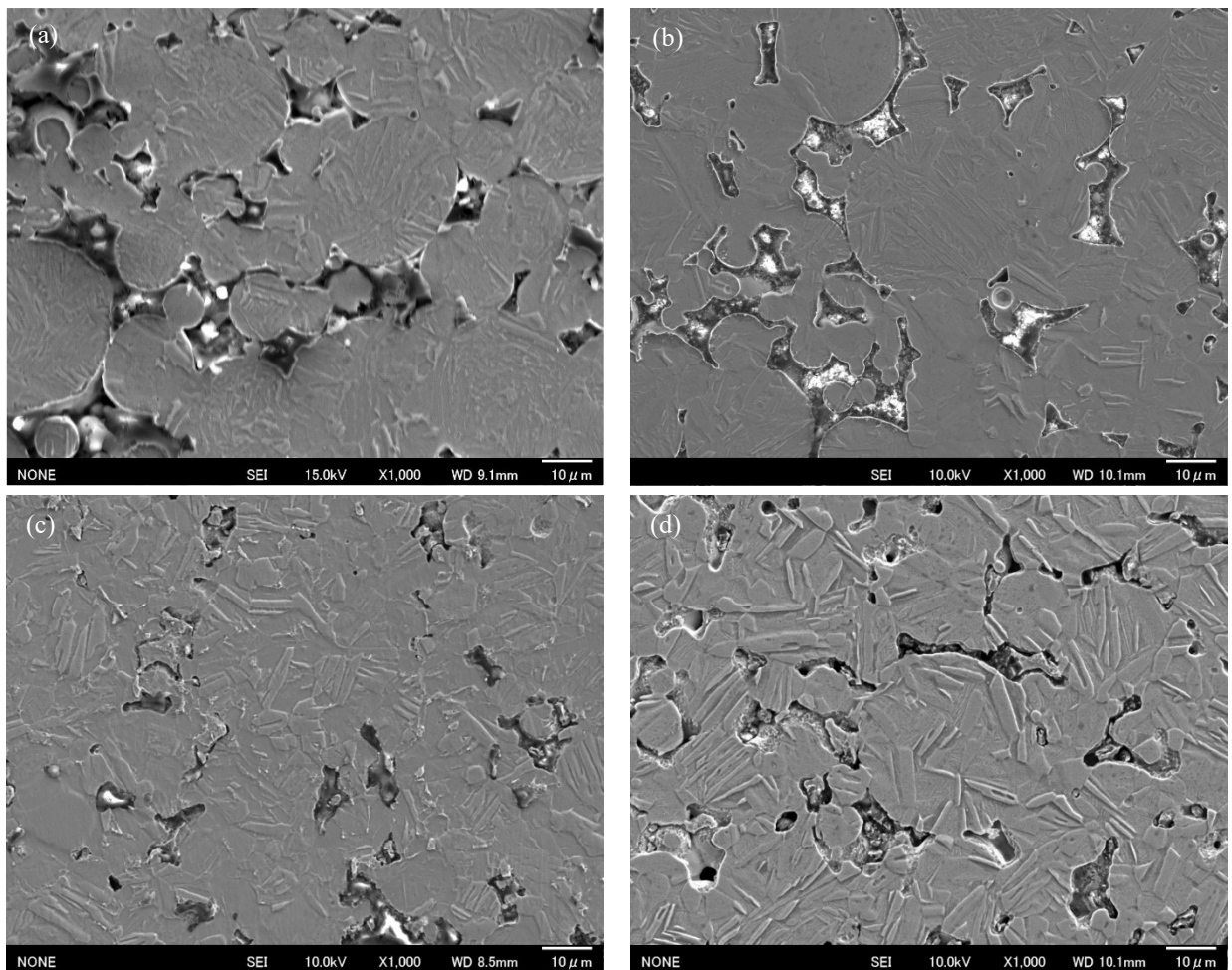


Figure 4. 3 SEM images of bulk Ti-6Al-4V sintered at 700 °C, 30 MPa after solution treatment (ST) at 850, 900, 980 and 1000 °C for 1 hour followed by ice water quenched at low magnification

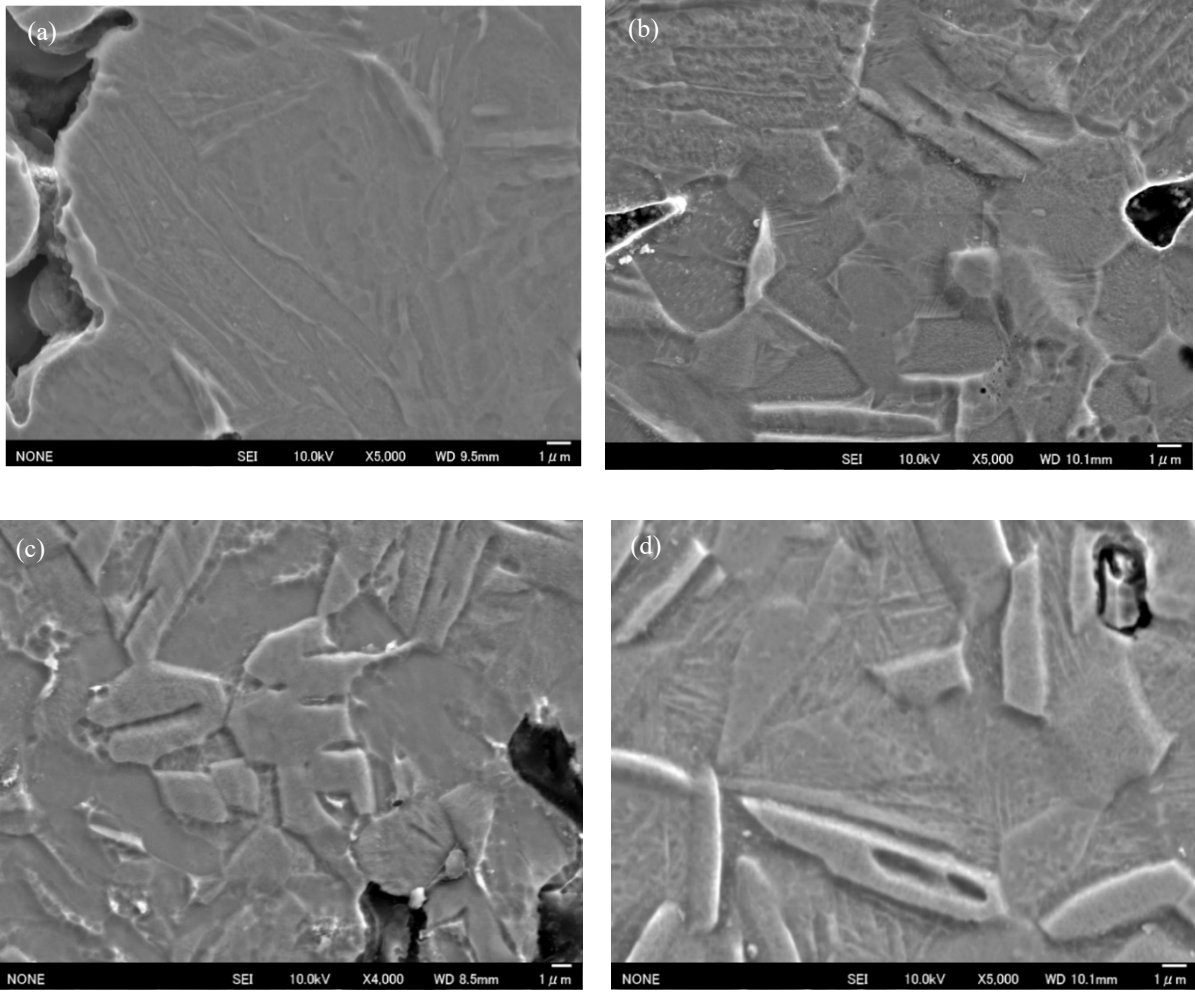


Figure 4. 4 SEM images of bulk Ti-6Al-4V sintered at 700 °C, 30 MPa after solution treatment (ST) at 850, 900, 980 and 1000 °C for 1 hour followed by ice water quenched at high magnification

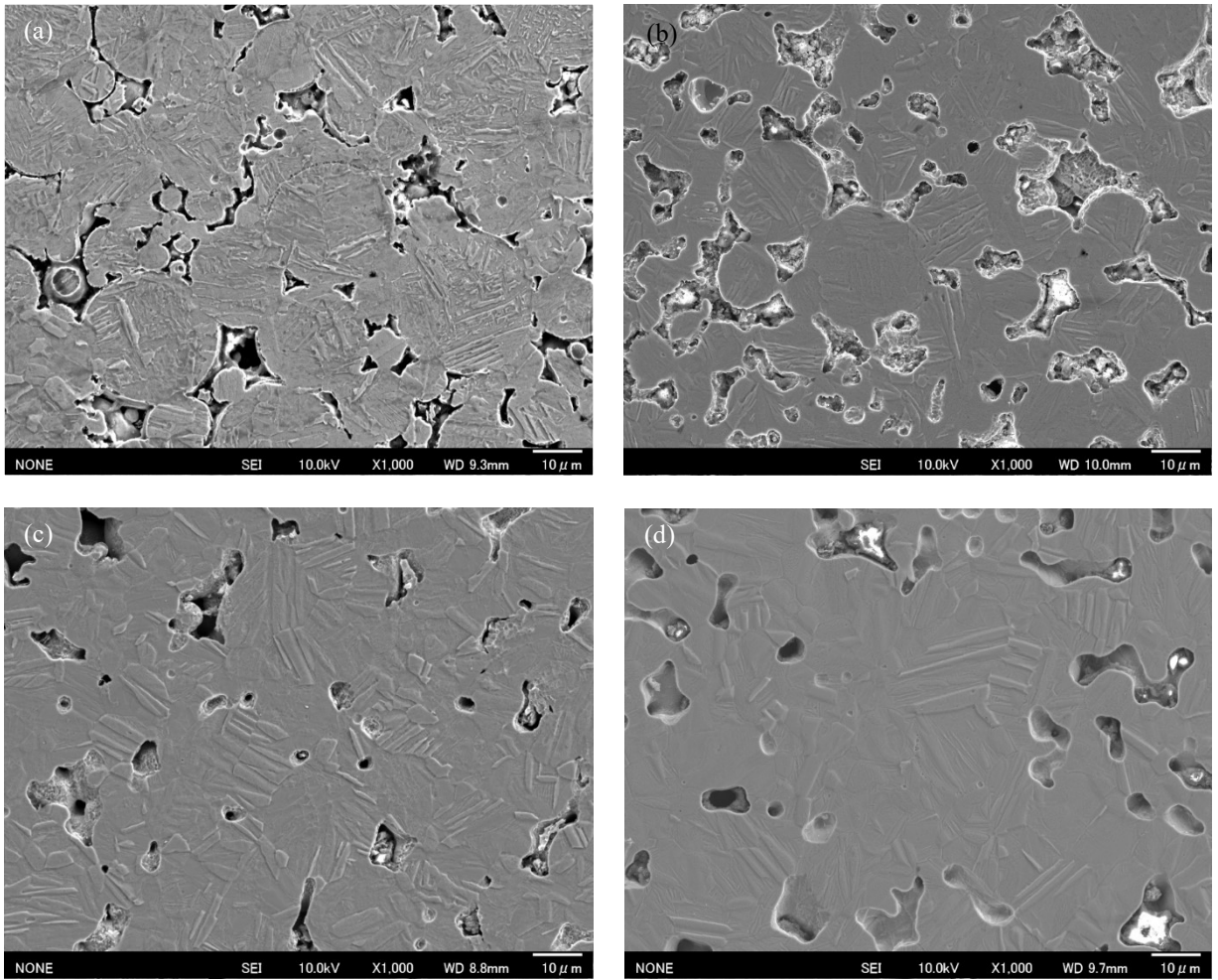


Figure 4. 5 SEM images of bulk Ti-6Al-4V sintered at 725 °C, 40 MPa after solution treatment (ST) at 850, 900, 980 and 1000 °C for 1 hour followed by ice water quenched at low magnification

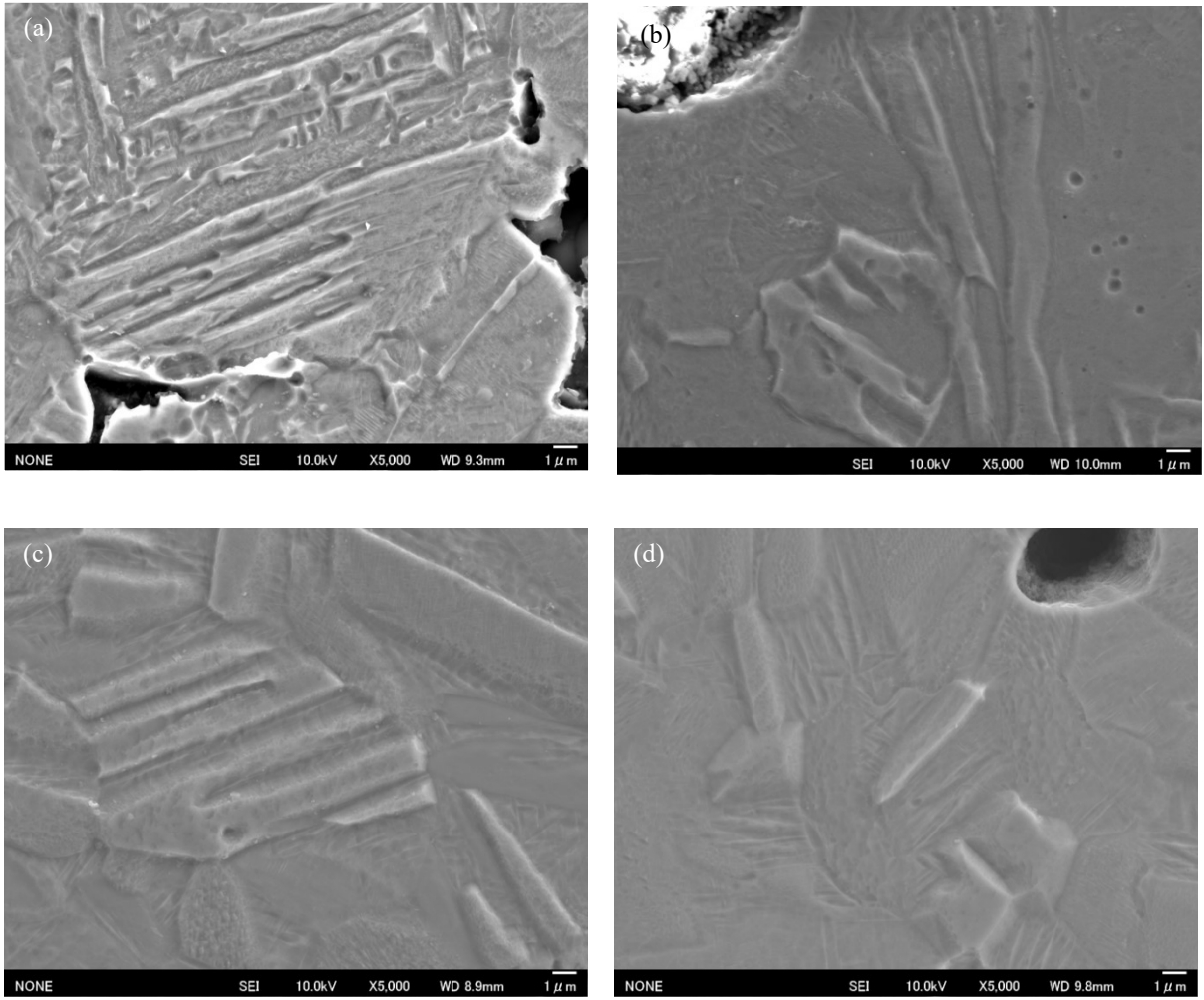


Figure 4. 6 SEM images of bulk Ti-6Al-4V sintered at 725 °C, 40 MPa after solution treatment (ST) at 850, 900, 980 and 1000 °C for 1 hour followed by ice water quenched at high magnification

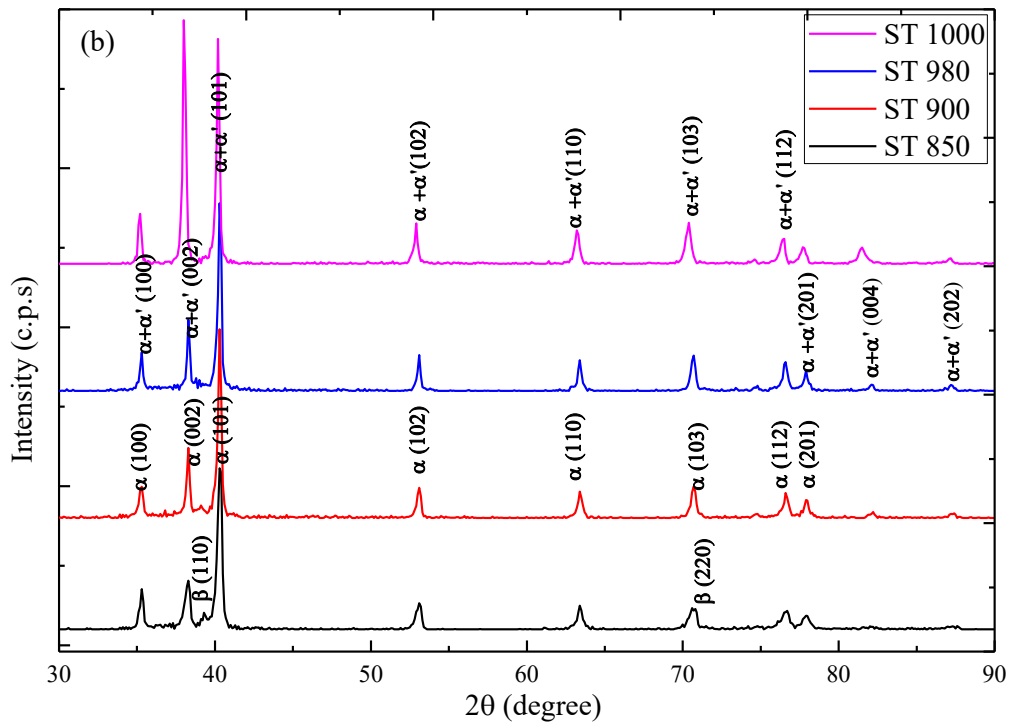
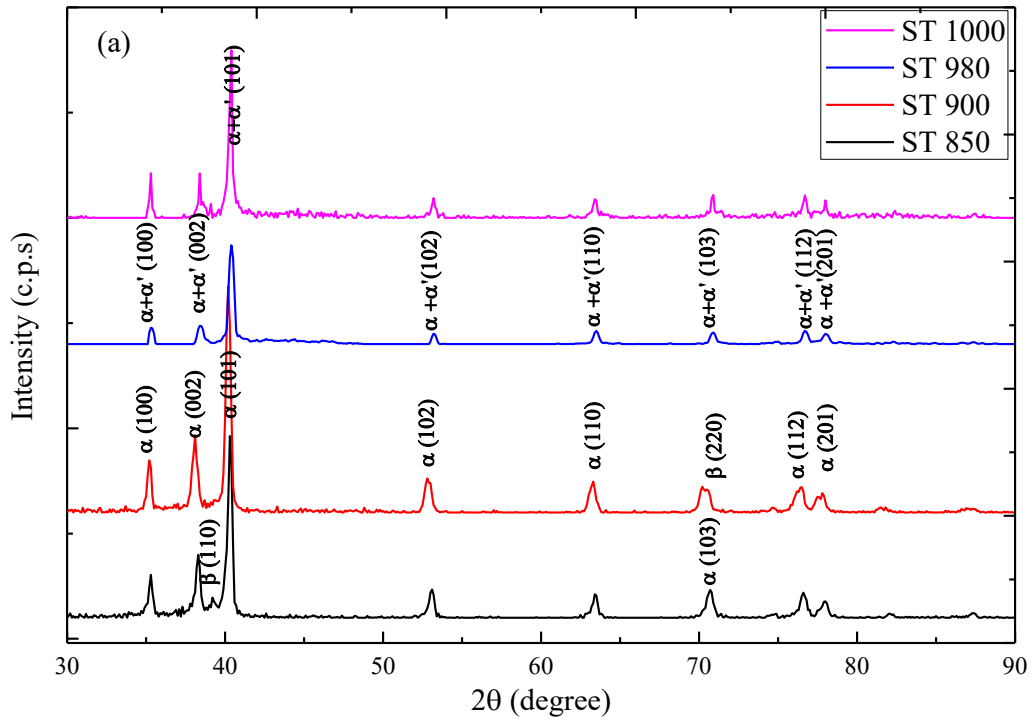


Figure 4. 7 XRD pattern of samples sintered at 700 C, 30 MPa (a) and 725, 40 MPa after solution treatment at several temperature for 1 hour followed by ice water quenching

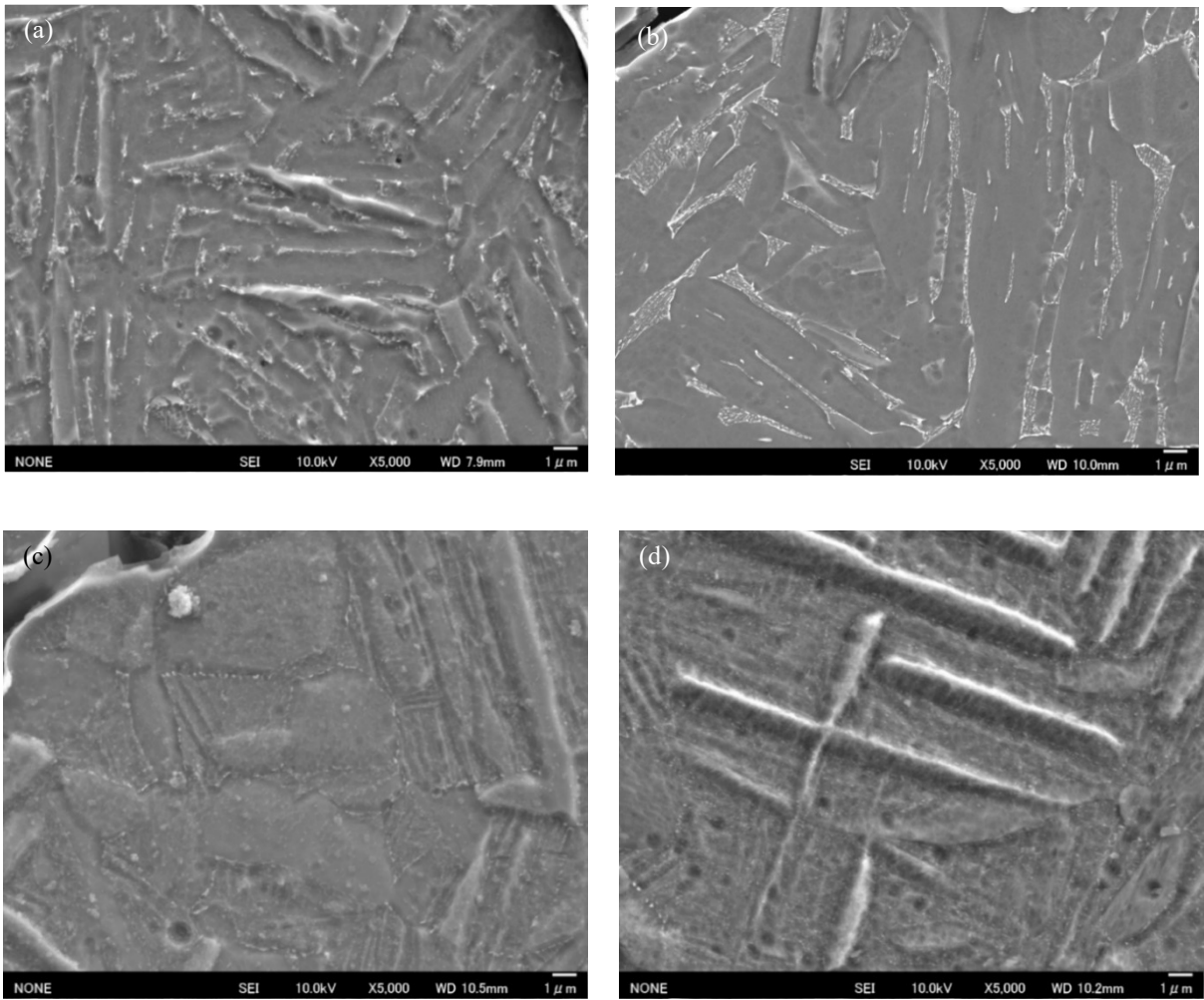


Figure 4. 8 SEM images of bulk Ti-6Al-4V sintered at 700 °C, 30 MPa after solution treatment (ST) at 850 (a), 900 (b), 980 (c) and 1000 °C (d) for 1 hour followed aging at 530 °C for 6 hours

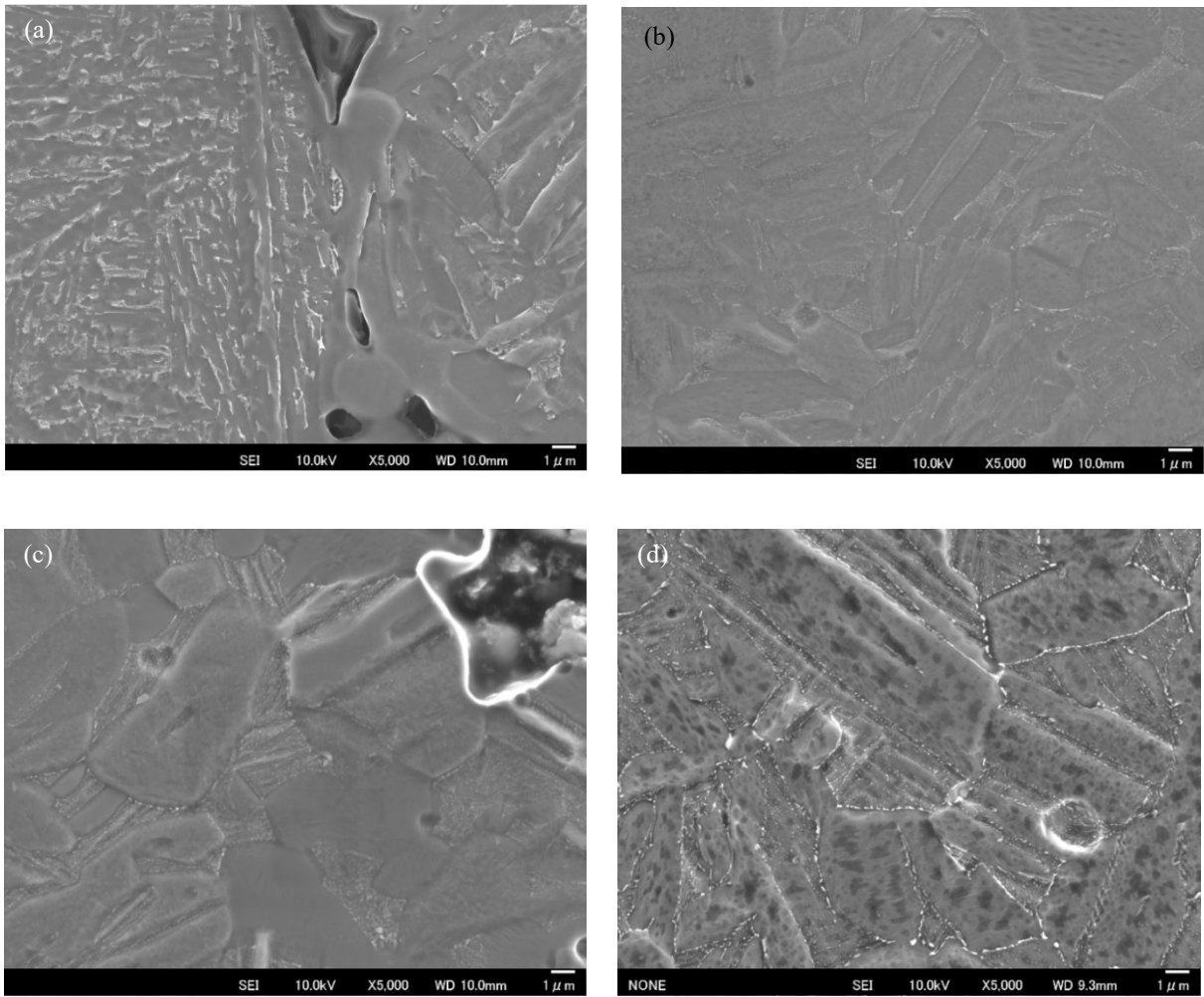
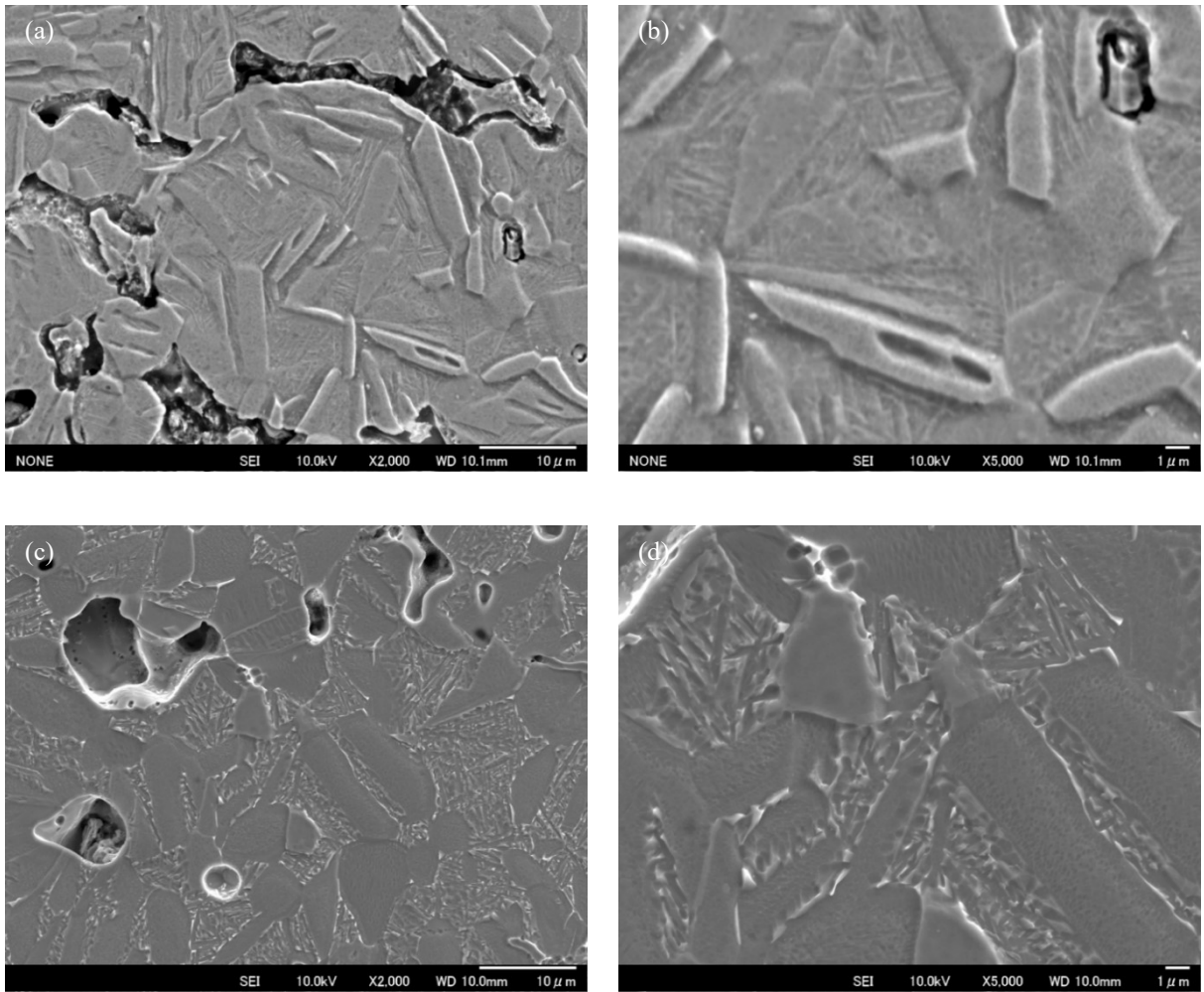


Figure 4. 9 SEM images of bulk Ti-6Al-4V sintered at 725 °C, 40 MPa after solution treatment (ST) at 850 (a), 900 (b), 980 (c) and 1000 °C (d) for 1 hour followed aging at 530 °C for 6 hours



Figure 4. 10 High magnification SEM image of sintered at 700 °C, 30 MPa sample solution treated at 1000 °C for 1 hour then aged at 530 °C for 6 hours

Higher magnification of aged samples shown in figure 4.10 and 4.13 shows that the small lighter particles inside α' martensite are aligned on the preferred direction along the direction of α' martensite. Li *et al.* on their work of aging response of laser melting deposited Ti-6Al-2Zr-1Mo-1V alloy reports β phase precipitate formation inside α' martensite plate and on the plate interfaces after isothermal aging at temperature between 550 – 600 °C [9]. Increasing aging temperature to 700 °C leads to the formation of coarser precipitates as shown in figure 4.11. The EDS result in figure 4.12 confirms the precipitates have higher vanadium content, the result suggests the precipitates are β phase.



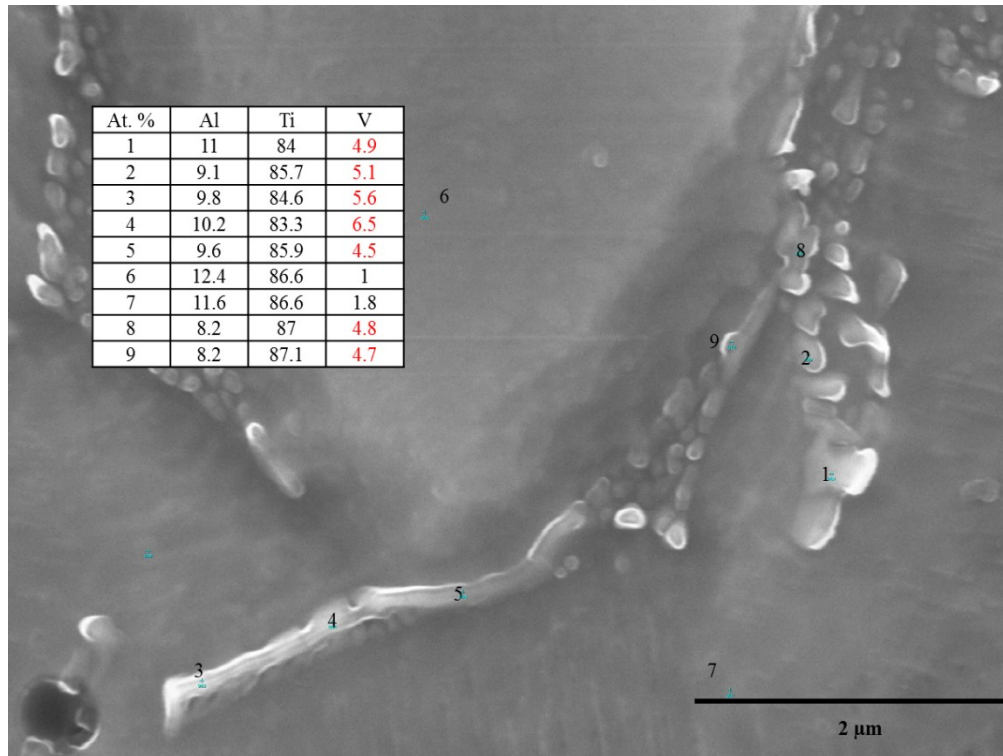
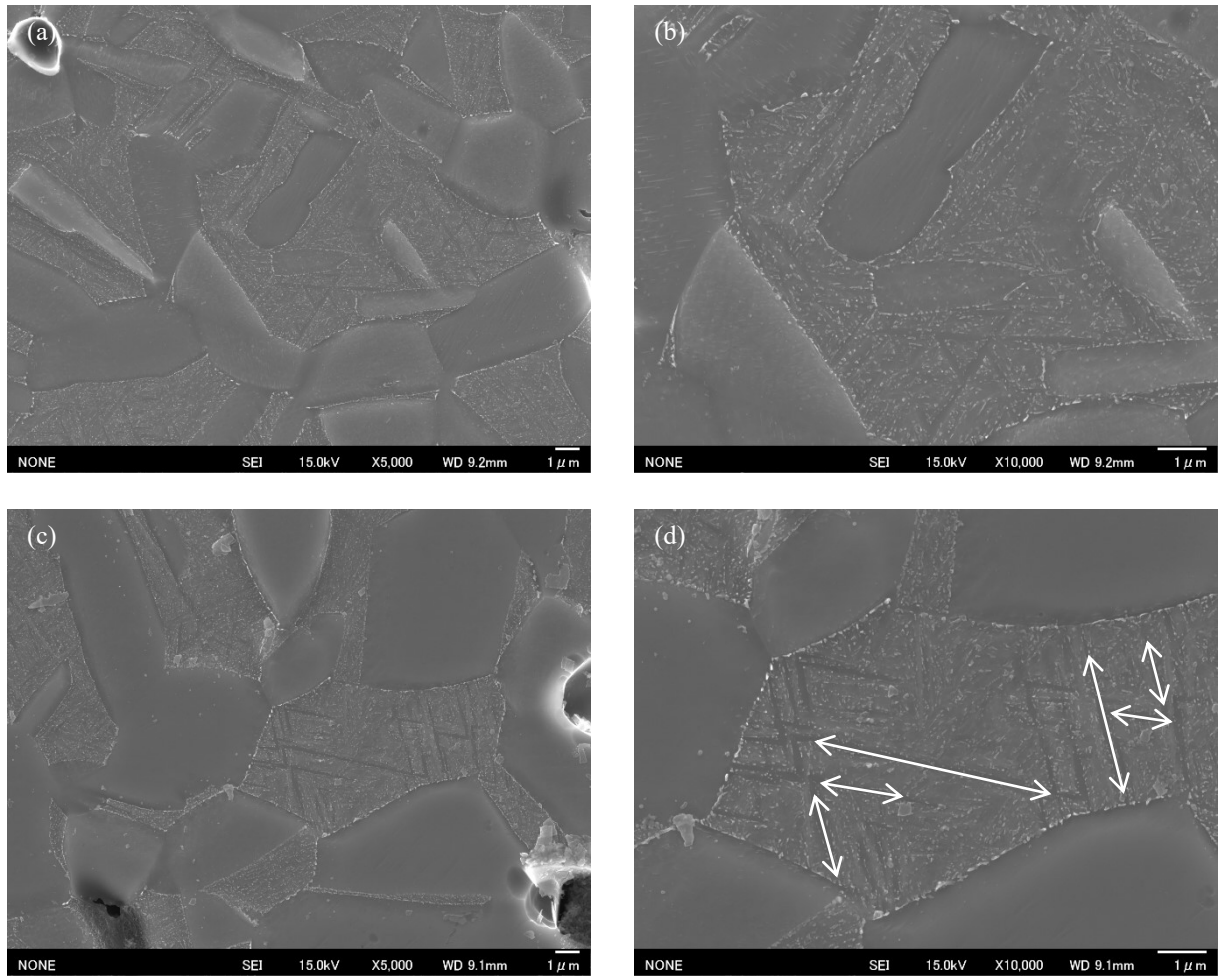


Figure 4. 12 EDS result of sintered at 725 °C, 40 MPa sample solution treated at 1000 °C for 1 hour and aged at 530 °C for 6 hours



4.3.2 Hardness after heat treatment

Micro-Vickers hardness test was performed in order to understand the hardness change before and after heat treatment. Figure 4.14 shows the summary of micro-Vickers hardness of as-sintered samples before and after solution treatment at several temperature. Sample sintered at 725 °C, 40 MPa has a slightly higher hardness than sample sintered at 700 °C, 30 MPa. At higher sintering temperature and pressure, β phase are likely formed more upon cooling. Thus, the hardness of sample is higher due to two phase strengthening. The other reason is at higher temperature and pressure, less micro-porosity produce in sample which increase its hardness. Both the hardness of samples sintered at different sintering pressure and temperature are increased as the solution treatment increase. After solution treatment at 850 and 900 °C, the hardness increase because the formation of metastable β phase and two phase strengthening while the formation of α' martensite causing the increment at solution treatment temperature of 980 and 1000 °C.

The micro-Vickers hardness change after and before solution treatment and aging is summarized in figure 4.15 and 4.16. It is shown from the figure that compare to as-sintered samples, both samples that solution treated and aged have higher hardness. However, compare to solution treated samples, aging treatment lowers the samples' hardness. After aging, α' martensite produced by samples solution treated at 980 and 1000 °C decomposes into α phase and precipitate of β phase. Therefore, the hardness decreases after aging at 530 °C for 6 hours. After solution treatment at 850 and 900 °C, the formation of more stable β phase precipitate generates the slight decrease of samples' hardness. Further martensite decomposition at higher aging temperature will decrease more samples' hardness as shown in figure 4.16.

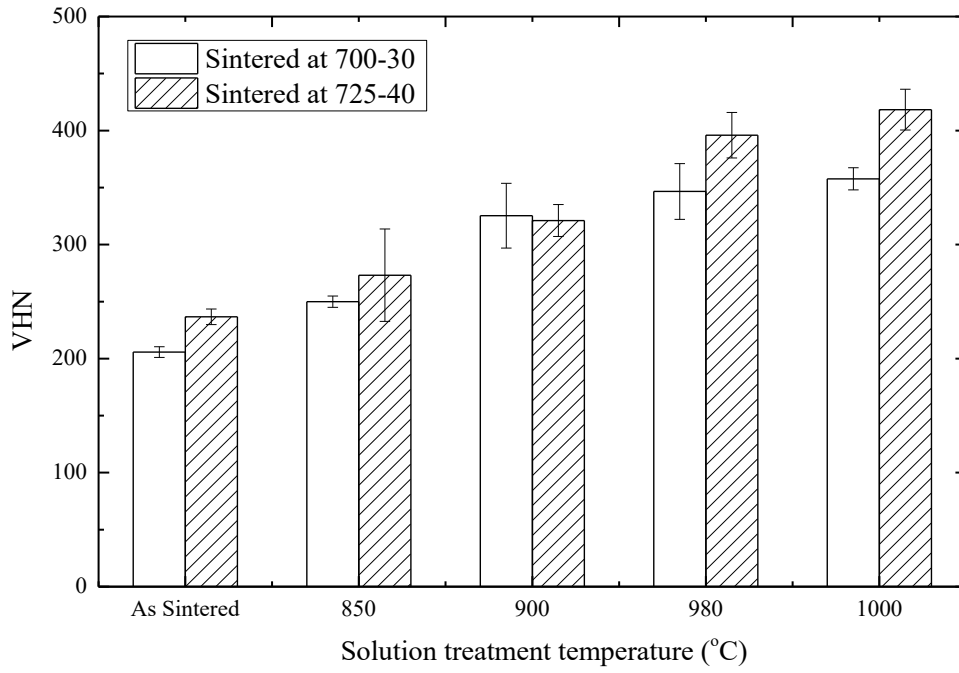


Figure 4. 14 Micro-Vickers results of sintered samples solution treated at different temperature for 1 hour

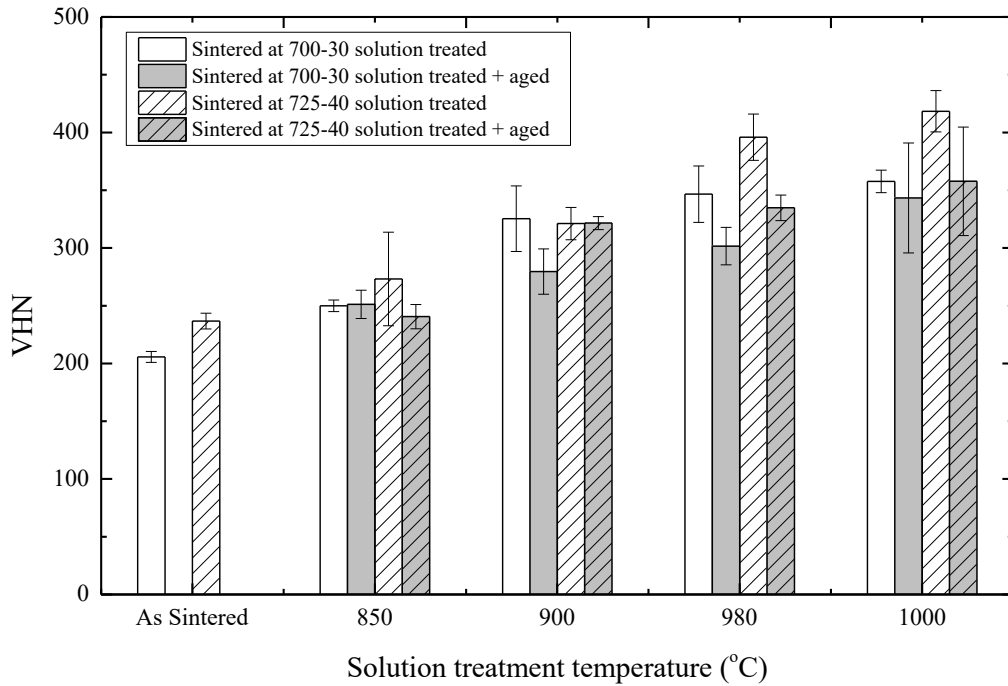


Figure 4. 15 Micro-Vickers results of sintered samples solution treated at different temperature for 1 hour and aged at 530 °C for 6 hours

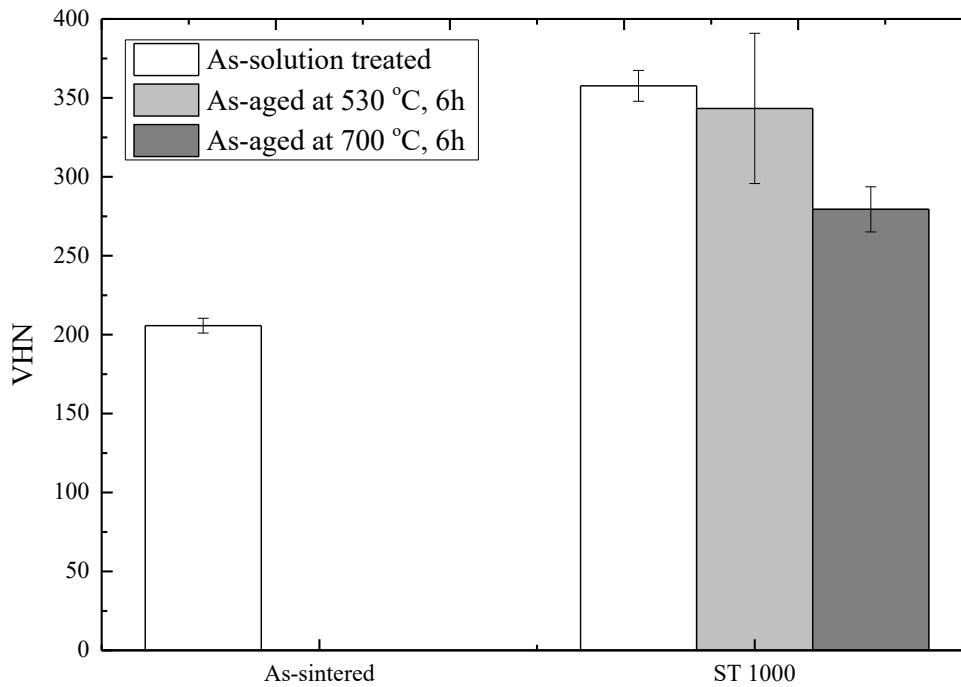


Figure 4. 16 Micro-Vickers results of sample sintered at 700 °C, 30 MPa solution treated at 1000 °C and aged at different temperature

4.4 Discussion

4.4.1 Influence of solution treatment to microstructure and hardness

According to phase diagram in figure 4.17 at room temperature due small amount of vanadium content as β stabilized element, this alloy contain α and β phases. Heating the alloy below its β solvus temperature will form two phases namely HCP α phase and BCC α phase with higher fraction of α phase. Figure 4.18 shows the decrease of α phase grain size as the temperature of solution treatment increase while β phase grain size increase as its volume fraction increase upon heating. After quenching, α phase retains its crystal. Upon cooling vanadium content in α phase changes a little along α solvus line. On the other hand, the enrichment of vanadium in β phase along α solvus line is observed. At 850 and 900 °C, vanadium content in β phase is about 12 wt. % and 10 wt. %. Thus, upon quenching β phase is able to keep its BCC structure at room temperature, namely metastable β phase which slightly increase the hardness. Also from the phase diagram, the β solvus temperature is about 980 °C. Heating the alloy higher than its β solvus temperature to 1000 °C will form β single phase.

Upon the quenching this β phase will transform into hexagonal α' martensite which increase the hardness of samples.

Table 4.2 shows the summary of phases after quenching of spark plasma sintered samples which are solution treated at different temperature. Comparing to the phases constituent from phase diagram, at 1000 °C notable amount of retained α phase is still observed in the microstructure of solution treated sample (figure 4.3(d) and 4.4(d)). This suggest that β solvus temperature of spark plasma sintered Ti-6Al-4V is higher than 1000 °C. Solution treatment at higher temperature 1050 °C is also formed retained α phase as shown in figure 4.11 (c-d).

Figure 4. 19 shows the schematic microstructural evolution of as-sintered samples during heating at prior solution temperature and quenching and during aging. At 850 – 900 °C the samples contain α and β phase. Upon quenching β phase maintain its BCC structure and stays as metastable β phase. Aging treatment generates the transformation of more stable β phase with higher vanadium content while vanadium lean phase transform to α phase. At solution treatment higher than 980 °C, β phase transform into α' martensite after quenching. Upon aging treatment, α' phase decomposes into α and β phases.

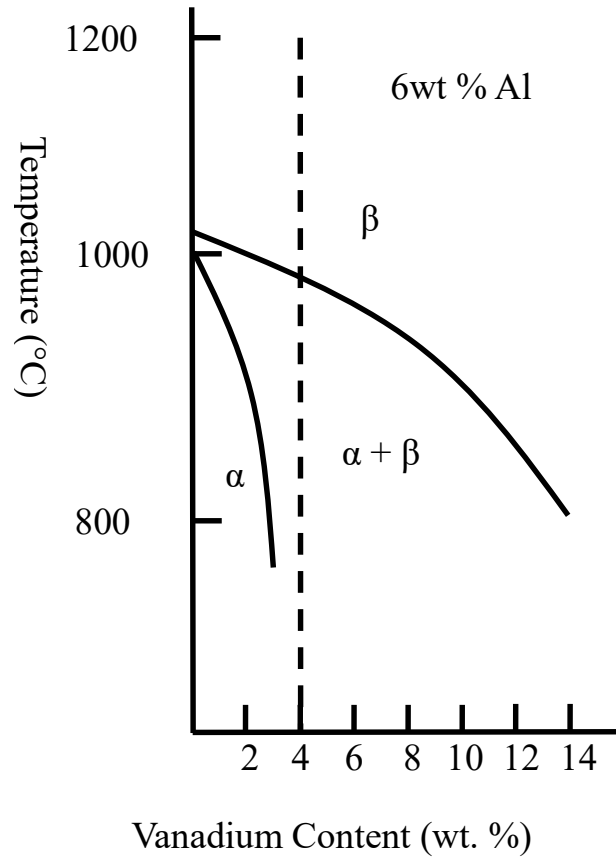


Figure 4. 17 Phase diagram of Titanium containing 6 wt. % Al with different vanadium content [7]

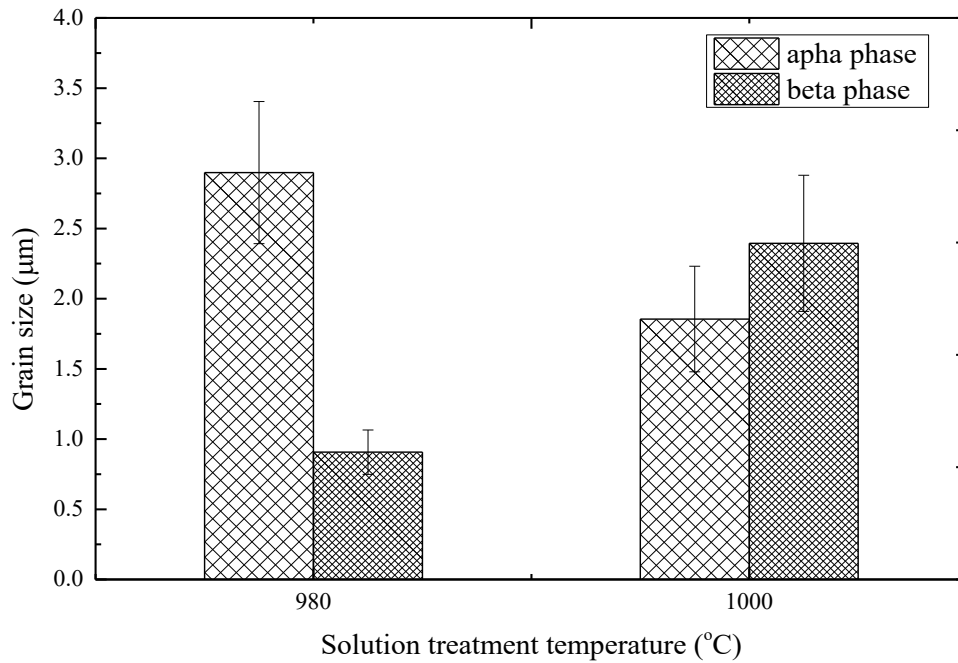


Figure 4. 18 Grain size of α - and β -phase which transform into α' martensite of samples sintered at 700 °C, 30 MPa solution treated at different solution treatment

Table 4. 2 Phase constitution of spark plasma sintered samples sintered at different sintering condition after solution treatment at different temperature followed by quenching

Sintering Condition	Solution treatment (°C)	Phases upon quenching
700 °C, 30 MPa	850	α +metastable β
	900	α +metastable β
	980	α + α'
	1000	α + α'
725 °C, 40 MPa	850	α +metastable β
	900	α +metastable β
	980	α + α'
	1000	α + α'

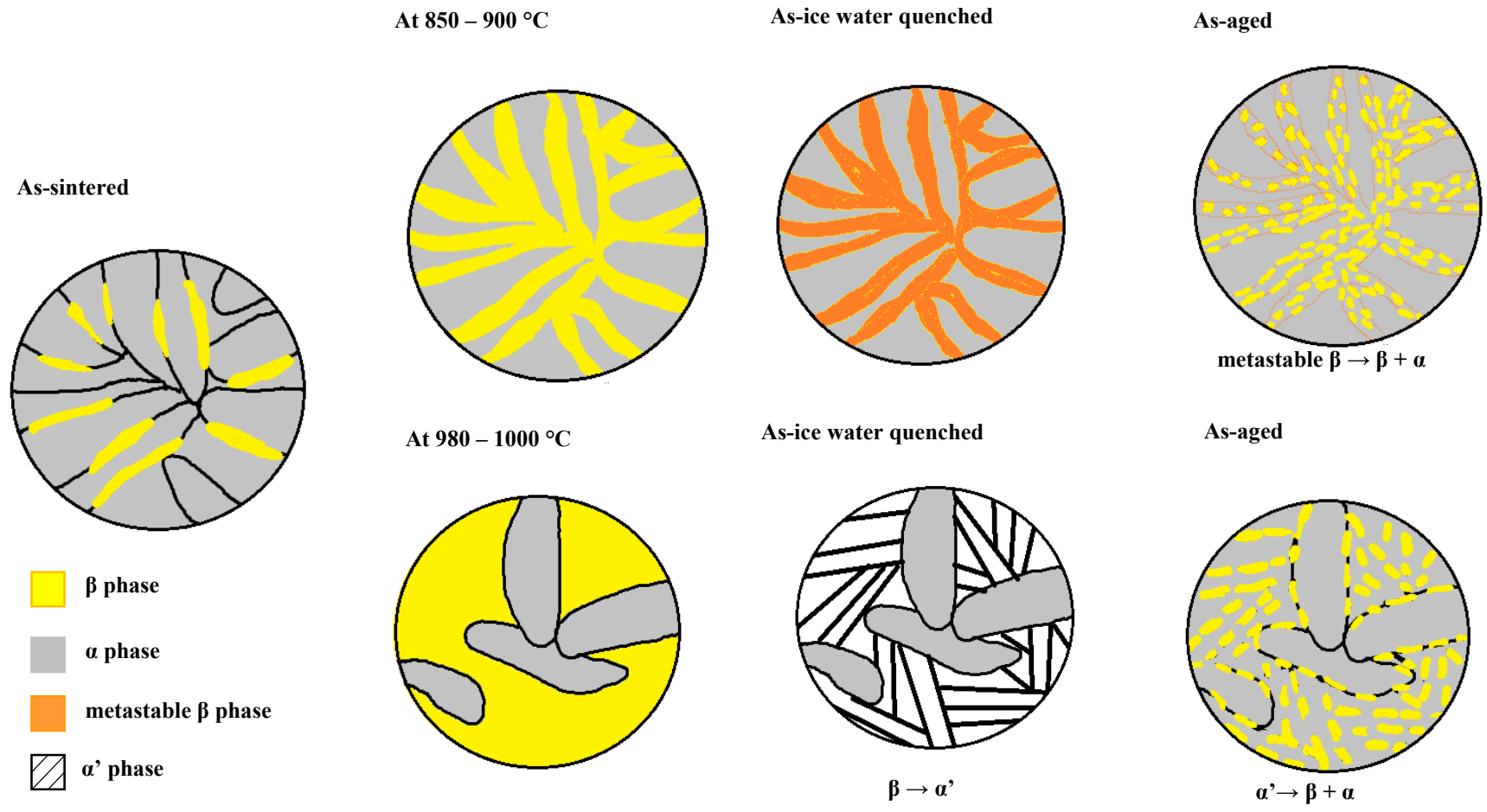


Figure 4. 19 Schematic microstructural evolution during solution treatment and aging

4.4.2 Influence of aging to microstructure and hardness

Aging treatment at both 530 and 700 °C enhances the decomposition of α' to α and β phase. Coarser α phase is formed at higher temperature. This β phase formed firstly along α' grain boundary and interface of α' plate [9] as shown in figure 4.11. The β phase aligned on certain direction parallel to the direction of martensite phase, marked by the arrow in figure 4.11. This decomposition generates the decrease of samples' hardness. In addition, comparing the microstructure as-solution-treated samples in figure 4.3 and figure 4.4 and as-aged samples in figure 4.6 and figure 4.7, it is shown that during aging α phase grows. Thus, the hardness of aged samples decrease. The highest hardness was achieved by sample contained α and α' result from solution treatment at 1000 °C.

4.5 Conclusions

In this chapter the influence of solution treatment and aging to the hardness of spark plasma sintered Ti-6Al-4V is summarized as follow:

- (1) Upon quenching, martensite phase only formed by sample solution treatment above 980 °C. Due to high vanadium content which stabilized the BCC structure, quenching below such temperature produces metastable β phase.
- (2) Aging treatment enhances formation of β phase precipitate. Thus, after aging martensite decomposes to rich vanadium β phase, which form along the grain boundary of martensite and aligned along interface of martensite plate, and lean vanadium α phase. The decomposition then decrease the hardness of the sample.
- (3) Even after heating at 1050 °C, retained α -phase is still observed, implies that the β tansus temperature of spark plasma sintered Ti-6Al-4V is higher than 1050 °C.

4.6 References

- [1] G. Lütjering, "Influence of processing on microstructure and mechanical properties of (α + β) titanium alloys," *Materials Science and Engineering: A*, vol. 243, no. 1-2, pp. 32-45, 1998.
- [2] S. L. Semiatin, V. Seetharaman and I. Weiss, "Advances in the Science and Technology of Titanium Alloy Processing," in *TMS*, Warrendale, Pennsylvania, 1996.
- [3] Y. Lee and G. Welsch, "Young's Modulus and Damping of Ti-6Al-4V Alloy as a Function of Heat Treatment and Oxygen Concentration," *Materials Science and Engineering A*, vol. 128, pp. 77-89, 1990.
- [4] Y. Lee, M. Peters and G. Welsch, "Elastic Moduli and Tensile and Physical Properties of Heat-Treated and Quenched Powder Metallurgical Ti-6Al-4V Alloy," *Metallurgical Transactions A*, vol. 22A, no. 3, pp. 709-714, 1991.
- [5] G. Welsch, R. Boyer and E. W. Collings, "Ti-6Al-4V," in *Materials Properties Handbook: Titanium Alloys*, Materials Park, Ohio: ASM International, 1994, pp. 483-636.
- [6] J.-T. Yeom, J. H. Kim, J.-K. Hong, N.-K. Park and C. S. Lee, "Prediction of Microstructure Evolution in Hot Backward Extrusion of Ti-6Al-4V Alloy," *Journal of Metallurgy*, vol. 2012, p. Article ID 989834, 2012.
- [7] R. Pederson, "Microstructure and Phase Transformation of Ti-6Al-4V," in *Microstructure and Phase Transformation of Ti-6Al-4V (Licentiate Thesis)*, Luleå, Luleå University of Technology, 2002, p. 14.
- [8] F. Hideki, "Strengthening of α + β titanium alloys by thermomechanical processing," *Materials Science and Engineering: A*, vol. 243, p. 103–108, 1998.
- [9] J. Li and H. Wang, "Aging Response of Laser Melting Deposited Ti-6Al-2Zr-1Mo-1V Alloy," *Materials Science and Engineering A*, vol. 560, pp. 193-199, 2013.

Chapter 5 Influence of Solution Treatment and Oxygen Content to Microstructure and Mechanical Properties of Porous Ti-6Al-4V

5.1 Introduction

From chapter 4, it was found rather than increase the hardness, aging treatment decrease the hardness of samples. In this chapter the effectivity of solution treatment to microstructure and mechanical properties of porous Ti-6Al-4V fabricated by solid-state space holder method will be discussed. Additionally, it also is revealed that even after heating the samples at 1050 °C, retained α phase is still observed at the microstructure, implies that the β transus temperature of spark plasma sintered Ti-6Al-4V is higher than 1050 °C. The increase the β transus temperature is most likely due to oxygen content in spark plasma sintered sample. Thus, solution treatment at temperature higher than 1050 °C also will be done. In addition, the effect of oxygen content to microstructure and mechanical properties of porous Ti-6Al-4V by oxygen dissolving process will also discussed.

5.2 Experimental Procedures

5.2.1 Fabrication of porous sample

Porous Ti-6Al-4V was prepared by solid-state space holder method. Metal powder in the size of ~45 μm and sodium chloride as space holder in the size 600 – 425 μm with 50 vol. %: 50 vol. % ratio were mixed with the addition of ethanol as process control agent (PCA). Powder mixture was compacted in a 20-mm inner diameter graphite die and then was sintered at 700 °C, 30 MPa under a vacuum condition about 13 Pa using a spark plasma sintering machine (SPS 511S, SPS Syntex) for 20 minutes with slow and high heating rate as described in figure 5.1.

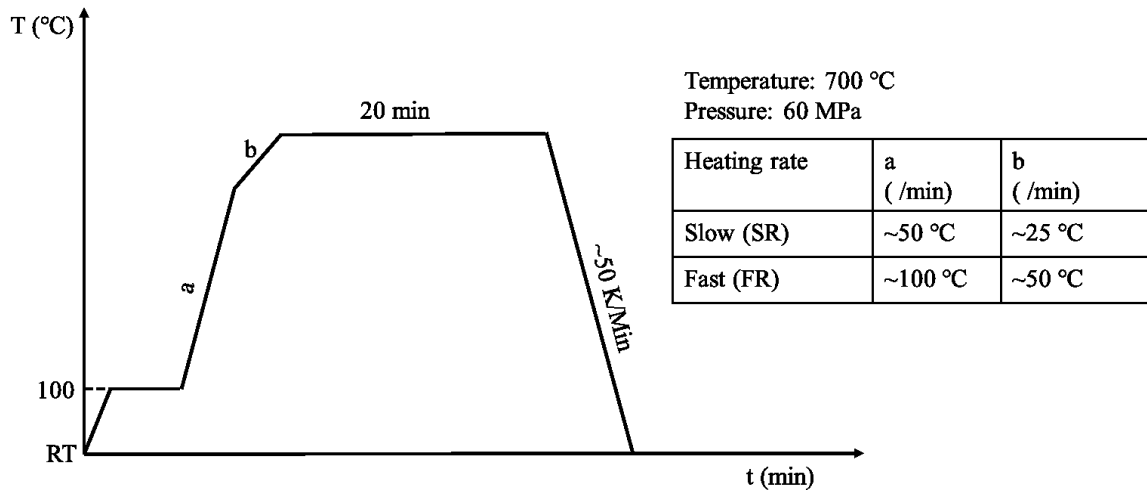


Figure 5. 1 Sintering program

Ti-6Al-4V/NaCl composite then was cut using micro-cutter into dimension of about 5 x 5 x 15 mm. Removal of sodium chloride is then performed by immersing the sample in warm distilled water (around 30 – 40 °C) for 2 hours with cycle of changing the water every 30 minutes in an ultrasonic cleanser machine. Density and open porosity of samples is calculated by equation 2.1 and 2.2.

5.2.2 Heat treatment

Porous Ti-6Al-4V is then subjected to solution treatment at temperature in the range of 850 – 1400 °C for 1 hour. Solution treatment at 850 – 1000 °C was performed in an argon flow furnace followed by ice water quenching (WQ) while at 1300 and 1400 °C was performed in an ultra-high-vacuum furnace followed by furnace cooling (FC). An elemental analysis by inert gas fusion (LECO) was performed in order to measure the oxygen composition of samples sintered with different sintering program and after solution treatment. For further understanding of the influence of oxygen, sample that solution treated at 1000 °C then heated at 530 °C for 6 hours followed by air cooling in the argon furnace to let oxygen diffuse to the samples. This process will be further called oxygen-dissolving process. The microstructural change of samples and mechanical properties of samples were examined respectively by High temperature-XRD (HT-XRD), SEM/EDS and compression test.

5.3 Results

5.3.1 Oxygen concentration change

Table 5.1 is the results of oxygen concentration test of both sintered Ti-6Al-4V and porous Ti-6Al-4V. Porous sample was produced from as-space-holder-removed composite contained 50 vol. % Ti-6Al-4V and 50 vol. % sodium chloride as the space holder. It is shown from the results that after sintering, oxygen concentration in sample increase, compare to oxygen concentration of powder in chapter 2 table 2.1. For sintered Ti-6Al-4V, changing total sintering time by varied its heating rate only results to a little increase of oxygen concentration. In contrast, a notable increment of oxygen concentration is observed for porous sample sintered with different heating rate. After heat treatment, the oxygen concentration of porous samples also increase.

Lefebvre *et al.* [1] described how oxygen content in titanium foams change during several heat treatment process in their work of oxygen concentration and distribution of titanium foams. It was reported that oxygen comes from the thin oxide surface layer (TiO_2), usually in the thickness between 2 – 7 nm [2], which is naturally formed by titanium alloys after they were expose to the atmospheric environment. During heat treatment, the oxide layer easily dissolved and the oxygen will interstitially solutes into titanium crystal structure [3], especially in α -titanium. Upon cooling and being exposed to the atmospheric condition, the oxide layer will form again. The cycle of dissolving and formation of the oxide layer during heating and cooling will increase the total oxygen concentration in samples. It was also reported that sample which has higher surface area exhibits higher total oxygen content.

Table 5. 1 Oxygen content results of sintered Ti-6Al-4V and porous Ti-6Al-4V at different sintering heating rate and heat treatment

Sample	Sintering heating rate	Heat treatment	Oxygen concentration (wt. %)
Ti-6Al-4V	Low heating rate	No	0.223
	High heating rate	No	0.222
Porous Ti-6Al-4V	Low heating rate	No	0.294
		Solution treatment @ 850 °C, 1h → Ice WQ	0.811
		Solution treatment @ 1000 °C, 1h → Ice WQ	0.961
		Solution treatment @ 1000 °C, 1h → Ice WQ + Oxygen-dissolving @ 530 °C, 6h → AC	1.74
	High heating rate	No	0.279

5.3.2 High-temperature XRD

Figure 5.2 is high temperature XRD results for powder Ti-6Al-4V at room temperature and elevated temperature until 1100 °C. At room temperature, the pattern shows α and β phase pattern. At high temperature the patterns are the mixed of several phases including α and β phase, Ti_3Al α_2 phase and TiC phase. Up to 600 °C small peak at low angle 2θ value between $20^\circ - 30^\circ$ is observed, indicates Ti_3Al α_2 phase.

Figure 5.3 and 5.5 are high temperature XRD results for spark plasma sintered Ti-6Al-4V at room temperature and elevated temperature until 1200 °C. At room temperature the results are similar to the pattern of Ti-6Al-4V powder, it contains XRD patterns of α and β phase. At high temperature, the result shows some more pattern of β phase at high angle 2θ value between $50^\circ - 55^\circ$ and around 70° . Contrarily, Ti_3Al α_2 phase peaks are only observed at temperature between 800 – 900 °C. XRD patterns at lower 2θ value, as shown in figure 5.4 and 5.6, confirms that at 1000 °C, α_2 peaks disappears in both samples sintered at different sintering condition. Table 5.2 shows the summary of phase constituent at elevated temperature based on HT-XRD. From the phase constituent summary in table 5.2, it is revealed that for both powder Ti-6Al-4V and as-sintered Ti-6Al-4V, even after heating as high as 1200 °C samples still contain α phase.

5.3.3 Microstructural change after solution treatment

The SEM images of porous Ti-6Al-4V solution treated at several temperatures in argon flow furnace followed by ice water quenched are shown in figure 5.7 – 5.9. At low magnification, pore surface is not clearly observed because the samples were embedded to epoxy resin. The epoxy resin was marked with red arrow. At higher magnification, the microstructure of solution treated porous samples have similar microstructure with spark plasma sintered Ti-6Al-4V. ST 850 sample has the structure of thin layer of metastable β phase, marked with white arrow, in between α phase. ST 980 and 1000 samples' microstructure contain needle-like α' and α phase.

Figure 5.10 is the SEM of samples solution treated at 1300 and 1400 °C in ultra-high-vacuum furnace followed by furnace cooling. At low magnification, it was observed a smoother macro-pore surface in both of solution treatment condition is observed. Denser structure and lesser micro-porosity are also observed. At higher magnification, the microstructure contains Widmanstätten structure of α and β phase without remaining retained α phase. The EDS results in figure 5.11 confirm the β phase is vanadium rich phase.

5.3.4 Mechanical properties after solution treatment

Figure 5.12 shows the mechanical properties of porous Ti-6Al-4V, including compressive strength (figure 5.12(a)) and Young's modulus (figure 5.12(b)), solution treated at several solution treatment temperatures in the argon flow furnace. Notable increment of compressive strength is observed at sample solution treated at 1000 °C while solution treatment at 850 and 980 °C only result a little increase of samples' strength. As shown in figure 5.12(b), solution treatment changes samples' Young's modulus a little. The lowest value of Young's modulus was resulted from samples solution treated at 850 °C. Increasing solution treatment temperature then increase sample's Young's modulus.

The compressive strength and Young's modulus of porous Ti-6Al-4V solution treated at 1300 and 1400 °C in vacuum furnace are summarized respectively in figure 5.13(a) and figure 5.13(b). Comparing the compressive strength of ST 1300 and ST 1400 samples and as-sintered sample, solution treatment at 1300 and 1400 °C increase sample's compressional strength until about twice. This increase is also followed by the increase sample's Young's modulus.

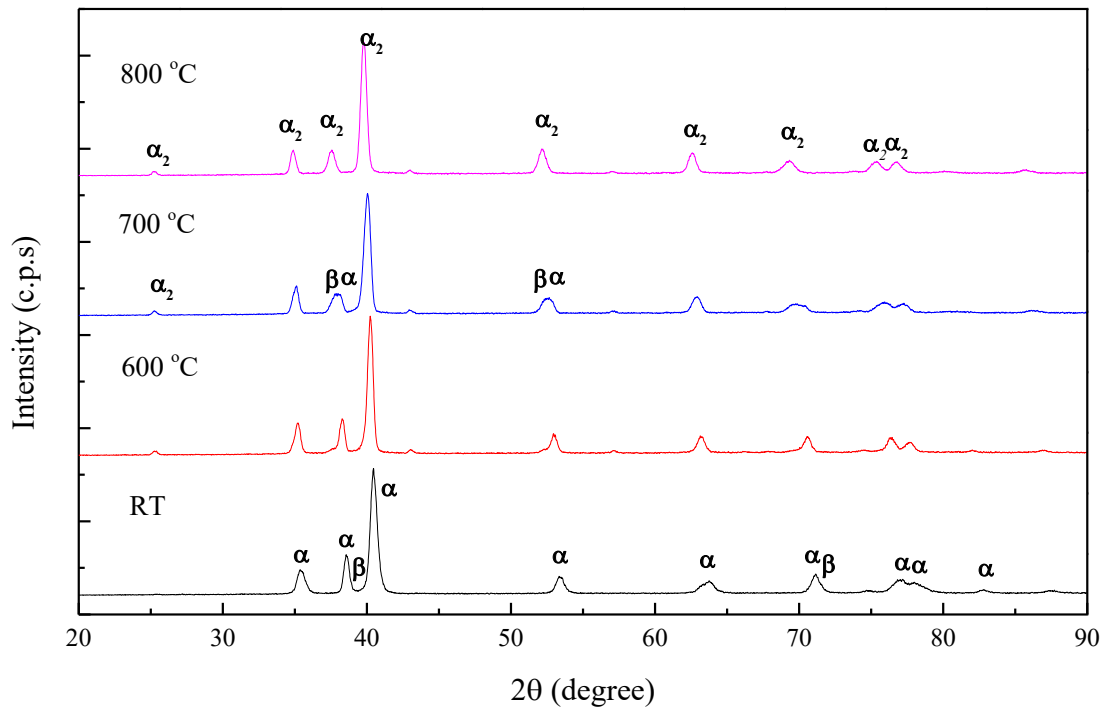
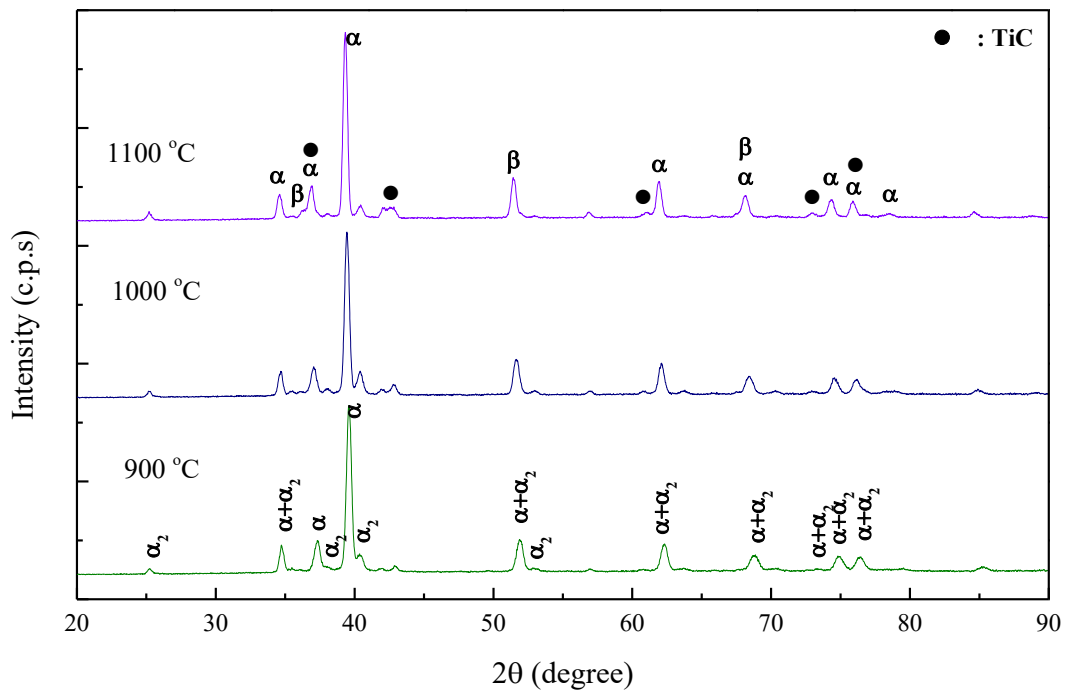


Figure 5. 2 High temperature XRD of powder Ti-6Al-4V at elevated temperature

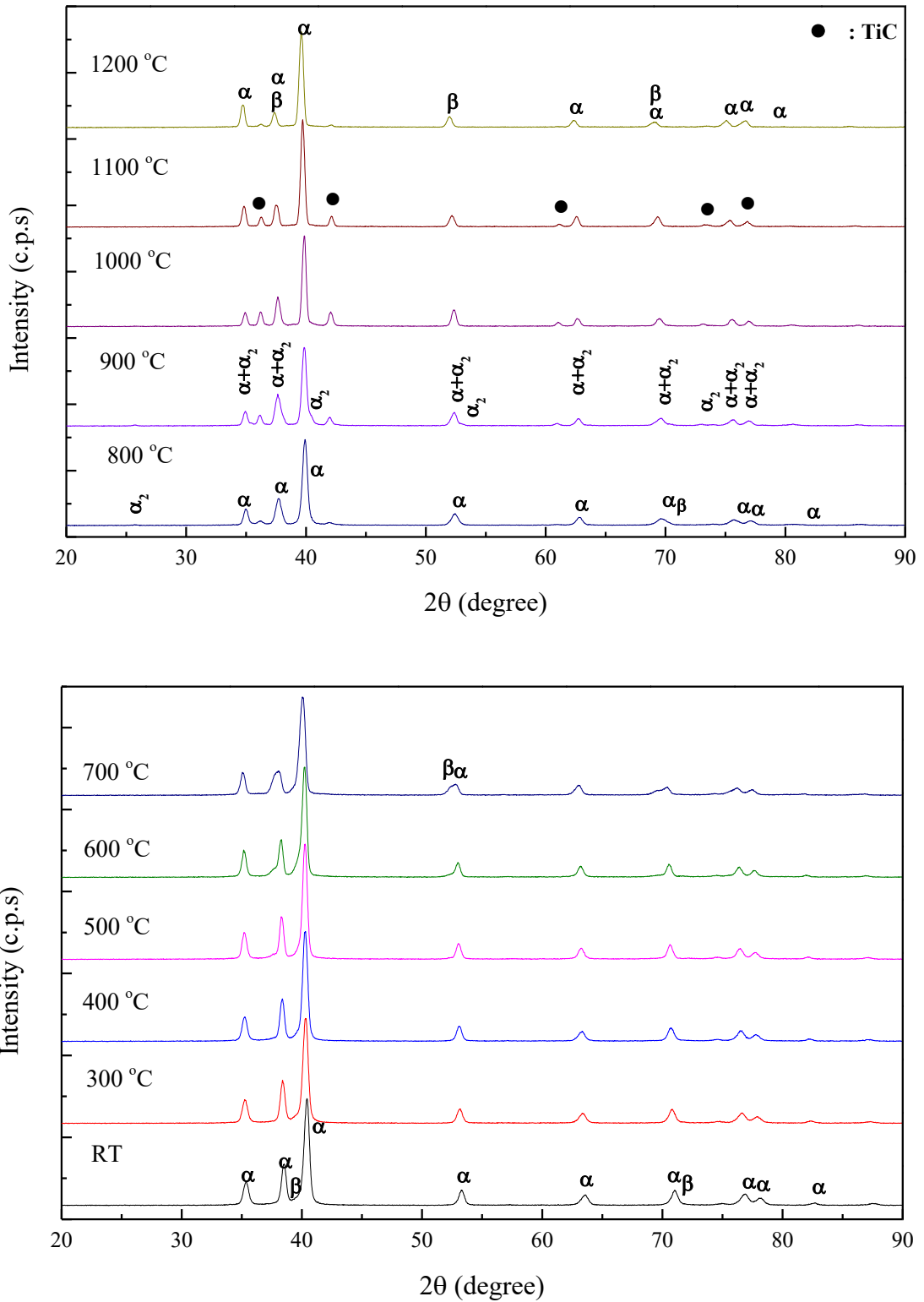


Figure 5. 3 High temperature XRD of Ti-6Al-4V sintered at 700 °C, 30 MPa at elevated temperature

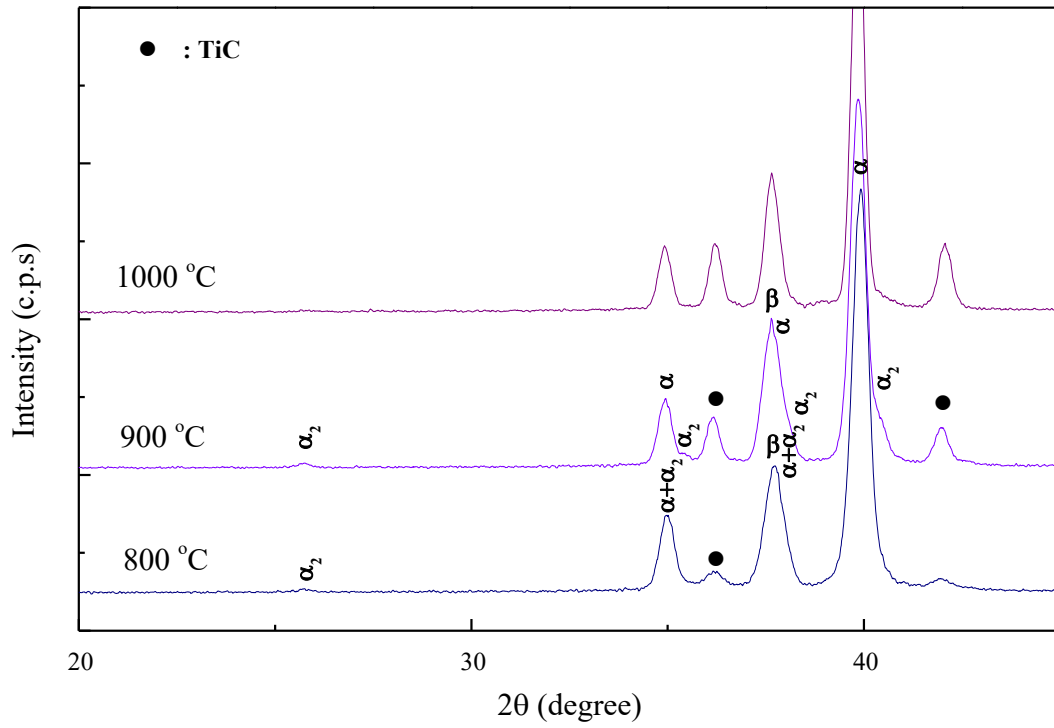


Figure 5. 4 High temperature XRD of Ti-6Al-4V sintered at 700 °C, 30 MPa at elevated temperature for low angle 2θ value between $20^\circ - 40^\circ$

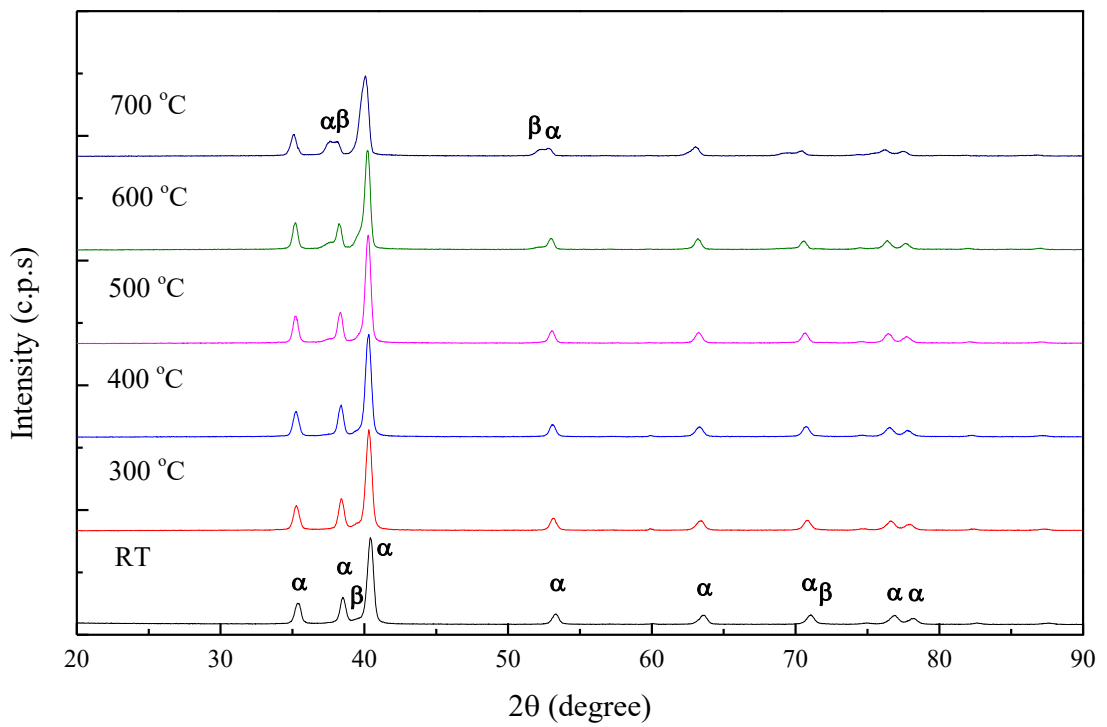
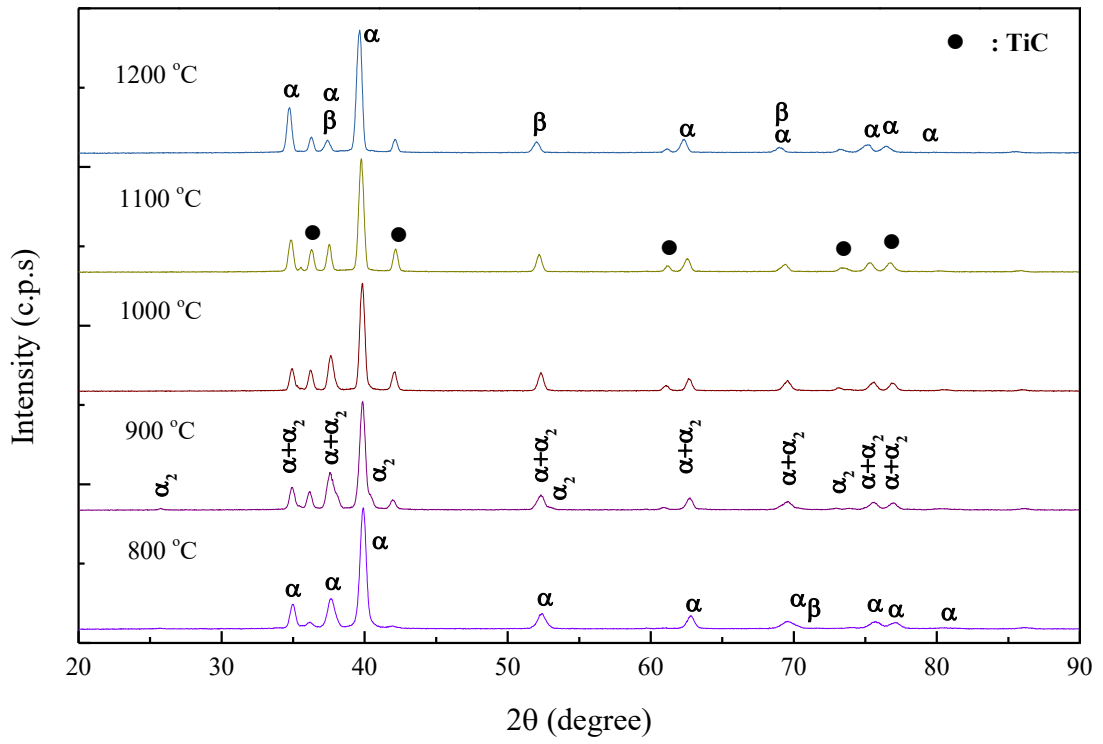


Figure 5. 5 High temperature XRD of Ti-6Al-4V sintered at 725 °C, 40 MPa at elevated temperature

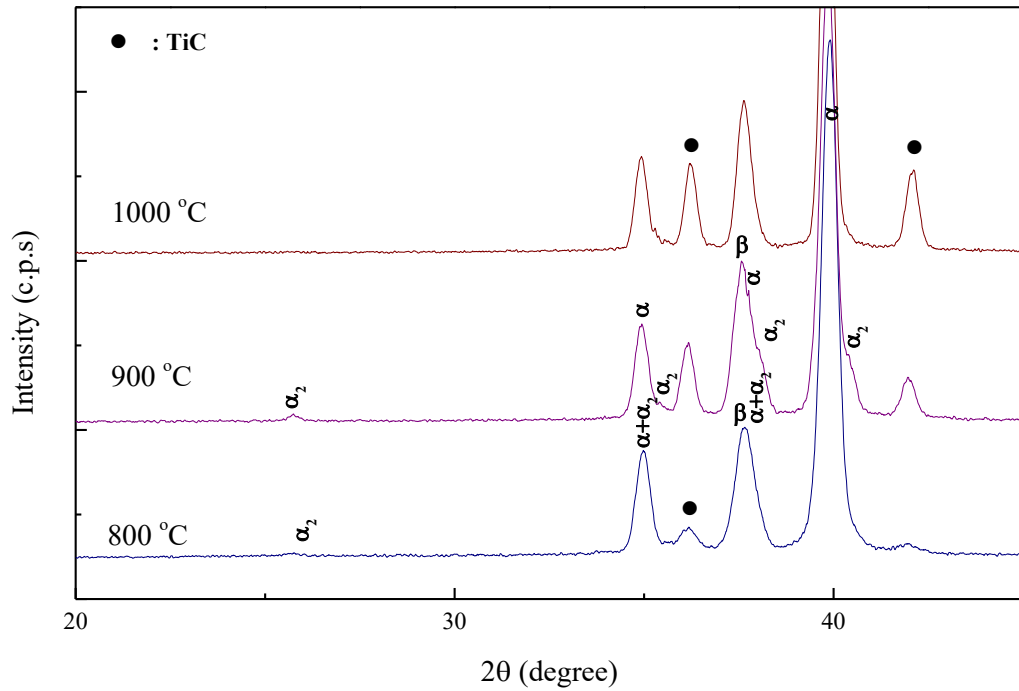


Figure 5. 6 High temperature XRD of Ti-6Al-4V sintered at 725 °C, 40 MPa at elevated temperature for low angle 2θ value between $20^\circ - 40^\circ$

Table 5. 2 Summary of phase constituent from HT-XRD results

Temperature (°C)	Sample		
	Powder	Sintered at 700 °C, 30 MPa	Sintered at 725 °C, 40 MPa
Room temperature	$\alpha + \beta$	$\alpha + \beta$	$\alpha + \beta$
300	-	$\alpha + \beta$	$\alpha + \beta$
400	-	$\alpha + \beta$	$\alpha + \beta$
500	-	$\alpha + \beta$	$\alpha + \beta$
600	$\alpha + \alpha_2 + \beta$	$\alpha + \beta$	$\alpha + \beta$
700	$\alpha + \alpha_2 + \beta$	$\alpha + \beta$	$\alpha + \beta$
800	$\alpha + \alpha_2 + \beta$	$\alpha + \alpha_2 + \beta + \text{TiC}$	$\alpha + \alpha_2 + \beta + \text{TiC}$
900	$\alpha + \alpha_2 + \beta + \text{TiC}$	$\alpha + \alpha_2 + \beta + \text{TiC}$	$\alpha + \alpha_2 + \beta + \text{TiC}$
1000	$\alpha + \alpha_2 + \beta + \text{TiC}$	$\alpha + \beta + \text{TiC}$	$\alpha + \beta + \text{TiC}$
1100	$\alpha + \alpha_2 + \beta + \text{TiC}$	$\alpha + \beta + \text{TiC}$	$\alpha + \beta + \text{TiC}$
1200	$\alpha + \alpha_2 + \beta + \text{TiC}$	$\alpha + \beta + \text{TiC}$	$\alpha + \beta + \text{TiC}$

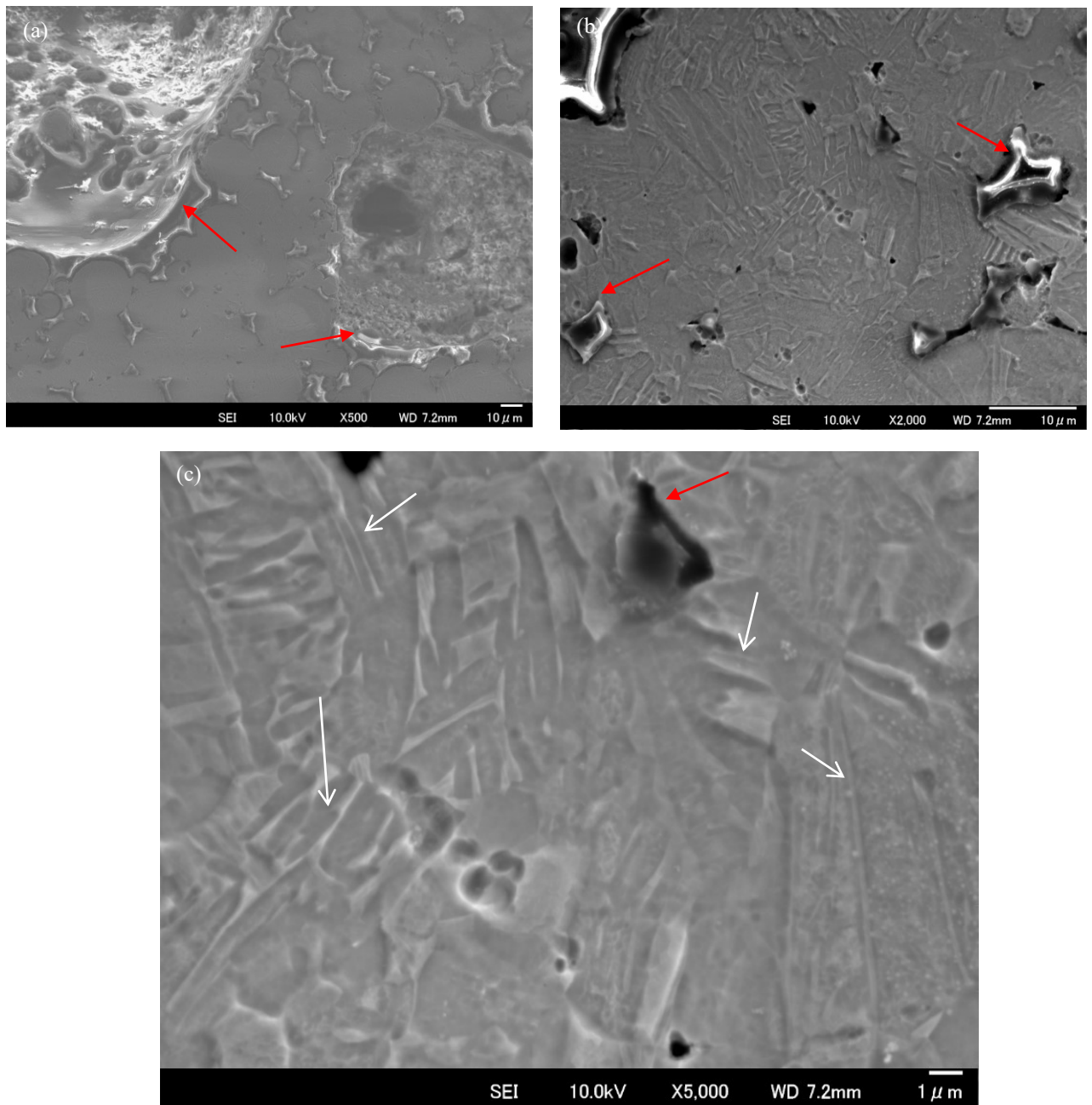


Figure 5. 7 SEM images of porous Ti-6Al-4V solution treated at 850 °C in argon flow furnace for 1h followed by ice water quenched at low magnification (a) and high magnification (b-c)

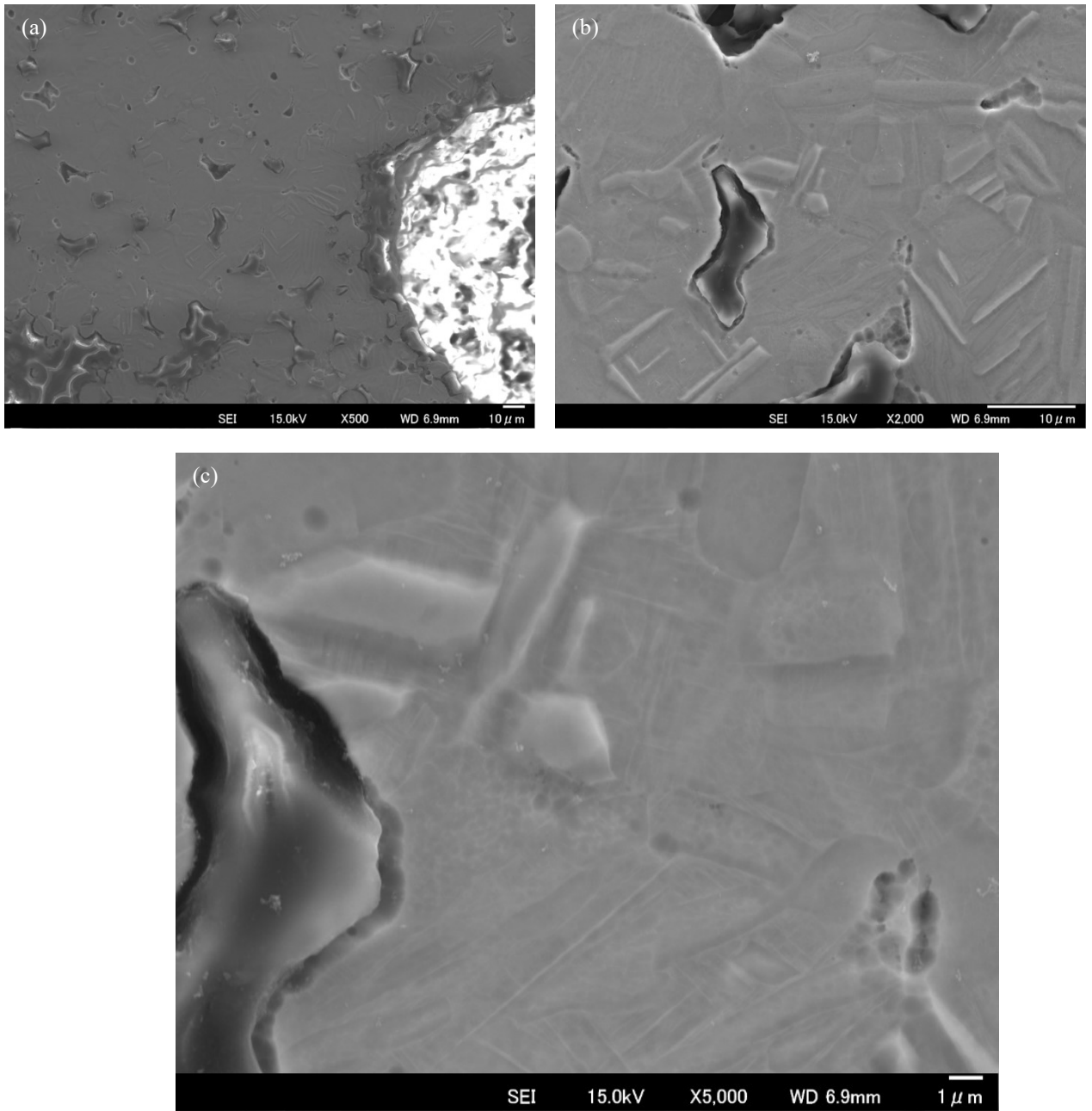


Figure 5. 8 SEM images of porous Ti-6Al-4V solution treated at 980 °C in argon flow furnace for 1h followed by ice water quenched at low magnification (a) and high magnification (b-c)

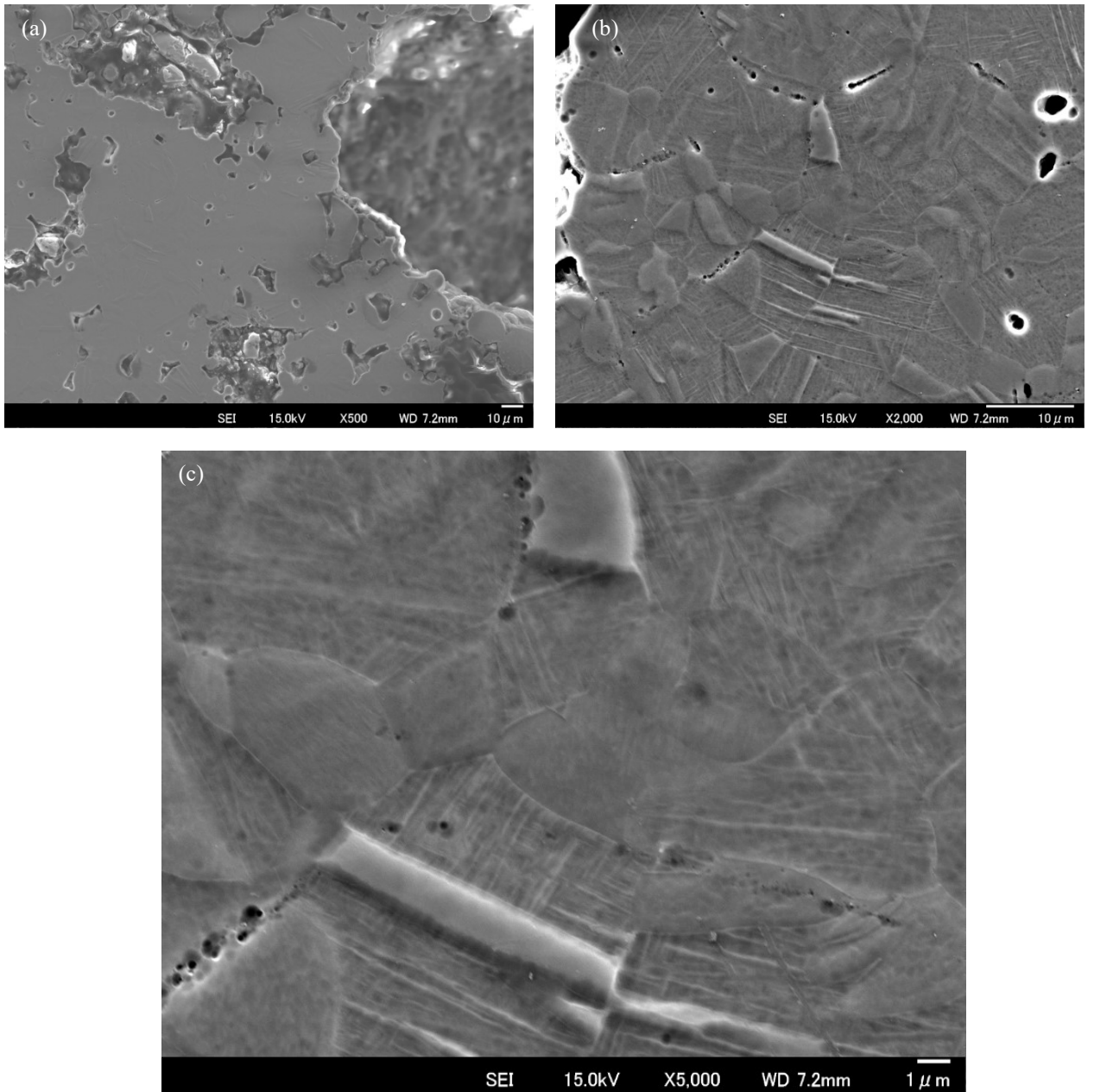


Figure 5. 9 SEM images of porous Ti-6Al-4V solution treated at 1000 °C in argon flow furnace for 1h followed by ice water quenched at low magnification (a) and high magnification (b-c)

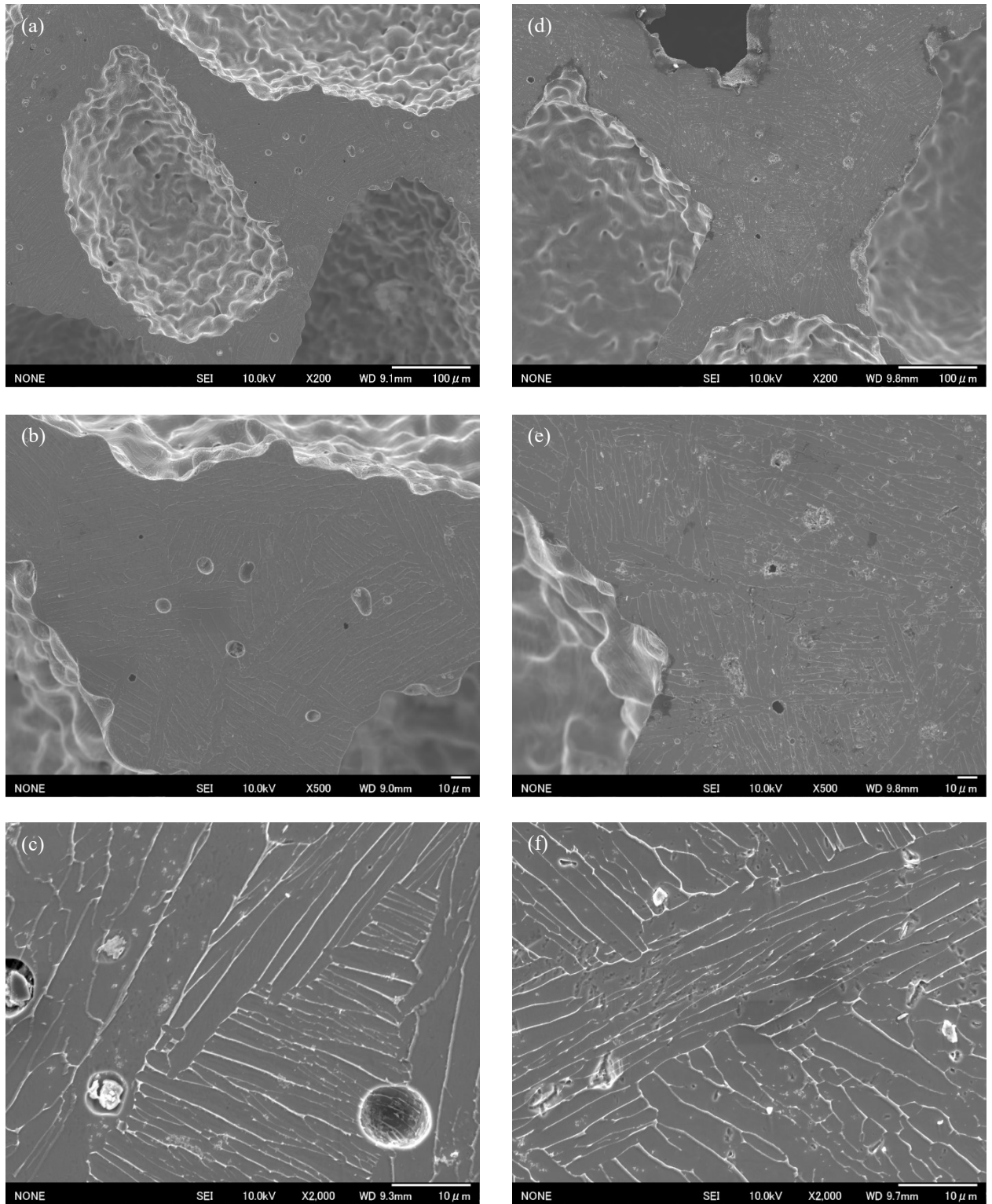


Figure 5. 10 SEM images of porous Ti-6Al-4V solution treated at 1300 °C at low magnification (a-b) and high magnification (c) and 1400 °C at low magnification (d-e) and high magnification (f) in ultra-high-vacuum furnace followed by furnace cooling

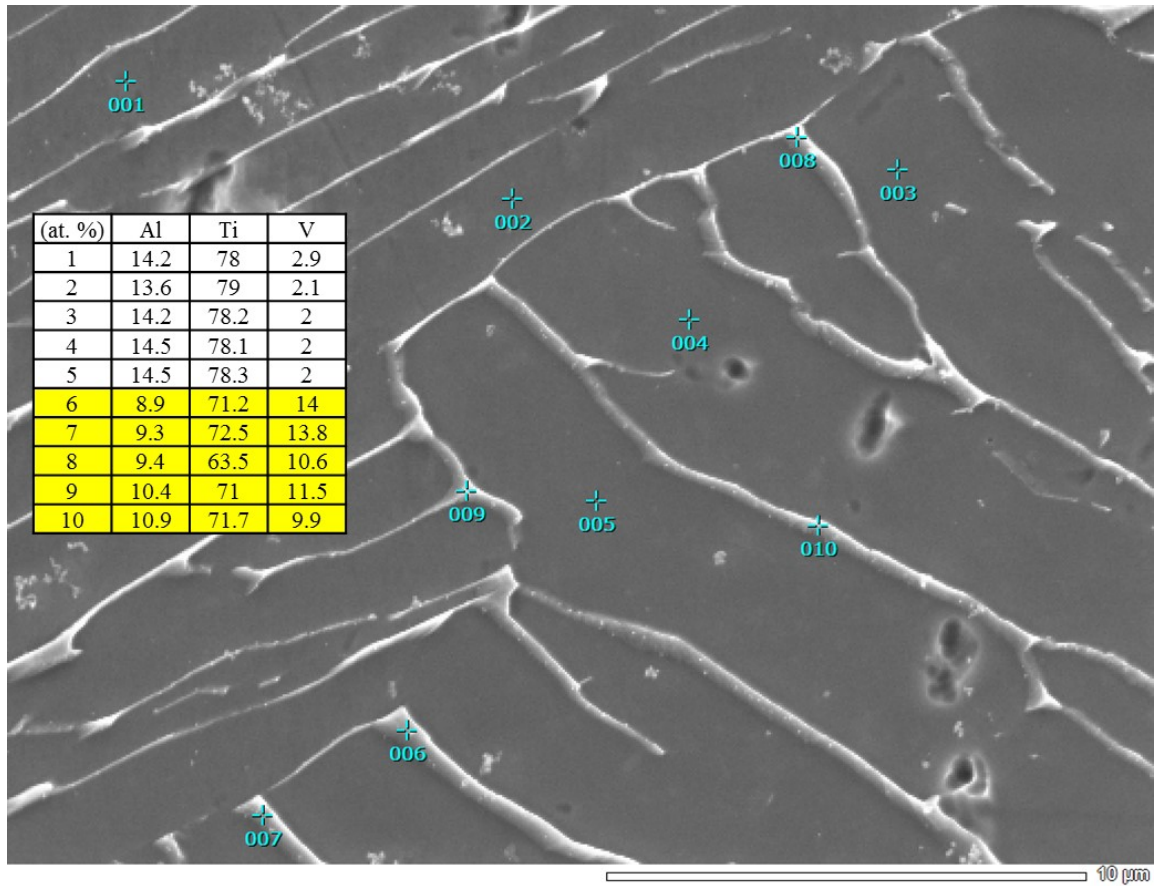


Figure 5. 11 EDS results of sample solution treated at 1400 °C in ultra-high-vacuum furnace followed by furnace cooling

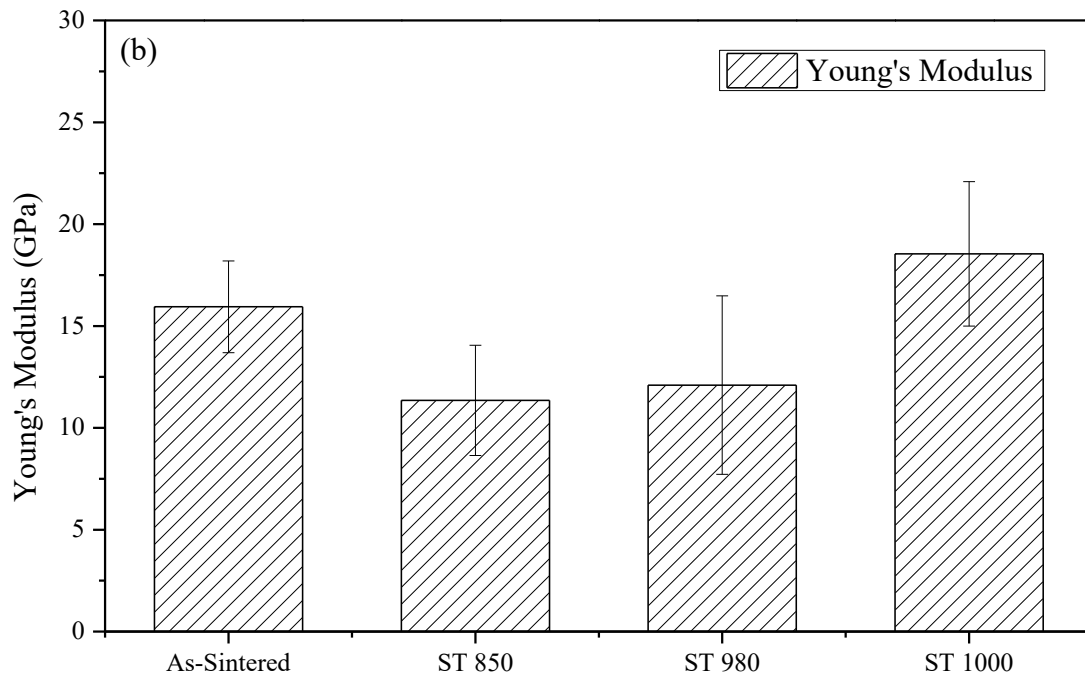
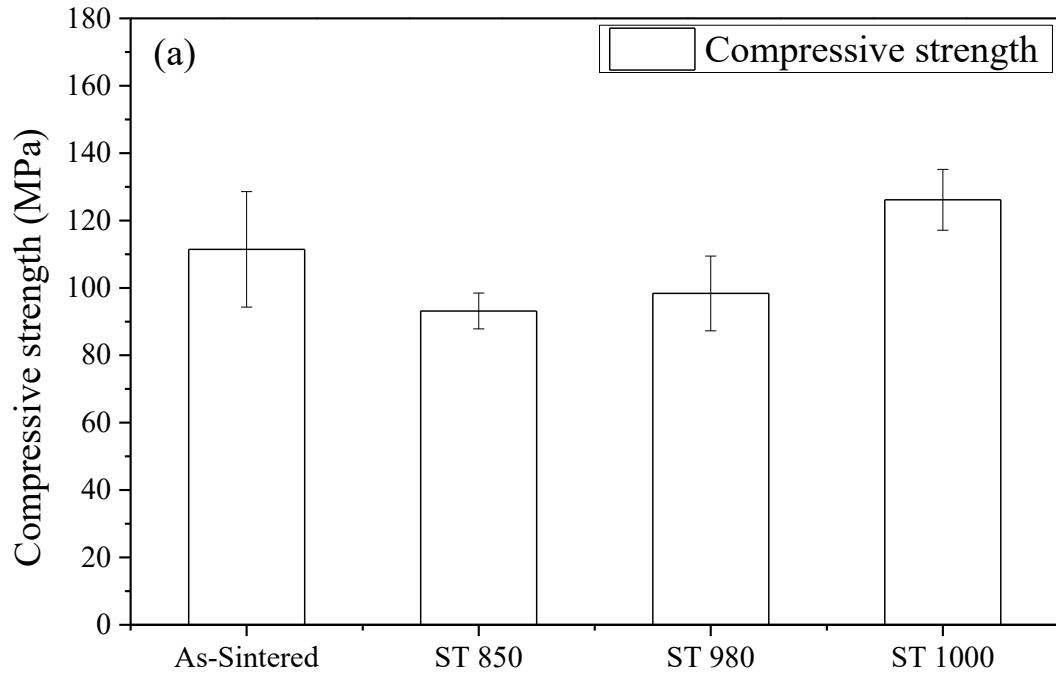


Figure 5. 12 Mechanical properties of porous Ti-6Al-4V after solution treatment in argon flow furnace at several temperature

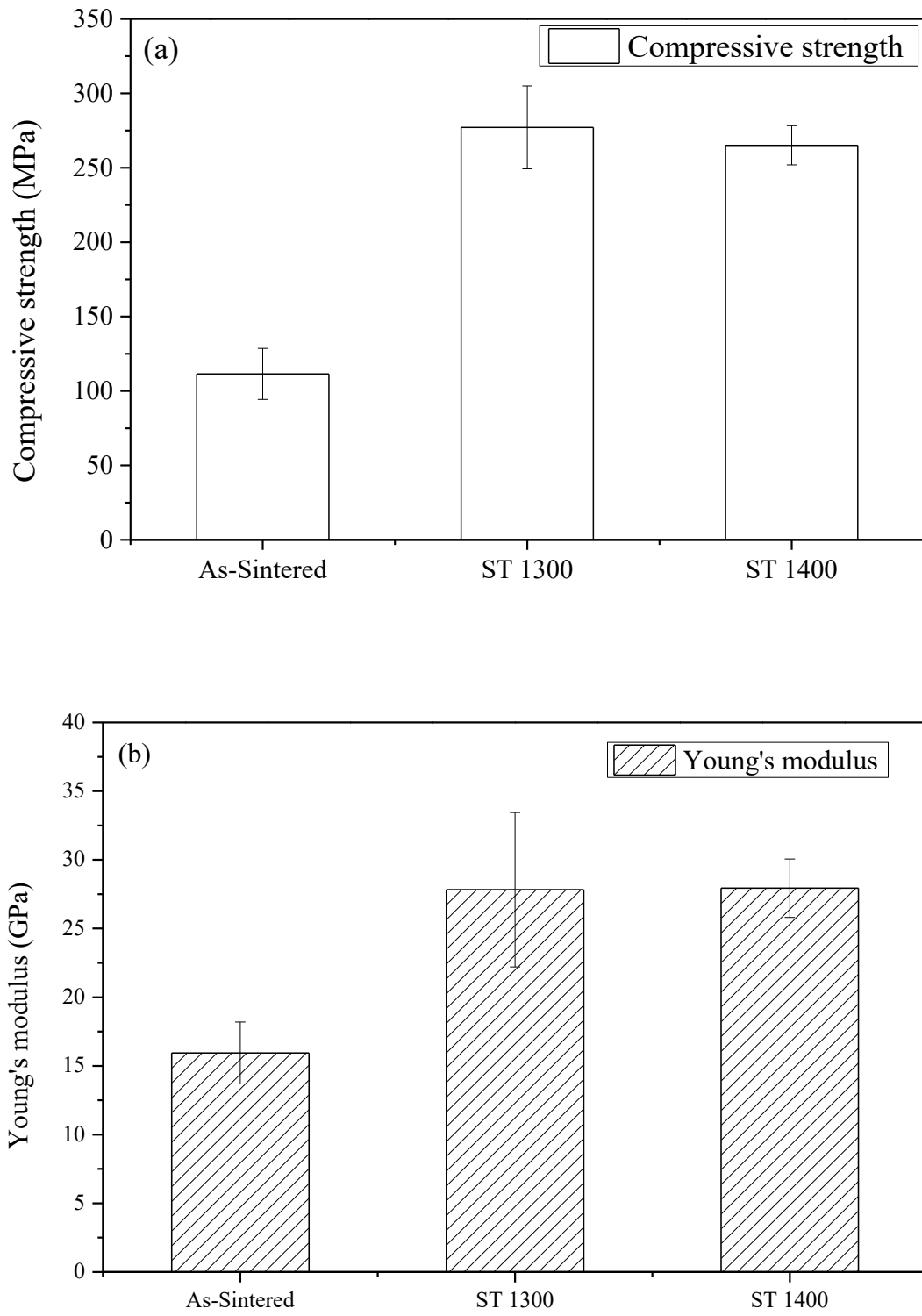


Figure 5. 13 Mechanical properties of porous Ti-6Al-4V after solution treatment in argon flow furnace at several temperature

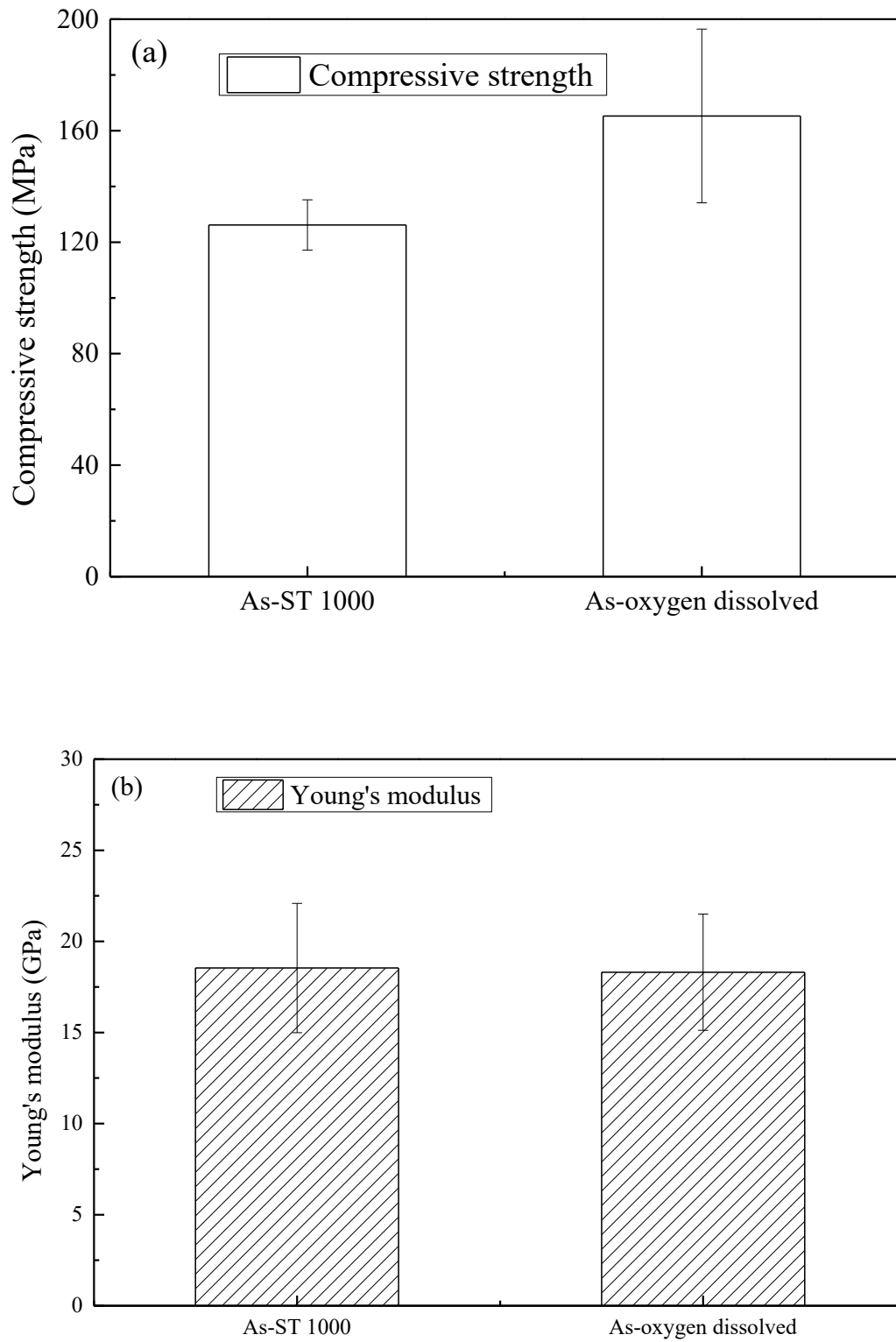


Figure 5. 14 Mechanical properties of as-solution treated sample and as-oxygen-dissolving process at 530 °C for 6h

5.4 Discussion

5.4.1 Influence of oxygen

From table 5.1, it is shown that during sintering and heat treatment process, the oxygen content in samples is changed. Oxygen as strong α phase stabilizer will increase the β transus temperature of Ti-6Al-4V. Equation 5.1 shows the relation between oxygen concentration and β transus temperature of this alloy [4].

$$T_{\beta\text{-transus}} = 937 + 242.7 [O] \quad 5.1$$

where [O] is the oxygen concentration in weight percent. After sintering, spark plasma sintered sample contained about 0.223 of oxygen, results the β transus temperature about 992 °C. While for porous samples, the β transus temperature is about 1010 °C. However, HTRD results from figure 5.2-6 implies that even after heating at 1200 °C, single β phase peak was not found. From SEM results of samples solution treated at several temperature, figures 5.7-10, retained α phase was not observed at sample solution treated at 1300 °C, implies the actual β transus of the alloy is between 1200 and 1300 °C. In fact, although it is not discussed in this research, other interstitial element such as carbon, nitrogen and iron act similarly with oxygen as α stabilizer elements. Equation 5.2 and 3 describes the oxygen equivalent value affected by each elements content in weight percent [5] [6].

$$[O]_{EQ} = [O] + 2[N] + \frac{2}{3}[C] \quad 5.2$$

$$[O]_{EQ} = [O] + 2.77 [N] + 0.1 [Fe] \quad 5.3$$

Yan *et al.* [7] reported the formation of nano-size α_2 phase in the α phase of as-sintered Ti-6Al-4V with interstitial oxygen content between 0.25 and 0.49 wt. %. Figure 5.15 shows the titanium alloys phase diagram of Ti-rich corner focusses on α and α_2 phases [8]. From the phase diagram, it was shown for 6 wt. % titanium, at elevated temperature α_2 phase is formed then disappeared, transformed into α phase. It was mentioned before in section 5.4.1 that oxygen content increase as surface area increase. Lim *et al.* [9] and Liu *et al.* [10] reported that oxygen increase the solvus line of $\alpha/(\alpha+\alpha_2)$. Thus, at HT-XRD α_2 still occurs at temperature above 1000 °C for Ti-6Al-4V powder. The influence of oxygen to the increase of $\alpha/(\alpha+\alpha_2)$ solvus line is described in equation 5.4 (in wt. %) [8] [9].

$$[Al]_{EQ} = 1[Al] + \frac{1}{3}[Sn] + \frac{1}{6}[Zr] + 10[O + C + 2N] \quad 5.4$$

The influence of oxygen content to mechanical properties of porous Ti-6Al-4V is summarized in figure 5.16. As oxygen content increase the mechanical properties of porous sample increase this result is comparable with Lefebvre *et al.* [1].

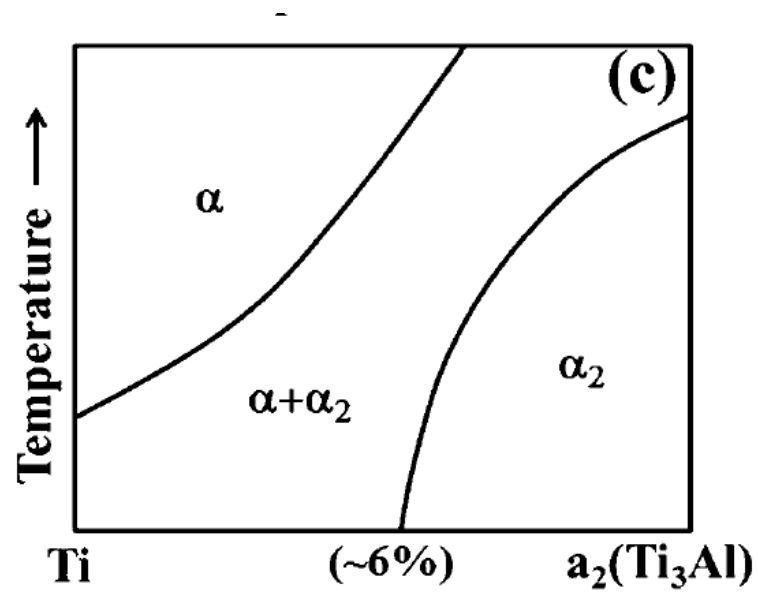


Figure 5. 15 Titanium alloys phase diagram of Ti-rich corner focusses on α and α_2 -phases [8]

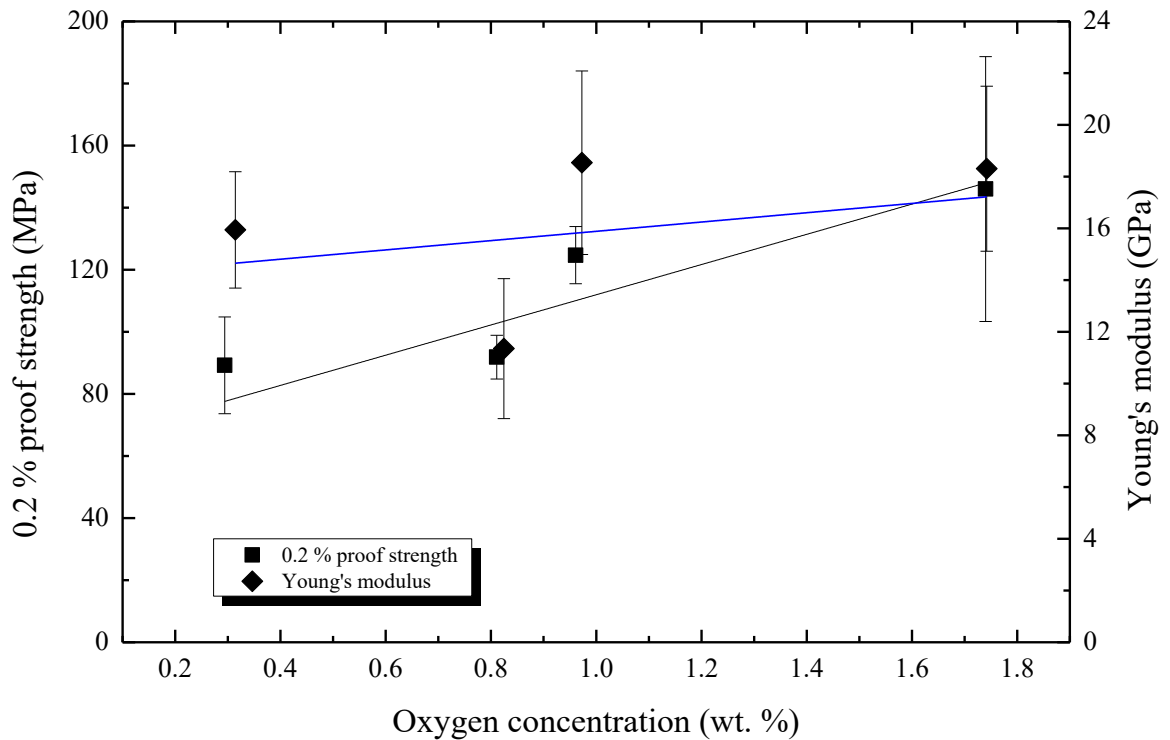


Figure 5. 16 Mechanical properties of porous Ti-6Al-4V with different oxygen content

5.4.2 Influence of solution treatment to micro-structure and mechanical properties of porous Ti-6Al-4V

Table 5.4 shows the summary of phase constituent after several solution treatments. Solution treatment at 980 and 1000 °C followed by ice WQ produced α' -phase while at 850 °C produced metastable β -phase which lead to increase of both compressive strength and Young's modulus of samples. Solution treatment at β single phase area at 1300 – 1400 °C followed by furnace cooling which produce Widmanstätten α and β phase more increase the mechanical properties of porous Ti-6Al-4V until the upper part of cortical bone properties, figure 5.17 marked by red circle.

Table 5. 3 Summary of phases after several solution treatment

Heat treatment	Phases
ST 850 → Ice WQ	$\alpha + \text{metastable } \beta$
ST 980 → Ice WQ	$\alpha + \alpha'$
ST 1000 → Ice WQ	$\alpha + \alpha'$
ST 1300 → FC	Widmanstätten $\alpha + \beta$
ST 1400 → FC	Widmanstätten $\alpha + \beta$

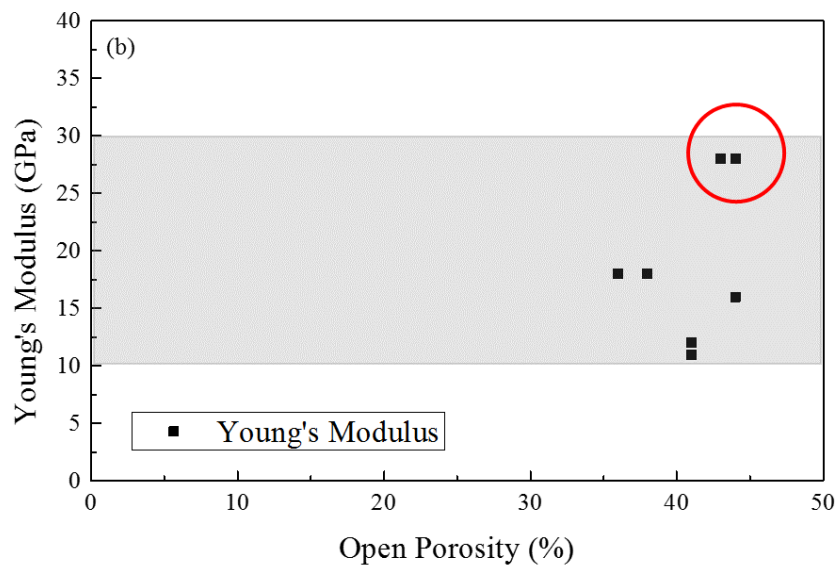
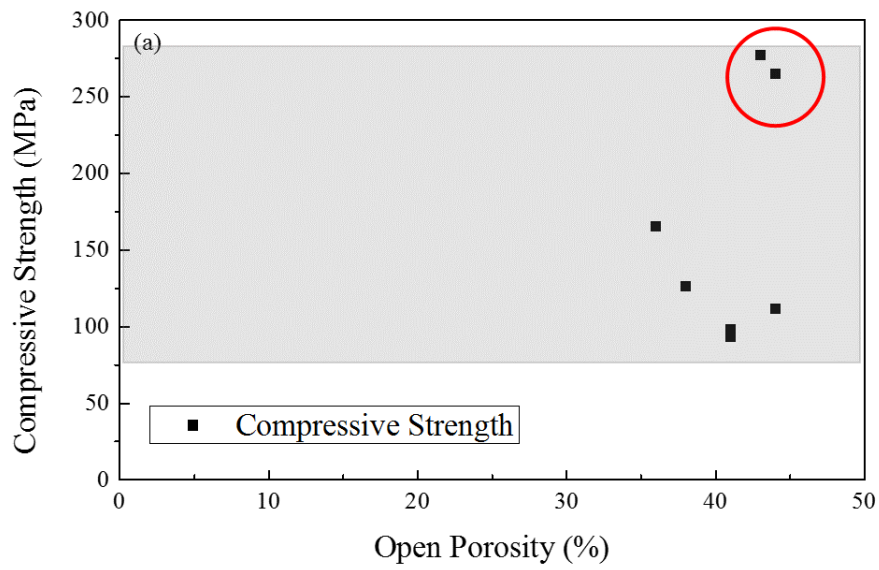


Figure 5. 17 Summary of mechanical properties of porous sample solution treated at different condition. The grey area is the range of cortical bone Young's modulus and compression strength

5.5 Conclusions

The influence of oxygen and solution treatment to micro-structure and mechanical properties of porous Ti-6Al-4V is discussed in this chapter. In summary the influence is define below:

- (1) Oxygen content affects the phase's constitution of porous sample at elevated temperature. Due to relatively high oxygen content the β transus temperature of the sample increase till between 1200 and 1300 °C. Although increasing the β transus temperature, oxygen increase the mechanical properties of porous Ti-6Al-4V.
- (2) Solution treatment at temperature 850 – 1000 °C followed by ice WQ produces microstructure which is similar to spark plasma sintered Ti-6Al-4V and increases the mechanical properties of porous Ti-6Al-4V.
- (3) Solution treatment at single β phase area at 1300 – 1400 °C produce a very fine Widmanstätten α and β phase which results to more increase of mechanical properties of porous Ti-6Al-4V comparable with cortical bone properties.

5.6 References

- [1] L.-P. Lefebvre and E. Baril, "Effect of Oxygen Concentration and Distribution on the Compression Properties on Titanium Foams," *Advanced Engineering Materials*, vol. 10, no. 9, pp. 868-876, 2008.
- [2] "ASTM standard F1580 - 01," in *Standard Specification for Titanium and Titanium-6 Aluminum-4 Vanadium Alloy Powders for Coating Surgical Implants*.
- [3] Y. Oshida, "Bioscience and Bioengineering of Titanium Materials," Oxford, Elsevier, 2002, p. 82.
- [4] A. Kahveci and G. Welsch, "Effect of oxygen on the hardness and alpha/beta phase ratio of Ti-6Al-4V alloy," *Scripta Metallurgica*, vol. 20, pp. 1287-1290, 1986.
- [5] H. Ogden and R. Jaffee, "The effects of carbon, oxygen and nitrogen on the mechanical properties of titanium and titanium alloys," Titanium Metallurgical Laboratory No.20, Ohio, 1955.
- [6] S. Soeda and H. O. M. H. H. Fujii, "High strength, high ductility titanium-alloy and process for producing the same". United State of America Patent 6063211, 2000.
- [7] M. Yan, M. Dargusch, T.Ebel and M. Qian, "A transmission electron microscopy and three-dimensional atom probe study of the oxygen-induced fine microstructural features in as-sintered Ti-6Al-4V and their impacts on ductility," *Acta Materialia*, vol. 68, pp. 196-206, 2014.
- [8] M. Yan, W. Xu, M. S. Dargusch, H. Tang, M. Brandt and M. Qian, "Review of effect of oxygen on room temperature ductility of titanium and titanium alloys," *Powder Metallurgy*, vol. 57, no. 4, pp. 251-257, 2014.
- [9] J. Y. Lim, J. C. J. McMahon, D. P. Pope and J. C. Williams, "The effect of oxygen on the stucture and mechanical behavior of aged Ti-8Al," *Metallurgical Transaction A*, vol. 7A, pp. 139-144, 1976.

- [10] Z. Liu and G. Welsch, "Effects of oxygen and heat treatment on the mechanical properties of alpha and beta titanium alloys," *Metallurgical and Materials Transactions A*, vol. 19, no. 3, pp. 527-542, 1988.

Chapter 6 General Conclusions

In *chapter 1 General Introduction*, basic theory of porous metal and the development of space holder technique to produce porous metal are presented. The basic introduction of heat treatment for Ti-6Al-4V alloy is also described.

In *chapter 2 Fabrication of Porous Ti-6Al-4V through space holder method*, in order to achieve the effective fabrication condition, the influence of sintering parameters, i.e. heating rate, sintering temperature and sintering pressure, space holder size and its distribution to the formation of both micro- and macro- porosity were investigated. Space holder distribution plays an important role to increase open porosity value of porous products. Open porosity of sample increase as the more homogenous space holder distribution produced suggests distribution of space holder is main aspect that control the macro-pore interconnectivity. There is no significant increase of open porosity number by varying the space holder size and shape implying the interconnectivity between macro-pore is independent on space holder size and shape Sintering temperature and pressure are the main parameter to control micro-porosity. Increasing sintering pressure is more effective to reduce micro-porosity in the samples. Relative density produced is independent on heating rate. The most effective condition to produce less micro-porosity and more interconnected macro-porosity is utilization of any kind of space holder size with the addition of 10 wt. % ethanol as PCA and sintering at 700 °C, 60 MPa.

In *chapter 3 Effect of Macro- and Micro-porosity on Mechanical Properties of a Porous Ti-6Al-4V*, the effect of macro-porosity and micro-porosity to the mechanical properties of porous Ti-6Al-4V fabricated by solid-state space holder method was discussed. Macro-porosity in the range of 50 – 800 μm plays more significant role to control mechanical properties of porous product. Irregular shape of macro-pore result about two times lower mechanical properties than cuboidal shape macro-pore while porous mechanical properties is insensitive to macro-porosity size. Homogenous macro-porosity will yield more pore connectivity which result to higher

number of open porosity and lower Young's modulus. Porous product strength is more dependent to pore wall thickness than its open porosity number. Micro-porosity in the size a few till a few ten micrometer has no significant effect to both Young's modulus and mechanical properties of porous product.

In *chapter 4 Influence of Solution Treatment and Aging to Microstructure and Hardness of Bulk Spark Plasma Sintered Ti-6Al-4V*, the effect of solution treatment and aging to the mechanical properties of spark plasma sintered Ti-6Al-4V was confirmed. Upon quenching, martensite phase only formed by sample solution treatment above 980 °C. Due to quite high vanadium content which stabilized the BCC structure, quenching below such temperature produced metastable β phase. Aging treatment enhances formation of β phase precipitate. Thus, after aging martensite decomposes to rich vanadium β phase, which form along the grain boundary of martensite and aligned along interface of martensite plate, and lean vanadium α phase. The decomposition then decrease the hardness of the sample. The results of solution treatment also imply that the β transus temperature of spark plasma sintered Ti-6Al-4V is higher than 1050 °C.

In chapter 5 *Influence of Solution Treatment and Oxygen Content to Microstructure and Mechanical Properties of Porous Ti-6Al-4V*, the influence of solution treatment and oxygen to microstructure and mechanical properties of porous Ti-6Al-4V are investigated. Solution treatment increase oxygen content in porous samples. Oxygen content affects the phase's constitution of porous sample at elevated temperature. Due to relatively high oxygen content the β transus temperature of the sample increase till between 1200 and 1300 °C. Even though oxygen increase the β transus temperature, it also increase the compressive strength of porous sample. Solution treatment at temperature 850 – 1000 °C followed by ice WQ produces microstructure similar to spark plasma sintered Ti-6Al-4V and increases the mechanical properties of porous Ti-6Al-4V. Solution treatment at single β phase area at 1300 – 1400 °C produce a very fine Widmanstätten α and β phase which successfully results to the increase of mechanical properties of porous Ti-6Al-4V, comparable with cortical bone properties.

Acknowledgements

I would like to thank supervisor Prof. Equo Kobayashi, vise supervisor Prof. Kumai, Prof. Sato and Prof. Tezuka for their kind assistance and patience guidance. From their critical advices and tremendous encouragements, I am able to finish my research. I also would like to express my gratitude to Prof. Takeyama, Prof. Kawamura and Prof. Ueda who allows me to use their laboratory's equipment, especially Prof. Takeyama who also help me to do oxygen concentration test. I also received so much help from Dr. Yoko Yamabe-Mitarai from NIMS to perform some experimental works such as high-temperature XRD and heat treatment using ultra-vacuum furnace. I am very thankful for her help and kindness. My endless gratitude for my parents and my sister and brother for every prayer times they gave. Because of their prayers, I am strengthen to do all things necessary to complete my study. I would like to thank all the members of Sato-Kobayashi Laboratory, Kumai-Kobayashi Laboratory and Kobayashi Laboratory. It is an honor to spend five years study here.

Dedicated to Thee who makes all things possible

*“To the King of the ages, immortal, invisible, the only God, be honor and glory forever and ever.
Amen.”*

1 Timothy 1: 17

Soli Deo Gloria,

Yorina Sarah Franscoise Lantang